INVESTIGATION OF THE SUDDEN AIR RELEASE UP THE AIRSHAFT OF THE BERG RIVER DAM BOTTOM OUTLET STRUCTURE DURING EMERGENCY GATE CLOSURE USING NUMERICAL MODELLING METHODS

by
Doreen Pulle

Thesis presented in fulfilment of the requirements for the degree
Master of Science in Water and Environmental Engineering at the
University of Stellenbosch

Supervisor: Prof. Gerrit Roux Basson
Faculty of Engineering
Department of Civil Engineering

December 2011

DECLARATION

By submitting this dissertation electronically, I declare that the entirety of the work contained therein is my own, original work, that I am the owner of the copyright thereof (unless to the extent explicitly otherwise stated) and that I have not previously in its entirety or in part submitted it for obtaining any qualification.

December 2011

i

ABSTRACT

The design of the Berg River Dam bottom outlet structure with multitude draw offs was based on various hydraulic model tests on a 1:40 model that was used for original design and a 1 in 20 physical model which was used to produce the final design. These tests indicated no foreseeable malfunction and showed that the 1.8 m^2 air vent would provide sufficient air flow to minimize the negative pressures that would develop behind the emergency gate during its closure or opening. However, during the first trial commissioning of the dam outlet structure, air was unexpectedly expelled through the air vent at a velocity so high that the recta-grids covering the shaft were blown to a height of over 3m while the gate was closing at a rate of approximately 0.0035 m/s. The air flow velocity up the air vent was approximately 45m/s and occurred when the gate was approximately 78% closed. A brief report on the test indicated that the source of air may have been a vortex formation in the vertical intake tower upstream of the emergency gate entraining air which was drawn through the gate and released up the air vent.

The purpose of this research was to utilize 3-dimensional numerical modelling employing Computational Fluid Dynamics (CFD) to carry out numerical simulations to investigate the above mentioned malfunction and thereby establishing whether the given hypotheses for the malfunction were valid. For purposes of validating the CFD modelling, a 1:14.066 physical model was constructed at the University of Stellenbosch hydraulics laboratory.

The 3-dimensional CFD model was used to investigate the said incident, using steady state simulations that were run for various openings of the emergency gate. The intenetion was to establish whether there was an emergency gate opening which would reproduce the air release phenomenon.

The results obtained from the numerical model showed a similar trend to those of the physical model although there were differences in values. Neither model, showed a sudden release of air through the vent. It was concluded that the unsteady air-water flow out of the air vent may have been caused by the variation of the discharge with time causing unbalanced negative pressures in the outlet structure. Therefore, it was recommended that further CFD transient simulations should be undertaken incorporating a moving emergency gate.

OPSOMMING

Die ontwerp van die bodemuitlaat van die Bergrivierdam met multivlakuitlate is gebaseer op verskeie hidrouliese modeltoetse op a 1:40 fisiese model wat vir die oorspronklike ontwerp gebruik is, asook 'n 1 tot 20 fisisiese model wat gebruik is om die finale ontwerp te lewer in 2003. Hierdie toetse het geen beduidende afwykings aangedui nie en het bewys dat die 1.8m^2 lugskag voldoende lugvloei sal toevoer om die negatiewe drukking wat stroomaf van die noodsluis ontstaan gedurende die sluitingsproses, sal minimaliseer. Gedurende die inlywingtoets in die veld in 2008 van die noodsluis, is lug onverwags teen 'n hoë snelheid deur die lugskag opwaarts uitgelaat, wat die rooster wat die skag beskerm teen 'n hoogte van oor 3m geblaas het terwyl die sluis teen 'n tempo van ongeveer 0.0035 m/s toegemaak het. Die lugvloeisnelheid in die lugskag was ongeveer 45m/s en het plaasgevind toe die sluis ongeveer 78% toe was. 'n Kort verslag oor die veldtoets dui aan dat die bron van die lug dalk werwelvorming in die vertikale inlaattoring stroomop van die noodsluis was, met lug wat deur die sluis getrek was en opwaarts in die lugskag vrygelaat is.

Die doel van die navorsing was om drie-dimensionele numeriese modellering met rekenaar vloeidinamika (RVD) te benut om numeriese similasies uit te voer om die bogenoemde abnormale werking van die lugskag te ondersoek en daarmee vas te stel of die gegewe aannames van krag is. Vir die doel om die RVD modellering te verifieer is 'n 1:14.066 fisiese model gebou by die Universiteit van Stellenbosch se waterlaboratorium.

Die 3-dimensionele RVD model is gebruik om die genoemde probleem te ondersoek, deur stasionêre simulasies wat vir verskillende openinge van die noodsluis geloop is te gebruik. Die doel was om vas te stel of daar 'n spesifieke noodsluisopening is wat die vrylating van die lug veroorsaak het.

Die uitslag verkry deur die numeriese model het dieselfde windrigting soos die van die fisiese model gewys, alhoewel daar verskille in die waardes was. Nie een van die modelle het 'n skielike vrystelling van lug deur die lugskag gewys nie. 'n Afleiding is gemaak dat die nie stasionêre lug-water vloei uit die lugskag moontlik veroorsaak was deur die verandering van die vloei met tyd veroorsaak deur ongebalanseerde negatiewe druk in die uitlaatstruktuur. Daarom is daar voorgestel dat verdere RVD nie stasionêre simulasies gedoen word met 'n bewegende noodsluis.

ACKNOWLEDGEMENTS

TABLE OF CONTENTS

vii

LIST OF ABBREVIATIONS

Symbol	**Description**
BRD	Berg River Dam
CFD	Computational Fluid Dynamics
ASHRAE	American Society of Heating, Refrigerating and Air Conditioning Engineers
Q	Discharge (m^3/s)
s	Seconds
V	Velocity (m/s)
g	Acceleration due to gravity (m/s^2)
m	meters
H, h	Head (m)
Fr	Froude number
C_c	Contraction coefficient
A	Area (m^2)
a, b	Rectangular dimensions
C_d	Discharge coefficient
β	Air entrainment coefficient
m_a	Mach number
D	Diameter
η	Relative gate opening
y	Contracted water depth (m)
K, n	Empirical coefficients

LIST OF FIGURES

LIST OF TABLES

CHAPTER 1

1. INTRODUCTION

1.1 Background

Bottom outlets are openings in a dam used to draw down the reservoir level or to release flow from the dam. According to the type of control gates (valves) and the position of the outflow in relation to the tail water, they operate either under pressure or free flowing over part of their length. The flow from the bottom outlets can be used as compensating flow for a river reach downstream of the dam where the flow would otherwise fall below acceptable limits. Outlets can also serve to pass density (sediment-laden) currents through a reservoir.

Controlled outlet facilities are required to permit water to be drawn off as is operationally necessary. Provision must be made to accommodate the required pipework and its associated control gates or valves (Novak et al., 2007). For embankment dams it is normal practice to provide a control structure or valve tower, which may be quite separate from the dam, controlling entry to an outlet tunnel or culvert. A bottom outlet facility is provided in most cases as a dam safety measure to rapidly drawdown and if necessary empty the reservoir. The bottom outlet must have as high a capacity as economically feasible consistent with the reservoir management plan. In most cases it is necessary to use special outlet valves and/or structures to avoid scouring and damage to the stream bed and banks downstream of the dam.

Gated tunnels are used for emergency drawdown of reservoirs, for regulating the reservoir water level and sometimes for flushing of sediment among other reasons (Vischer and Hager, 1998). In gated tunnels a high-speed flow issuing from the gate drags and entrains a lot of air and that is why in the construction of dam bottom outlet structures, emphasis is made on the provision of an air vent immediately downstream of the emergency gate so as to accommodate for the negative pressures that develop behind the gate during its closure and/or opening. This is crucial because the aeration deficit behind the emergency gate may lead to adverse effects such as cavitation and vibration of the gate.

1.1.1 The Berg Water Project (BWP)

The Berg River Project comprises the Berg River Dam, Dasbos Pump Station and pipeline to Dasbos Tunnel and Adit situated approximately 6km northwest of Franschhoek in the Berg River Valley. The Drakenstein Abstraction Works and Pump Station are situated approximately 10km downstream of the

Dam site on the right bank of the Berg River on the grounds of Drakenstein Correctional Services, and 1.5km west of the R301 to Paarl.

The increasing demand for water in the Greater Cape Town region led to the Department of Water Affairs (DWA) identifying the Berg Water Project (BWP) which included the Berg River Dam (previously known as the Skuifraam Dam) and a supplement scheme located approximately 12 km downstream of the dam. The supplement scheme was constructed to provide excess water from high winter flows back into the Berg River Dam while maintaining the downstream environmental requirements.

The upper catchment of the Berg River to the South of the Dam site is one of the most productive water catchments in the country and the BWP harnesses this resource primarily for the benefit of the City of Cape Town but also for the bulk of water users in the urban and agricultural sectors of the Western Cape. The BWP augments the yield of the Western Cape Water System by $81Mm^3$ (to $523Mm^3$) per year and integrates with the Riviersonderend – Berg River Government Water Scheme (Abban B. et al., unknown).

The project was funded and implemented by the Trans-Caledon Tunnel Authority (TCTA), which in December 2002 appointed the Berg River Consultants, a joint venture between Knight Piesold Consulting, Goba Consulting Engineers and Project Managers and Ninham Shand Consulting Engineers, as design and construction supervising consultants (Abban B. et al., unknown).

The Project components are owned by TCTA but are operated and maintained as part of the Western Cape Water System by DWAF.

1.1.1.1   Components of the Berg River Dam

The Berg River Dam is located on the upper Berg River in the La Motte forest. The dam is a concrete-faced-rockfill dam (CFRD), with a crest length of approximately 938 m, 62.5 m high, and 220 m dam width. The appurtenant structures include a 65m high intake tower, a 5.5m diameter concrete outlet conduit, outlet works and an un-gated side channel spillway (Van Vuuren, 2003).

The dam has a gross storage capacity of 130 million m^3 and a surface area of 537 ha at full supply level (FSL) and it provides an additional $56Mm^3$/a of water to the Greater Cape Town region (Van Vuuren, 2003), and an additional $25Mm^3$/a of water is supplied by the supplement scheme.

1.1.2   Problem Statement

On 12th June, 2008, at the commissioning of the Berg River Dam bottom outlet structure large volumes of air were released up the air vent while the gate was gradually being closed. When the gate was approximately 78% closed, the high up-flow air velocity blew the mentis grid cover off the top of the air vent about 3m high into the air causing injury to an observer who was monitoring the air flows at the air vent (Commissioning report, Appendix A). This issue raised various concerns, questions and comments as to the cause of the continuous release of such large volumes of air from the air intake shaft which was designed to deliver a down-flow of air to negate the effects of pressure reduction, or vacuum formation behind the emergency gate.

1.1.3   Hypotheses

Based on the commissioning report and meetings held thereafter regarding the said incident, the following hypotheses were drawn as to the cause of the high velocity air flow up the air vent.

➢ Vortex formation in the intake tower may have resulted in entrainment of air in the flow. The entrained air would then have flowed underneath the emergency gate and have been released immediately downstream of the gate.

➢ During the gradual closing of the emergency gate, the varying discharge capacity could have resulted in air trapped in the conduit being pushed backwards in the conduit and eventually up the air vent by the surging of the air-water mixture in the conduit.

1.1.4   Objective

In 2009, investigations of the unexpected sudden air and water gust up the air vent that occurred during the trial commissioning of the Berg River Dam bottom outlet structure commenced with the aid of a 1:40 scale physical model and a two-dimensional Computational Fluid Dynamics (CFD) numerical model (Calitz, 2009). The results from these studies were inconclusive owing to the small scale of the physical model and the inadequate geometry of the Computational Fluid Dynamics (CFD) model which did not accurately represent actual conditions(Calitz, 2009).

Recommendations were made that a larger scale physical model be studied alongside a 3-dimensional CFD model in order to provide a more detailed study of the problem, which also implied higher model construction costs.

3

The purpose of this research was to utilise CFD (numerical simulation) methods and a 3-dimensional model of the Berg River Dam bottom outlet structure to investigate and study the above mentioned malfunction. Since this was the first time a 3-dimensional CFD model had been used for the research, the study entailed the monitoring of fluid flow in the outlet structure for different static openings of the emergency gate for steady state simulations. This helped establish whether there is an emergency gate opening for which the air vent is inadequate to provide the aeration demand behind the emergency gate. It should be noted, however, that the conditions during the commissioning were such that the emergency gate was closed at a given rate.

1.1.5   Motivation

Water is a very important natural resource whose management must be properly handled so as to minimise the negative effects of poor resource management. It can be seen worldwide how countries with inadequate water management structures struggle to reap the benefits of the God given resource. Among other mechanisms, dams are one of the major means by which water is controlled to provide for the various needs of the environment. Such needs include flood control, hydropower generation, potable water supply, maintaining downstream flow conditions, recreation, and irrigation, to mention but a few.

Over the years, the need for adequate resource management will definitely increase given the increasing population and potential climate change that would affect the availability of the resource. As such, it is expected that structures such as dams constructed to fulfil these purposes will be stable, efficient and reliable since they will be required to be functional for long periods of time.

The rapid growth in demand for water has put pressure on engineers and designers to expedite the design of water retaining structures and as such computer-aided programs have been developed to expedite the design process since physical modelling is not only expensive but also requires time assigned for construction and testing. Advancement in technology has introduced new methods of designing or investigating engineering complexities alongside physical experimental procedures. The use of computer software whose codes have engineering theory incorporated into them is being widely used to simulate various engineering conditions. Such technology may be employed where physical modelling proves expensive or highly unreliable.

Current research involving flow problems is being handled using CFD methods (numerical methods) which provide results that are reliable. Also, more complex situations are able to be modelled where

physical modelling wouldn't be easily handled, such as hazardous projects. For this research, ANSYS FLUENT, a software package that uses CFD codes to solve for flow problems in fluid flow analysis is utilised.

1.2   What is CFD?

Computational fluid dynamics (CFD) is a branch of fluid mechanics that uses numerical methods and algorithms to solve and analyze problems that involve fluid flows. It may also be defined as the analysis of systems involving fluid flow, heat transfer and other associated phenomena like chemical reactions by means of computer-based simulation. (Versteeg and Malalasekera , 2007). Computational Fluid Dynamics is a design tool that has been developed over the past few decades and will be continually developed as the understanding of the physical and chemical phenomena underlying CFD theory improves.

Computers are used to perform the calculations required to simulate the interaction of liquids and gases with surfaces defined by boundary conditions. With high-speed supercomputers, better solutions can be achieved. On-going research, however, yields software that improves the accuracy and speed of complex simulation scenarios such as transonic or turbulent flows.

The goals of CFD are to be able to accurately predict fluid flow, heat transfer and chemical reactions in complex systems, which involve one or all of these phenomena. Presently, CFD is being increasingly employed by many industries either to reduce manufacturing design cycles or to provide an insight into existing technologies so that they may be analysed and improved. Examples of such industries include power generation, aerospace, process industries, automotive, chemical engineering and construction.

As a design tool in water resources applications, CFD presently is used together with experimental analysis where CFD does not produce absolute results. In order to provide validation and verification of CFD solutions, experimental methods are normally conducted in conjunction with numerical simulations to provide more realistic results. The reason for this is that the numerical methods, which govern the solutions in a CFD problem, rely on several modelling assumptions that may not have been validated to a satisfactory level.

The schematic below shows a rough sketch of how the problem relates to the analytical solution depending on which approach is chosen to determine the required solution.

5
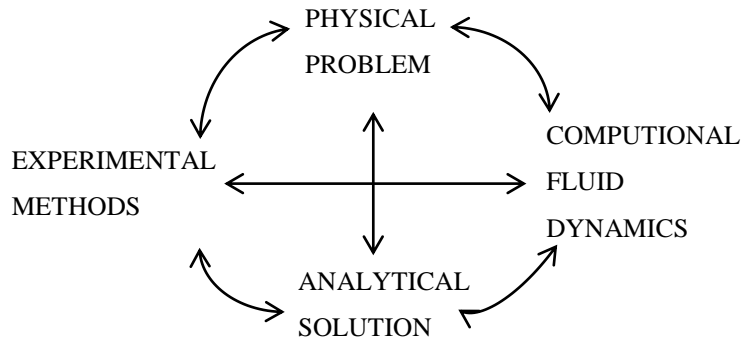
Figure 1.2-1: Schematic of approach to tackling engineering flow problems (Veersteg, 2007).

CFD presently offers itself as a powerful design tool and even more so in the future because:

(a) Dangerous or expensive trial and error experiments can be simulated and design parameters observed prior to any physical prototype being constructed;

(b) Computers are becoming more powerful and less expensive, thus allowing larger CFD simulations to be calculated, or more detailed simulations of present CFD problems;

(c) The numerical schemes and physical models that are the building blocks of CFD are being continually improved.

(d) If a CFD model can be established yielding accurate results on one particular design, then the model can be used as a tool of prediction for that design under many different operating conditions.

CFD modelling involves iteratively solving partial differential equations in time and/or space (which in this case describe the flow of fluids) to obtain a final numerical description of the total flow field under consideration. The computer program utilises the theory available on fluid flow dynamics to determine the solution for the problem at hand.

1.2.1   Errors and uncertainty in CFD modelling

The benefits of CFD, over time, have been recognised by large corporations, small and medium sized alike, and it is now used in design/development environments across a wide range of industries. This has focussed attention on 'value for money' and potential consequences of wrong decisions made on

6

the basis of CFD results. The consequences of inaccurate CFD results are at best a waste of time, money and effort and at worst catastrophic failure of components, structures or machines. Moreover, the costs of a CFD capability may be quite substantial (Versteeg et al, 2007):

- Capital cost of computing equipment

- Direct operating cost: software licence(s) and salary of CFD specialist, if solicited

- Indirect operating cost: maintenance of computing equipment and provision of information resources to support CFD activity

The value of a modelling result is clear – time saving in design and product improvement through enhanced understanding of the engineering problem under consideration – but is rather difficult to quantify. The application of CFD modelling as an engineering tool can only be justified on the basis of its accuracy and the level of confidence in the results. With its roots in academic research, CFD development was initially focused on new functionality and improved understanding without the need to make very precise statements relating to confidence levels. Also, the engineering industry has a long tradition of making things work within the limitations of the current state of knowledge, provided that the confidence limits are known. Assessment of uncertainty in experimental data is a well-established practice and the relevant techniques form part of every engineer's basic education.

For this reason, extensive reviews of the factors influencing simulation results have been carried out and a systematic process developed to estimate uncertainty in experimental results for the quantitative assessment of confidence levels.

In the context of trust and confidence in CFD modelling, the following definitions of error and uncertainty have now been widely accepted:

1.2.1.1 Error

This may be defined as a recognisable deficiency in a CFD model that is not caused by lack of knowledge. Causes of errors defined in this way include (Malalasekera, 2007):

i.) Numerical errors – Computational Fluid Dynamics solves systems of non-linear partial differential equations in discretised form on meshes of finite time steps and finite control volumes that cover the region of interest and its boundaries. This gives rise to three recognised sources of numerical error:

- Round off errors – These are the result of representation of real numbers by means of a finite number of significant digits, which is termed the machinery accuracy. These types of errors contribute to the numerical error in a CFD result and can be generally controlled by careful arrangement of floating-point arithmetic operations to avoid subtraction of almost equal-sized large numbers or the addition of numbers with very large differences in magnitude. In CFD computations it is common practice to use gauge pressures relative to a specified base pressure, for example, in incompressible flow simulations a zero pressure value is set at an arbitrary location within the computational domain. This is a simple example of error control by good code design, since it ensures that the pressure values within the domain are always of the same order as the pressure difference that drives the flow. Thus, the calculation with floating-point arithmetic of pressure differences between adjacent mesh cells is not spoilt by loss of significant digits as would be the case if they were evaluated as the difference between comparatively large absolute pressures.

- Iterative convergence errors – The numerical solution of a flow problem requires an iterative process and the final solution exactly satisfies the discretised flow equations in the interior of the domain and the specified conditions on its boundaries. If the iteration sequence is convergent the difference between the final solution of the coupled set of discretised flow equations and the current solution after k iterations reduces as the number of iterations increases. In practice, the available resources of computing power and time dictate that we truncate the iteration sequence when the solution is sufficiently close to the final solution. This truncation generates a contribution to the numerical error in the CFD solution. The most commonly constructed truncation criterion in CFD is one based on so-called residuals. The discretised equation for general flow variables, Ø, at mesh cell, i, can be written as follows:

$$(a_P \emptyset_P)_i = \left(\sum_{nb} a_{nb} \emptyset_{nb} \right)_i + b_i$$

where the subscript i indicates the control volume and a_P, a_{nb} and b_i are constants.

The final solution will satisfy the equation above exactly at all cells in the mesh but after k iterations there will be a difference between the left and right hand sides. The absolute value of this difference at the mesh cell i is termed as the local residual, $R_i^{\emptyset}$, whose sum over all control volumes within the computational domain gives an indication of the convergence behaviour

8

across the whole flow field, also defined as the global residual, $\hat{R}^{\emptyset}$. This global residual is always equal to zero when the final solution is reached and it is a satisfactory average measure of the discrepancy between the final solution and the computed solution after k iterations. In commercial CFD codes, such as ANSYS FLUENT, the convergence test in the iterative sequences involves the specification of tolerances for the normalised global residuals for mass, momentum and energy. An iteration sequence is automatically truncated when all these residuals are smaller than their pre-set maximum values. Default values for the tolerances, which have been determined by systematic trials to give acceptable results for a wide range of flows, are supplied by the code vendors but for high accuracy work it may be necessary to reduce these values of tolerance from their default values to control and reduce the magnitude of the contribution to the numerical error due to early truncation of the iterative sequence.

- Discretisation errors – temporal and spatial derivatives of the flow variable, which appear in the expressions for rates of change, fluxes, sources and sinks in governing equations are approximated in the finite volume method on the chosen time and space mesh and this involves simplified profile assumptions for flow variable Ø, a practice that corresponds to the truncation of a Taylor series. This discretisation error is associated with the neglected contributions due to the higher-order terms, which give rise to errors in CFD results. Control of the magnitude and distribution of discretisation errors through careful mesh design is a major concern in high-quality CFD and in theory, the discretisation error can be made arbitrarily small by progressive reductions in the time step and space mesh size but this requires increasing amounts of memory and computing time. Thus, the ingenuity of the CFD user as well as resource constraints dictate the lowest achievable level of the contribution to the numerical error due to the simplified profile assumptions.

ii.) Coding errors – This involves mistakes or 'bugs' in the software and is one of the most insidious forms of error.

iii.) User errors – Entails human errors through incorrect use of the software. Such error may be reduced or eliminated to a large extent through adequate training and experience

1.2.1.2   Uncertainty

This may be defined as a potential deficiency in a CFD model that is caused by lack of knowledge. The main sources of uncertainty are (Veersteg and Malalasekera, 2007):

9

i.) Input uncertainty – Consists of inaccuracies due to limited information or approximate representation of geometry, boundary conditions, and material properties among others. It is associated with discrepancies between the real flow and the problem definition within a CFD model. There are three categories of input data that can lead to uncertainty in CFD, namely:

- Domain geometry – The definition of domain geometry involves specification of the shape and size of the region of interest. In industrial applications this may come from a CAD model. It is impossible to manufacture the desired structure perfectly to the design specifications; manufacturing tolerances will lead to discrepancies between the design intent and a manufactured part. Furthermore, the CAD model needs to be converted to be suitable within CFD and this conversion process could lead to discrepancies between the design intent and the geometry within CFD. Similar comments apply to the surface roughness. The boundary shape in CFD is a discrete representation of the real boundary. In summary, the macroscopic and microscopic geometry within the CFD model will be somewhat different from the real flow passage, which contributes to input uncertainty in the model results.

- Boundary conditions – Apart from the shape and surface state of solid boundaries, it is also necessary to specify the conditions on the surface for all other flow variables, such as velocity, temperature, species and so on. It can be difficult to acquire this type of input to a high degree of accuracy. The choice of type and location of open boundaries through which flow enters and leaves the domain is a particular challenge in CFD modelling. Boundary conditions are chosen from a limited set of available boundary types for inlets and outlets. There must be compatibility between chosen open boundary condition type and the flow information available on the chosen surface location. In some cases, we only have partial information, such as average velocity and some indication of velocity distribution but no information on the turbulence parameters. Missing information must now be generated on the basis of past experience or inspired guesswork. In other cases, the assumed boundary condition may only be uniform on a fixed pressure boundary, but might actually be somewhat non-uniform. A contribution to the input uncertainty is associated with the inaccuracy of all assumptions involved in the process of defining the boundary conditions. The location of the open boundaries must be sufficiently far from the area of interest so that it does not affect the flow in this region. Solution economy on the other hand dictates that the domain should not be excessively large, so a compromise must

be found, which may cause discrepancies between the real flow and the CFD model, resulting in a contribution to the input uncertainty.

- Fluid properties – All fluid properties like density, viscosity and the like depend to a greater or lesser extent on the local values of flow parameters, such as pressure. Often the assumption of a constant fluid property is acceptable provided that the spatial and temporal variations of the flow parameters influencing that property are small. The application of this assumption also benefits solution economy since CFD models converge more quickly if fluid properties remain constant; however, errors are introduced if the assumption of constant fluid properties is inaccurate. If the fluid properties are allowed to vary as functions of flow parameters we have to contend with errors due to experimental uncertainty in the relationships describing the fluid properties.

  ii.) Physical model uncertainty – This involves discrepancies between real flows and CFD due to inadequate representation of physical or chemical processes such as turbulence, or due to simplifying assumptions in the modelling process such as incompressible flow, or steady state.

- Lack of validity of sub-models – CFD modelling of complex flow phenomena such as turbulence, combustion, heat and mass transfer involves semi-empirical sub-models such as the turbulence models for Reynolds-averaged Navier-Stokes (RANS) equations. They encapsulate the best scientific understanding of complex physical and chemical processes. The sub-models invariably contain adjustable constants derived from high-quality measurements on a limited class of simple flows. In applying the sub-models to more complex flows we extrapolate beyond the range of these data. There are several reasons why the application of sub-models brings uncertainty in a CFD result:

  ➢ A complex flow may involve entirely new and unexpected physical/chemical processes that are not accounted for in the original sub-model. In the absence of a better sub-model the user has no option but to work with less sophisticated description of the flow.

  ➢ In spite of the availability of a more comprehensive sub-model the user may deliberately select a simpler sub-model with a less accurate account of physics/chemistry to save time in computation.

  ➢ A complex flow may include the same mixture of physics/chemistry as the original simple flows but not exactly in the same blend, requiring adjustments of the sub-model constraints.

➢ The empirical constants within the sub-models represent a best fit of experimental data which will themselves have some uncertainty.

These sub-models contain adjustable constants that can only be used to capture exactly the class of flows that were used to calibrate their values and each sub-model will contain empirical constants that have limited validity. The empirical nature of the sub-models inside a CFD code, the experimental uncertainty of the values of the sub-model constants and the appropriateness of the chosen sub-model for the flow to be studied together determine the level of error in the CFD results due to physical model uncertainty. Section 4.1.1.1 gives details on the sub-model chosen in this research.

- Lack of validity of simplifying assumptions – At the start of each CFD modelling exercise it is common practice to establish whether it is possible to apply one or more potential simplifications. Considerable simplification can be achieved if the flow can be treated as:
  ➢ Steady vs. transient
  ➢ Two-dimensional, axisymmetric, symmetrical across one or more planes vs. fully three dimensional
  ➢ Incompressible vs. compressible
  ➢ Adiabatic vs. heat transfer across the boundaries
  ➢ Single species/phase vs. multi-component/phase

The simplification must be justifiable to good accuracy. Many flows exhibit geometrical symmetry about one or two planes. However, unless the inlet flow possesses the same symmetry, a model simplification based on geometrical symmetry will be inaccurate. For example, previous studies on the Berg River Dam outlet structure using a simplified 2-dimensional CFD model were inconclusive. The accuracy and appropriateness of all simplifying assumptions for a given flow determine the size of their contribution to physical model uncertainty.

1.2.2   Verification and validation

Once it is recognised that errors and uncertainty are unavoidable aspects of CFD modelling, it becomes necessary to develop rigorous methods to quantify the level of confidence in its results.

1.2.2.1   Verification

This may be defined as the process of determining that model implementation accurately represents the developer's conceptual description of the model and the solution, as Roache (1998) puts it, 'solving the

equations right'. The verification process involves quantification of the errors. Since computer coding and user errors are ignored, the round-off error, iterative convergence error and discretisation error need to be estimated.

- *Round-off error* can be assessed by comparing CFD results obtained using different levels of machine accuracy.
- *Iterative convergence error* can be quantified by investigating the effects of systematic variation of the truncation criteria for all residuals on target quantities of interest such as, the velocity at one or more locations of interest. Differences between the values of a target quantity at various levels of the truncation criteria provide a quantitative measure of the closeness to a fully converged solution.
- *Discretisation error* is quantified by systematic refinement of the space and time meshes. In high-quality CFD work we should aim to demonstrate monotonic reduction of the discretisation error for target quantities of interest and the flow field as a whole on two or three successive levels of mesh refinement.

Such methods merely estimate the numerical error of the code as it is and do not test whether the code itself accurately reflects the mathematical model of the flow envisaged by the code designer. Oberkampf and Truncano (2007), therefore, argued that a complete programme of verification activities should always include a stage of systematic comparison of CFD results with reliable benchmarks, that is, high accurate solutions of flow problems, such as analytical solutions or highly resolved numerical solutions.

1.2.2.2   Validation

This may be defined as the process of determining the degree to which a model is an accurate representation of the real world from the perspective of the intended uses of the model. Roache (1998) called this 'solving the right equations'. The process of validation involves quantification of the input uncertainty and physical model uncertainty.

- *Input uncertainty* can be estimated by means of sensitivity analysis or uncertainty analysis. This involves multiple test runs of the CFD model with different values of input data sampled from probability distributions based on their mean and expected variations. The observed variations of target quantities of interest can be used to produce upper and lower bounds for their expected

range and hence are a useful measure of the input uncertainty. In sensitivity analysis the effects of variations in each item of input data are studied individually. Uncertainty analysis, on the other hand, considers possible interactions due to simultaneous variations of different pieces of input data and uses Monte Carlo techniques in the design of the programme of CFD test runs.

- Oberkampf and Truncano (2007) stated that quantitative assessment of the *physical modelling uncertainty* requires comparison of CFD results with high-quality experimental results. They also noted that meaningful validation is only possible in the presence of good quantitative estimates of (i) all numerical errors, (ii) input uncertainty, and (iii) uncertainty of the experimental data used in the comparison.

Thus, the ultimate test of a CFD model is a comparison between its output and experimental data. However, the way in which such a comparison should best be carried out is still a subject of discussion. The most common way of reporting the outcome of a validation exercise is to draw a graph of a target quantity on the *y*-axis and a flow parameter on the *x*-axis, and if the difference between computed and experimental values looks sufficiently small then the CFD model is considered to be validated. The latter judgement is rather subjective, and Coleman and Stern (1997) proposed a more rigorous basis for validation comparisons drawing on the practise of estimating uncertainty in experimental results involving several independent sources of uncertainty. They suggested that the errors should be combined statistically by calculating the sum of squares of estimates of numerical errors, input uncertainty and experimental uncertainty from an estimate of validation uncertainty. A simulation is considered to be validated if the difference between experimental data and CFD model results is smaller than the validation uncertainty. The level of confidence in the CFD model is indicated by the magnitude of the validation uncertainty.

Oberkampf and Truncano (2007) pointed out that this approach would have the slightly paradoxical implication that it is easier to validate a CFD result with poor-quality experimental results containing a large amount of scatter. They suggested an alternative validation metric, which includes a statistical contribution, the influence of which decreases as the variance of the experimental data decreases with increase in the number of repeat experiments. Thus, the metric indicates increased levels of confidence in a validated CFD code if (i) the difference between the experimental data and CFD results is small, and (ii) the experimental uncertainty is small.

Since it is now clear that the accuracy of CFD results cannot be taken for granted, verification and validation are mission-critical elements of the confidence-building process. For this reason, we require experimental data with:

i.) Comprehensive documentation of problem geometry and boundary conditions.

ii.) Detailed measurements of distributions of flow properties, such as velocity components, static or total pressure and so on.

iii.) Complementary overall measurements such as mass flow rate.

Naturally, we should limit ourselves to information from trusted sources to generate a sufficiently credible validation. If suitable experimental results for a comprehensive validation are not available it will be necessary to identify a dataset for a closely related problem. If the problem chosen for validation is sufficiently close to the actual problem to be studied, we should be able to apply roughly the same CFD approach in both cases. It should be noted that a sufficient level of confidence in CFD simulations can only be achieved through rigorous verification and validation. If the search for validation data draws a complete blank then it is essential that a reasonable programme of experimentation be undertaken alongside CFD to provide solid foundations for design recommendations.

CHAPTER 2

2. METHODOLOGY

2.1   Literature review

Various written papers, publications and books on the mechanics of aeration behind gates have been referenced. Most of the information refers to the theory available on orifice flow for gated tunnels, given that this research entails flow through a gate whose opening is being varied.

2.1.1   Numerical model study

Computational Fluid Dynamics (CFD) codes are structured around numerical algorithms that can handle fluid flow. In order to provide easy access to their solving power, all commercial CFD packages include sophisticated user interfaces to input problem parameters and to examine the results. A three-dimensional model of the Berg River Dam bottom outlet structure was studied using the resources of the ANSYS GAMBIT and ANSYS FLUENT packages. The ANSYS processing package codes contain three main elements: (i) a pre-processor, (ii) a solver and (iii) a post processor.

2.1.1.1   Pre-Processing

This element consists of the input of a flow problem to a CFD program by means of an operator-friendly interface and the subsequent transformation of this input into a form that is suitable for use by the solver. The activities at the pre-processing stage involve:

2.1.1.1.1 Construction of model geometry

The first stage in any CFD model is to create a geometry which represents the object being modelled. This entails a definition of the geometry of the region of interest; the computational domain. Analysis begins with a mathematical model of a physical problem and conservation of mass, momentum and energy must be satisfied throughout the region of interest. Engineering assumptions are made to simulate the real process and modelling requires material properties and appropriate boundary and initial conditions. For this exercise the use of the AutoCAD package was employed to construct the model geometry. In order for the CAD drawings to be usable in any meshing tool application, they have to be exported in a format that is readable in the said application. The ANSYS GAMBIT application was used as the meshing tool before files were exported to ANSYS FLUENT for processing.

The Berg River Dam model geometry used for the simulations was constructed for various static emergency gate openings: 20%, 30%, 40%, 50%, 60% and 70%. The given emergency gate openings were chosen because tests on the physical model revealed that they were among the most critical. The 10% emergency gate opening was not tested because it was feared that the physical model could not handle the pressures developed in the outlet structure, as previous tests on the physical model had caused it to break during testing.

2.1.1.1.2 Meshing

Meshing entails breaking up or sub-division of the domain into a collection of smaller, non-overlapping sub-domains also called a grid (or mesh) of cells (or control volumes or elements). CFD then utilizes numerical/discretisation methods to develop algebraic equations that approximate the governing differential equations of fluid mechanics in the domain to be studied. The system of algebraic equations is solved numerically for the flow field variables in each computational cell.

Herewith, the properties of the fluid are defined and appropriate boundary conditions are specified at cells which coincide with the domain boundary. The solution to a flow problem (velocity, pressure, temperature, and so on) is defined at nodes inside each cell. The accuracy of a CFD solution is governed by the number of cells in the grid: the larger the number of cells, the better the solution accuracy. The accuracy of a solution and its cost in terms of necessary computer hardware and calculation time are dependent on the fineness of the grid. Optimal meshes are often non-uniform: finer in areas where large variations occur from point to point and coarser in regions with relatively little change. Over 50% of the time spent on a CFD project is devoted to the definition of the geometry and grid generation. Most CFD codes include their own CAD (Computer Aided Design) style interface and/or facilities to import data from proprietary surface modellers and mesh generators. Most current pre-processors provide access to a library of material properties for common fluids and a facility to invoke special physical and chemical process models alongside the main fluid flow equations.

2.1.1.2   Processing

2.1.1.2.1 Solver

The solver employs the use of Computational Fluid Dynamics and most CFD codes are solely concerned with the finite volume method, a special finite difference formulation. In outline the numerical algorithm consists of the following steps:

- Integration of the governing equations of fluid flow over all the (finite) control volumes of the domain

- Discretisation, conversion of the resulting integral equations into a system of algebraic equations

- Solution of the algebraic equations by an iterative method

The control volume integration distinguishes the finite volume method from all other CFD techniques such as finite element and spectral methods. The resulting statements express the conservation of relevant properties for each finite size cell. The conservation of a general flow variable ϕ such as velocity within a finite volume can be expressed as a balance between the various processes tending to increase or decrease it. In words (Veersteg and Malalasekera, 2007):

$$\begin{bmatrix} Rate\ of\ change \\ of\ \phi\ in\ the \\ control\ volume \end{bmatrix} = \begin{bmatrix} Net\ rate \\ of\ increase \\ of\ \phi\ due\ to \\ convection \\ into\ the \\ control\ volume \end{bmatrix} + \begin{bmatrix} Net\ rate \\ of\ increase \\ of\ \phi\ due\ to \\ diffusion \\ into\ the \\ control\ volume \end{bmatrix} + \begin{bmatrix} Net\ rate \\ of\ creation \\ of\ \phi\ \ inside \\ the\ control \\ volume \end{bmatrix}$$

CFD codes contain discretisation techniques that are suitable for the treatment of the key transport phenomena, convection (transport due to fluid flow) and diffusion (transport due to variation of ϕ from point to point) as well as for the source terms (associated with the creation or destruction of ϕ) and the rate of change with respect to time. The underlying physical phenomena are complex and non-linear so an iterative solution approach is required. The following simulation in ANSYS FLUENT utilises the SIMPLE algorithm to ensure correct linkage between pressure and velocity.

2.1.1.2.2 Post processing

This involves the collection and analysis of the results from the simulation using the CFD code and analysis and verification and validation of the results. Using the solver's post-processing capabilities results can be displayed using versatile data visualisation tools such as;

- Domain geometry and grid display

- Vector plots

- 3D surface plots

- Path lines

- Tabulated results

- View manipulation (translation, rotation, scaling)
- Colour PostScript output

Results from the simulations have been displayed with some of the visualization tools mentioned above.

2.1.2   Comparison of mathematical and experimental results

The final part of the study involved the comparison of results from the numerical model to those from the experimental model. Parameters to be compared included velocities of air and/or water in the air vent, pressures at various sections of the outlet structure and discharges.

CHAPTER 3

3. LITERATURE REVIEW

3.1 Introduction

Dam hydraulics considers all hydraulic questions that relate to the construction, the management and the safety of dams. It is thus directed to the hydraulic design of diversions during construction, bottom outlets, intake structures, and overflow structures.

3.1.1 Cavitation

Given the high velocities and varying pressures in dam outlet structures, cavitation is a very common occurrence in their operation. Cavitation occurs whenever the pressure in the flow of water drops to the value of the pressure of the saturated water vapour and cavities filled by vapour, and partly by gases excluded from the water as a result of the low pressure are formed. When these 'bubbles' are carried by the water into regions of higher pressure, the vapour quickly condenses and the bubbles implode, the cavities being filled suddenly by the surrounding water. Not only is this process noisy with disruption in the flow pattern, but more importantly, if the cavity implodes against a surface, the violent impact of the water particles acting in quick succession at very high pressures, if sustained for long periods of time can cause substantial damage to the surface, which can lead to a complete failure in the structure. (Novak P. et al, 2007). Thus cavitation corrosion (pitting) and the often accompanying vibration is a phenomenon that has to be taken into account in the design of hydraulic structures, and prevented whenever possible. (Knapp, Daily and Hammit, 1970).

3.1.2 Hydraulics of Dam Bottom Outlets

The design of a bottom outlet is not obligatory in the construction of a dam structure but its inclusion is strongly recommended in all instances. Primarily a bottom outlet is a safety structure often used for water releases and it can be used secondarily for the flushing of sediment deposits or for discharging surplus water. Recently, bottom outlets linked to a multi-level intake tower have been designed to release floods required for the in stream flow requirement (Vischer and Hager, 1998). A bottom outlet serves various purposes such as draw-down of the reservoir when it is open, flushing of sediments, flood and residual discharge diversion and environmental flood releases. The velocity V at the bottom outlet is large and can be approximated by the Torricelli (1643) formula, $V = (2gH_o)^{1/2}$, where H_o is the head on the outlet and g the gravitational acceleration. Cavitation, abrasion and aerated flow are

particular hydraulic problems. A bottom outlet has to be designed such that it may be operated under all conditions for which it was planned. Usually, two outlet gates are provided, namely, the safety gate which is either open or closed, and the service gate or the regulating gate with variable opening.

The technical requirements for a bottom outlet may be summarized as follows (Giesecke, 1982):

- Smooth flow for completely opened outlet structure with excellent performance for all flows under partial opening
- Effective energy dissipation at terminal outlets
- Structure without leakage
- Simple, immediate use of the outlet
- Easy access for maintenance and service
- Economic, useful design with a long life

A bottom outlet may not always be a structure for permanent use due to the limitations regarding cavitation, hydrodynamic forces, abrasion, vibrations, vortex formation at intakes, air entrainment, energy dissipation and erosion. In the case of the Berg River Dam, some of the above hydraulic problems may only occur during an emergency when the emergency gate in the conduit has to be closed.

Figure 3.1.2-1 below shows the hydraulic configuration of a typical bottom outlet.
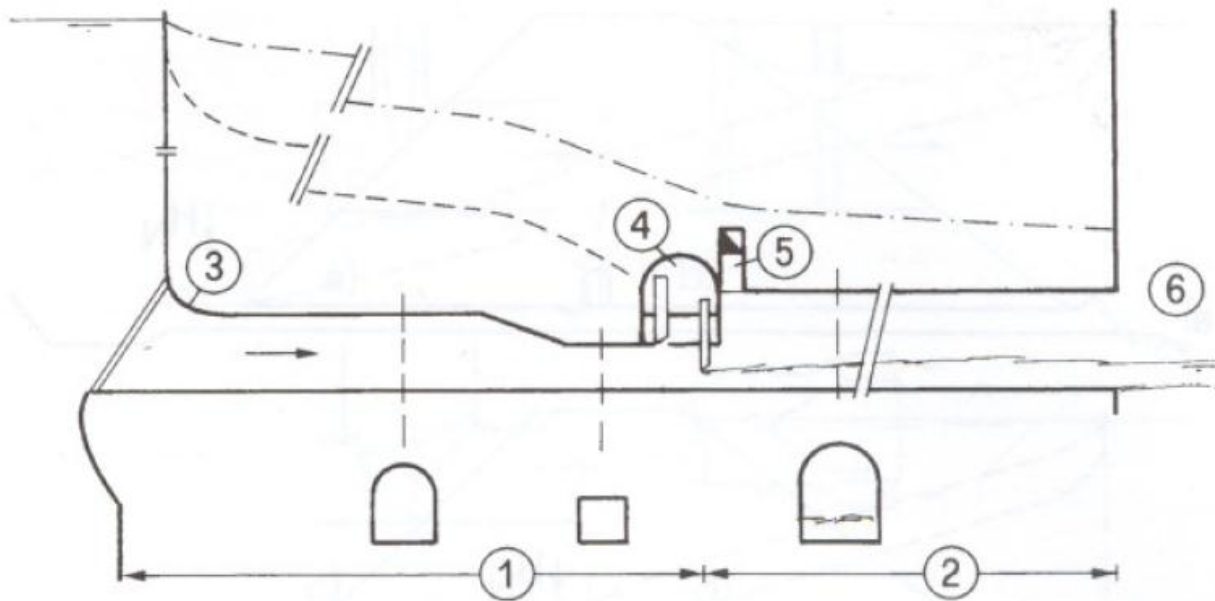
Figure 3.1.2-1: Hydraulic configuration of a bottom outlet with (---) pressure head line, (-.-) energy line, 1-pressurized and 2-free flow portion, 3-tunnel inlet, 4-gate chamber, 5-air supply, 6-tunnel outlet (Vischer and Hager, 1998)

Note the pressurized flow upstream, and the free-surface flow downstream from the gate, and that at the tunnel inlet the water is accelerated to the tunnel velocity. Immediately upstream from the gate chamber, the section contracts to a rectangular cross-section to cause sufficient backpressure and also to accommodate the gates. For long tunnels relative to the tunnel diameter, an aeration conduit discharging behind the gate chamber provides sufficient air for free flow under practically atmospheric pressure. The air supply conduit has to be designed so that the gate chamber is safe against submergence from the tunnel. During design, it is imperative that downstream submergence of the bottom outlet is prevented (Vischer and Hager, 1998).

Note that, accordingly, the transition from pressurized to free surface flow has to be located exactly behind the gate chamber, and therefore sufficient aeration, and a tunnel large enough to avoid surging flow in the downstream tunnel must be provided, the discharge being fully controlled with the gate (Vischer and Hager, 1998).

3.1.3   Flow patterns behind gates in conduits

Multicomponent, air-water flow in a closed conduit can be classified according to the type of flow pattern (Falvey, 1980). The flow patterns which develop depend on the air flow rate to water flow rate

22

ratio, slope of the conduit and existence of a hydraulic jump. In the pressurised section upstream of the gate water fills the whole system and flow is single component. Downstream of the gate, during gate closure all types of multi-component air-water flows may exist temporarily at certain sections, and finally after complete closure of the gate and single component flow of air starts from the gate region and continues until water is totally drained from the penstock. From a design point of view different categories of air-water flow in closed conduits may be considered depending on the mechanisms that create the air demand.

The aeration of flow may originate from three different sources (Figure 3.1.3-1):

1. From the downstream conduit
2. From the air vent
3. From upstream of the gate
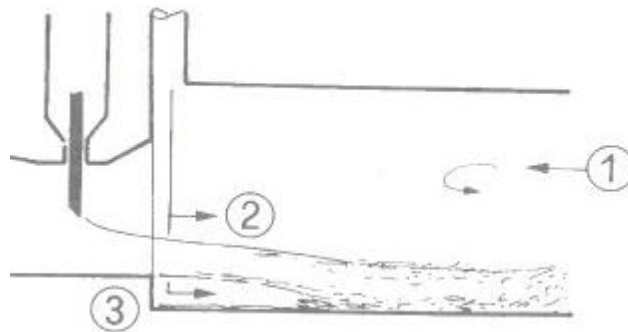
Figure 3.1.3-1: Air entrainment by gated outflow in bottom outlet tunnel, gate chamber with 1) counter-current air from tunnel, 2) air supply conduit for surface aeration, 3) bottom aerator (Vischer and Hager, 1998)

Sharma (1976) has introduced a classification of flow types for bottom outlets without a bottom aerator (Figure 3.1.3-2):

a) Spray flow for relative gate opening below 10%, with an extremely high air entrainment,
b) Free flow as typical for bottom outlets, and accompanied by features of supercritical flow, such as shockwaves and two phase flow,

23

c) Foamy flow for tunnel almost full with an air-water flow,

d) Hydraulic jump with a free surface tail-water flow due to a tail-water submergence,

e) Hydraulic jump with transition to pressurized tail-water flow, and

f) Fully pressurized flow caused by deep tail-water submergence.

In applications, only a) to c) should occur because of the dangerous surging conditions otherwise. Figure 3.1.3-2 shows the types of flow that may be experienced in bottom outlets without a bottom aerator.
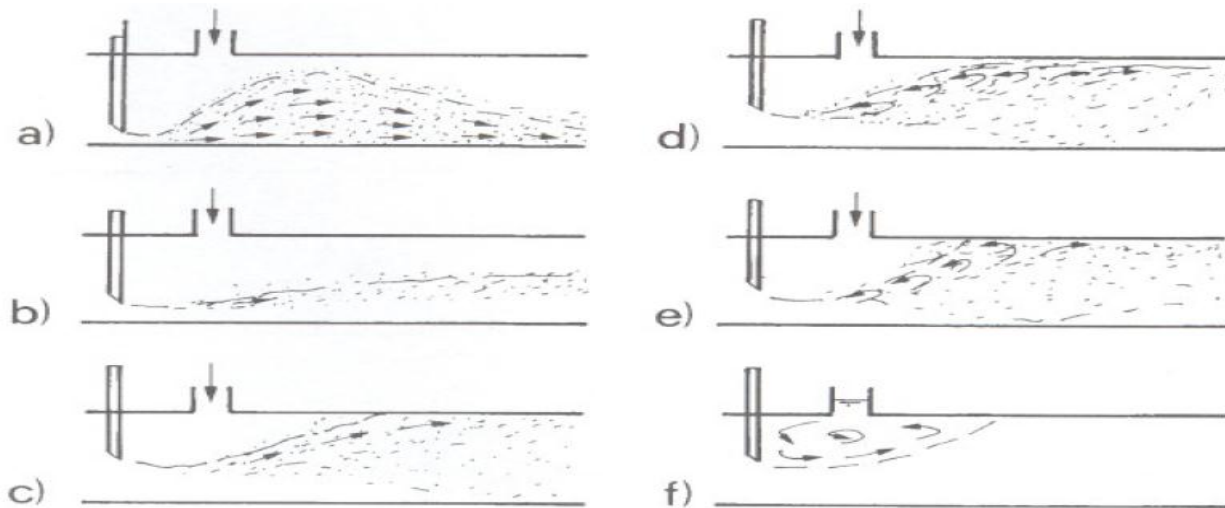
Figure 3.1.3-2: Classification of flow types in bottom outlets without a bottom aerator (Sharma, 1976)

The hydraulics of air-water flows in bottom outlets is actually not yet fully understood and hydraulic modelling based on sufficiently large scale models is recommended (Vischer and Hager, 1998). It is not always practical to study the specific patterns of air-water flows that may develop during gate closure to determine the overall air demand because no dependable solution is yet available to determine the quantity of air for different flow types (Sharma, 1976).

3.1.4   Hydraulics of gated conduits

When a vertical lift gate in a conduit is opened and the downstream section of the conduit contains no water, a demand for air arises due to entrainment of air in the issuing jet. The total air demand consists of two different parts, air entrainment in the water flow as bubbles or larger air pockets in the air-water transition region, and air flowing above the transition zone because of the drag of the flowing mixture. At initial gate openings the issuing jet is accompanied by spray which entrains high proportions of air

24

space. In gated conduits that do not discharge directly into the atmosphere such as bottom outlets, a high velocity flow occurs downstream of the gate resulting in sub-atmospheric pressures. This drop in pressure which is dependent on the flow rate, the gate opening and the geometry of installation, theoretically can be as low as the vapor pressure of water and may disturb the gate operation, due to occurrence of vibration and cavitation.

On the other hand, if air is introduced into a conduit upstream of the gate, severe pressure fluctuations can occur at the gate due to the build-up of stagnated air under high pressure at the conduit crown upstream of the gate. Air may exist in the form of bubbles being entrained in the conduit or owing to the development of vortices, which may be a source of trouble. As the air pockets continue to accumulate upstream of the gate they are eventually partially drawn under the gate and the air that is entrained into the water is instantly forced downstream in the form of small air bubbles such that when the pressurized air is released, it reaches atmospheric value almost instantaneously with an explosive force (Lewin, 1995).

In order to avoid such situations, air vents designed to admit large quantities of air into the water passages have to be employed closely adjacent to the downstream leaf face to keep the pressure near to atmospheric. Hydro-mechanical equipment for low-level water outlets operating under high pressure (H>50m) and high velocities (over 60 m/s) must be highly dependable and long-lasting. The aeration vent supplying the air behind low-level gates plays a considerable part in ensuring this dependability (Borodina, 1969). The general opinion is that aeration of the cavity behind the gates is the most effective means for combating such detrimental phenomena as vibration and cavitation of the gates and adjacent parts of the waterway. Aeration, provided the air vent is correctly designed, diminishes these detrimental effects, decreases the pulsation amplitude of hydrodynamic loads on the gates, stabilizes the hydraulic operating conditions behind the gates, and also decreases the vacuum among other remedies (Borodina, 1969). One of the basic conditions for dependable equipment operation is the selection of an air passage cross section which will provide the necessary air discharge and decrease the vacuum to a permissible level. Partial gate opening at the intake is a favorable condition for the formation of a hydraulic jump and therefore consequent air entrainment. When the gate of a high-head outlet conduit is partly opened, a negative pressure draws the air in through the air vent. Whereas the flow is pressurized upstream from the gates of a bottom outlet, free surface flow may develop in the tail-water of the gate, depending on the flow characteristics in the outlet tunnel.

25

3.1.4.1   Gate Discharge Equations

Gate flow may be either free or submerged. For free gate flow, the space behind the gate is filled with air of pressure head, h_a. If the outflow is to the atmosphere then $h_a = 0$ (Figure 3.1.4.1-1).
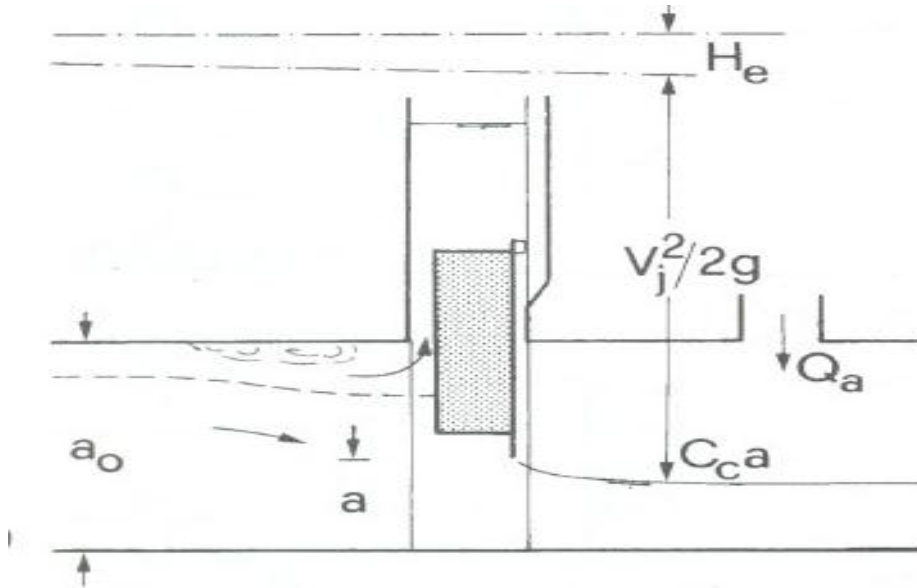
Figure 3.1.4.1-1: Definition sketch for free gate flow based on an experimental setup (Vischer and Hager, 1998)

Submerged gate flow in bottom outlets should be avoided as earlier noted and based on energy considerations. The underflow discharge of a gate is given by (Naudascher, 1991):

$$Q = C_c ab[2g(H - H_e - C_c a - h_a)]^{1/2}$$

where C_c is the contraction coefficient, a the gate opening, b the gate width, and $H\text{-}H_e$ the head on the gate with H_e the energy loss from the entrance to the gate section.

The underflow discharge Q_o of a high head gate is,

$$Q_o = C_o a_3 b[2g(H - H_e - H_{ce} - h_s - h_a)]^{1/2}$$

Where C_o is the discharge coefficient for the seal system, a_3 the width between the slot and the gate, H_{ce} the head loss between the approach flow and the upstream face of the gate, and h_s the vertical

distance between the datum and the section of jet issue. The discharge coefficient C_d of gate flow is the ratio:

$$C_d = Q/(2g\Delta H)^{1/2}$$

with ΔH as the difference in head according to the underflow discharge equation. The parameter C_d depends on a number of parameters such as the relative gate opening, $\eta = C_c ab/A_o$, with $A_o = a_o b_o$ at the approach section, the loss factor, the aspect ratio and the approach velocity distribution. Accordingly, one should rather use the contraction coefficient C_c than the lump parameter C_d.

The contraction coefficient C_c depends on the efflux Froude number, $Fr = V/(gC_c a)^{1/2}$, where V is the efflux velocity (m/s), g is the acceleration due to gravity (m/s^2) and a is the gate opening (m), provided $Fr > 4$. For large Froude numbers typically encountered in prototype high head gates neither this free surface effect nor the effect of viscosity have to be accounted for, and one may consider a potential flow with the gravity effect absent, i.e. the gate geometry had the significant effect on C_c.

Chadwick et. al. (2004) recommends a contraction coefficient of 0.61 for free surface flow in gated tunnels.

Figure 3.1.4.1-2 below shows the details of flow in a gated conduit.
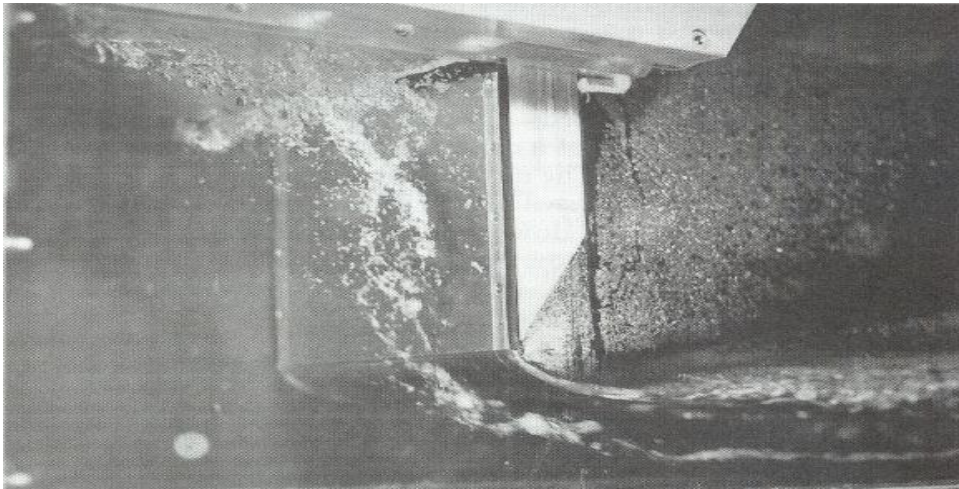
Figure 3.1.4.1-2: Detail of gate flow (Vischer and Hager, 1998)

3.1.4.2   Aeration behind gates in conduits

It is not permitted to draw the air either from structural cavities or from the areas where men work or machinery is installed. The air velocity should not exceed 40 to 50 m/s, otherwise the noise level would have a harmful effect on the health of the operating personnel, and head losses along the length and at the points of local resistance and the vacuum behind the gates would considerably increase (Borodina, 1969). An incident in Brazil occurred when alterations were introduced to the original design of the air vent. The alterations caused ineffective aeration leading to vibration of the tower on which the gate chamber stood (Erbisti, 2004). The depression created downstream of the gate drained the air from the nearby region with which it communicated through openings for the passage of the hoist stems and of the maintenance staff, that is, from the tower, creating great discomfort to the persons in the gate operating floor. The problem was partly solved by limiting the maximum gate opening and the construction of walls and doors for separation of the operating room from the depression area.

In an emergency, when the gates are lowered much faster than normal, the air passage should be able to supply enough air to decrease the sudden pressure to such an extent as to protect the emergency gates. Gates may be subjected to large down pull forces and severe vibration as a result of high speed fluid around the gate lip and low pressures due to suction induced by high momentum fluid downstream of the control section (Naudascher 1991). Common application to reduce suction and adverse effects of it is aeration of the downstream face of the gate by means of ventilation shafts located immediately after the gate.

In a study by Aydin, the falling water surface elevation behind a high head leaf gate during emergency closure and the consequent air flow patterns and the pressure drop were investigated. As the gate is closed, water flowing into the intake from the reservoir is gradually decreased (Aydin, 2002). Reduction in discharge upstream of the gate occurs simultaneously with the gate motion even in emergency closures. However, deceleration of fluid downstream of the gate, where a big volume may be flowing, is not at the same rate as the upstream, and the water volume in the conduit continues to flow by inhaling air from the ventilation shaft. Large amounts of air may enter through the ventilation shafts in a short period of time to maintain volumetric continuity so as to prevent large negative pressures behind the gate.

In the design of a ventilation shaft the maximum airflow rate must be estimated first (Sharma, 1976). Appropriate dimensioning and determination of the pressure drop across the shaft allows estimation of

28

the reduced pressure acting downstream of the gate which is an essential parameter in the analysis of the structural components which must withstand the imposed loads. The pressure downstream of the gate must be prevented from becoming too low as cavitation damage may result during prolonged periods of operation. If the pressure in the water body drops below the vapor pressure of water, water column separation and re-joining may occur, which induces water hammer problems, (Aydin, 2002).

Unfortunately, up to the present time, the air supply system behind the gates is often designed without a sound theoretical background and is based mainly on practical recommendations or empirical formulae (Borodina, 1969). Computational Fluid Dynamics (CFD) models describing the air-water systems have been used in the recent past but have not been well validated against physical models or field case studies. The air supply designers are often faced with a number of problems which can only be solved by physical model tests, although there always is doubt as to the correctness of adjusting the model test results to the prototype.

3.1.4.2.1 Air Demand ratio

Kalinske and Robertson (1943) suggested a hydraulic jump as a means to remove air pockets from pipelines, and quantified how much air a hydraulic jump that filled the entire conduit could remove through air entrainment. The research by Kalinske and Robertson (1943) determined that air entrainment was a function of the Froude number upstream of the hydraulic jump. Kalinske and Robertson (1943) expressed the entrainment coefficient in terms of the ratio of air flow to water flow. Design procedures were developed for determining the air-entrainment coefficient $\beta = Q_a/Q_w$ where Q_a is the air discharge and Q_w is the water discharge. With β and the water discharge Q_w known we can determine the air discharge Q_a and the cross section of the air passage (Kalinske and Robertson, 1943):

$$A_a = \frac{Q_a}{V_a} = \frac{\beta Q_w}{V_a}$$

The β ratio is a function of various parameters such as the conduit geometry, the velocity and depth of the vena contracta and the water head. Most published papers suggest the following for the determination of the air-demand ratio:

$$\beta = K(Fr - 1)^n$$

Where Fr = Froude number at vena contracta

K and n = empirical coefficents

29

Air entrainment without jumps has been investigated by a number of researchers and the suggested design assumption of the U.S Army Corps of Engineers (USACE, 1964):

$$\beta = 0.03(Fr - 1)^{1.06}$$

Where β is as described above

Fr is the Froude number, $V/\sqrt{(gy)}$, and the velocity V can be expressed in terms of the head, H, at the vena contracta as, $V = \sqrt{(2gH)}$

V is the flow velocity at the vena contracta

y is the water depth at the vena contracta

Earlier work by Campbell and Guyton (1953) suggested a slightly different equation for determining the aeration ratio, β:

$$\beta = 0.04\ (Fr - 1)^{0.85}$$

Where,

Fr = Froude number at vena contracta

The authors pointed out that maximum air demand takes place with the gate 80 per cent open and a gate lip with a 45-degree angle on the bottom can be expected to have a contraction coefficient of approximately 0.80. The Froude number should be based on the effective depth at the vena contracta which is therefore given by:

$$h_c = 0.8(0.8h)$$

where,

h_c is the effective depth at the vena contracta.

h is the height or maximum opening of the gate.

It is also recommended that the maximum air velocity in the air vent be limited to 45m/s (USACE, 1964).

Winser (1965) as cited in Sharma (1976) suggested that the air demand ratio was also dependent on the ratio of the cross-sectional area of the air vent to the cross-sectional area of the conduit. Winser

concluded that when the air vent to conduit area ratio was greater than 1/40 that air demand was only a function of the Froude number according to the equation below:

$$\beta = \frac{Q_a}{Q_w} = 0.024(Fr - 1)^{1.4}$$

Where Q_a is the air discharge, Q_w is the water discharge and Fr is the Froude number.

It should be noted, however, that this equation does not take into consideration the length of the tunnel. For longer tunnels, less air is entrained because of de-aeration processes.

3.1.4.2.2 Air vent design

Air vents are indispensable in high head installations of gates with a downstream skin plate and seals. The primary functions of the air vent are (Erbisti, 2004):

a) To reduce or eliminate sub-atmospheric pressure in the conduit during emergency closure or partial gate operation
b) To permit drainage of the conduit
c) To allow air to escape when the conduit is being filled

Special care should be taken when designing the air vent for bottom outlet segment gates since it is not always possible to provide a free passage in the vertical shaft so as to permit adequate aeration. For greater effectiveness, the lower end of the air vent should be located in the conduit ceiling, as close as possible to the gate, at a distance of not over 2m. The vent inlet should be located sufficiently far above the maximum reservoir water level to avoid interference with the air flow. The air vent should be as straight as possible, with the minimum number of bends and sharp corners, and without abrupt changes in section.

The determination of the flow coefficient of the air vent is usually carried out by trial and error, starting with the knowledge of the tube geometry and of a value estimated for the diameter. With these, head losses and the cross section area can be determined. Then the diameter is checked and if this differs from the value initially attributed to it, another value is selected and the above calculation is repeated (Erbisti, 2004).

Air velocity, V_a, in the air vent depends directly on the depression, H_d, i.e the difference in pressure between the inlet and outlet of the vent, expressed in meters of water. For a mach number, m_a, (air flow coefficient) below 0.5, the air velocity is given by the equation (Erbisti, 2004):

$$V_a = 28m_a\sqrt{2gH_d}$$

And

$$m_a = \frac{V}{a_a}$$

Where V – velocity of water (m/s) and a_a – speed of sound (m/s).

The depression, H_d, downstream of the gate must not be allowed to exceed certain limits otherwise one risks a greater likelihood of the occurrence of pulsation and cavitation. Levin (1965), states that depressions for head of 1.5m can be tolerated without problems in well-designed installations. The U.S, Army Corps of Engineers suggests limiting the air velocity to 45m/s which, for an air flow coefficient of 0.5, is equivalent to a depression of about 0.3m head.

Air vents with rectangular cross-section are calculated as if sections were circular. The equivalence of the circular and rectangular sections for pipes of the same length, flow and head losses, is given by the following ASHRAE (American Society of Heating, Refrigerating and Air Conditioning Engineers) formula:

$$D_e = 1.3 \frac{(ab)^{0.625}}{(a + b)^{0.25}}$$

where:

D_e = diameter of the equivalent circular section

a and b = rectangular dimensions

in the particular case of a square section, the equivalence is given by:

$$D_e = 1.093a$$

where a is the length of the square side.

3.2   The Berg River Dam (BRD) prototype

The basic structure of the BRD was constructed with a multi-level vertical intake tower: 3 levels of 6 m by 4 m paired rectangular gates behind trash racks. The intake tower is connected to a 3.8 m by 3.2 m rectangular conduit by a rectangular bell-mouthed section. The rectangular section of the conduit contains the emergency gate structure and an air vent is located immediately downstream of the emergency gate. Beyond the rectangular section of the conduit is a 5.5 m diameter horseshoe shaped conduit that extends approximately 175 m downstream to a radial gate structure and ski jump.

Figure 3.2-1 below shows the plan view of the BRD bottom outlet structure.
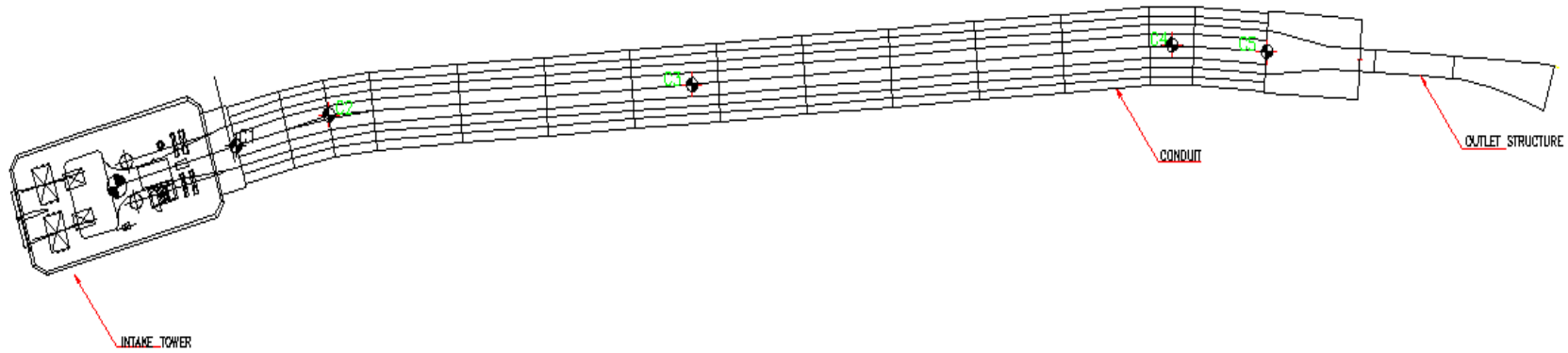
Figure 3.2-1: Plan view of the BRD bottom outlet structure.

The horseshoe shaped conduit has two horizontal bends. The angle of the first bend, located approximately 27 m from the beginning of the horseshoe shaped conduit is 12 degrees and the second bend of 8 degrees, located about 15 m before the end of the conduit is 8 degrees.

The base of the outlet conduit attaches to the radial gate and asymmetrical ski-jump with both vertical and horizontal slopes and one corner raised higher than the other. The roof of the conduit is lower at the transition from the horseshoe conduit to the rectangular shaoe for the radial gate.

Figure 3.2-2 below shows the side view of the BRD bottom outlet structure and Figure 3.2-3 that follows shows the front elevation of the wet well tower.

.
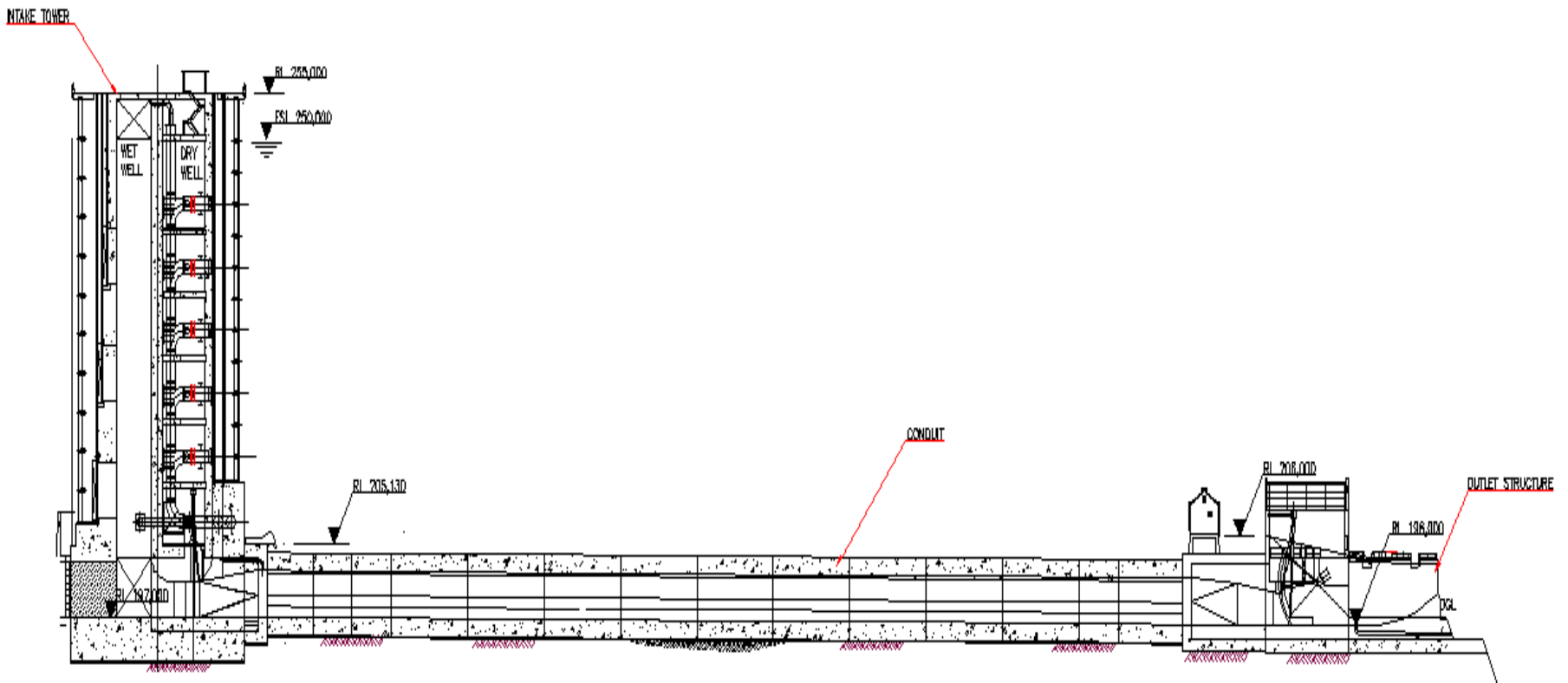
Figure 3.2-2: Side view of the BRD bottom outlet structure.

The area of the rectangular conduit, at the emergency gate, is smaller than the downstream horseshoe shaped conduit and this difference in cross-sectional area leads to higher velocities in the rectangular conduit at the gate. The enlargement of the cross-sectional area immediately downstream of the emergency gate decreases the water velocity when the conduit is flowing full and the air vent is required to provide enough aeration below the gate during gate closure to prevent the pressures from dropping to sub atmospheric levels.

35
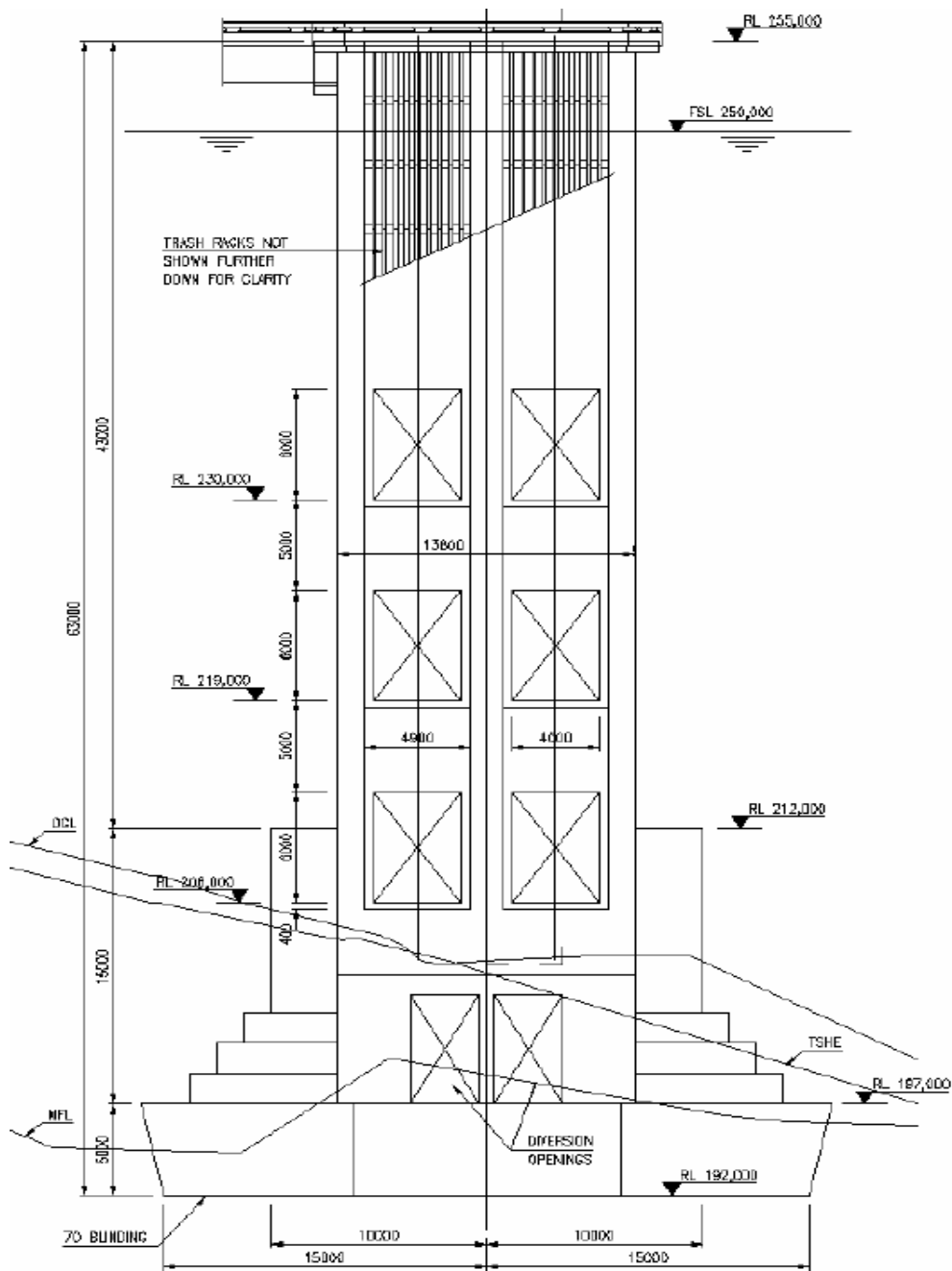
Figure 3.2-3: Front view of the wet well tower

3.2.1   The Berg River Dam air vent

Based on the equations presented in Section 3.1.4 above, the adequacy of the air vent on the Berg River Dam bottom outlet structure was assessed for the following assumptions:

- The contraction coefficient is 0.8 (U.S Army Corps of Engineers, 1964).
- The rectangular conduit at the gate chamber is 3.8 m x 3.2 m.
- The rectangular air vent immediately downstream of the emergency gate is 1 m x 1.8 m.

The calculations are shown in Table 3.2.1-1 below:

Table 3.2.1-1: Determination of the adequacy of the air vent on the Berg River Dam outlet structure with the reservoir at the commissioning water level.

	Assumptions: Contraction coefficient = 0.8							
Gate opening (%)	Contracted flow depth (m)	Contracted flow Area (m^2)	Head (m)	Water discharge Q_w (m^3/s)	Water velocity V_w (m/s)	Fr	Aeration demand ratio β	Air velocity V_a (m/s)
10	0.304	0.973	40.12	27.190	27.950	16.185	0.536	8.101
20	0.608	1.946	39.74	53.910	27.709	11.346	0.357	10.695
30	0.912	2.918	39.36	80.155	27.465	9.182	0.278	12.400
40	1.216	3.891	38.98	105.919	27.220	7.881	0.232	13.638
50	1.520	4.864	38.6	131.194	26.972	6.985	0.200	14.570
60	1.824	5.837	38.22	155.974	26.722	6.317	0.176	15.280
70	2.128	6.810	37.84	180.251	26.470	5.793	0.158	15.820
80	2.432	7.782	37.46	204.019	26.215	5.367	0.143	16.223
90	2.736	8.755	37.08	227.269	25.958	5.011	0.131	16.511
100	3.040	9.728	36.7	249.994	25.698	4.706	0.120	16.703

The empirical discharge equation for gated conduits above is utilised for the calculation of the discharge for the bottom outlet structure, that is:

$$Q = C_c ab[2g(H - H_e - C_c a - h_a)]^{1/2}$$

where C_c is the contraction coefficient, a the gate opening, b the gate width, and $H\text{-}H_e$ the head on the gate with H_e the energy loss from the entrance to the gate section.

Using the determined Froude number, the air demand ratio is calculated using the U.S. Army Corps of Engineers, (1964) equation:

$$\beta = 0.03(Fr - 1)^{1.06}$$

where Fr is the Froude number.

As stated earlier, U.S Army Corps of Engineers, 1964 recommends that the maximum air velocity in the air vent is limited to 45 m/s.

From the results obtained above, the actual 1.8 m^2 air vent should be sufficient to provide the required aeration demand downstream of the emergency gate at all static gate openings as the calculated air velocities are lower than 45m/s.

CHAPTER 4

4. NUMERICAL MODELLING

4.1 Theoretical information

4.1.1 Governing equations of fluid flow

The governing equations of fluid flow represent mathematical statements of the conservation laws of physics, namely:

   i.)   The mass of a fluid is conserved

   ii.)   The rate of change of momentum equals the sum of the forces on a fluid particle (Newton's second law)

   iii.) The rate of change of energy is equal to the sum of the rate of heat addition to and the rate of work done on a fluid particle (first law of thermodynamics)

The fluid will be regarded as a continuum. For the analysis of fluid flows at macroscopic length the molecular structure of matter and molecular motions may be ignored. The behaviour of the fluid is described in terms of macroscopic properties, such as velocity, pressure, and density and their time and space derivatives.

For all flows, ANSYS FLUENT solves the conservation equations for mass and momentum. Additional transport equations are also solved when the flow is turbulent.

A flow is incompressible when changes in density are negligible, both with respect to time and space. Below are the governing equations for an incompressible Newtonian fluid.

Continuity
$$div(\rho \boldsymbol{u}) = 0$$

x-momentum
$$div(\rho u \mathbf{u}) = -\frac{\partial p}{\partial x} + div(\mu\, grad\, u) + S_{Mx}$$

y-momentum
$$div(\rho v \mathbf{u}) = -\frac{\partial p}{\partial y} + div(\mu\, grad\, v) + S_{My}$$

z-momentum
$$div(\rho w \mathbf{u}) = -\frac{\partial p}{\partial z} + div(\mu\, grad\, w) + S_{Mz}$$

Where,

μ - Constant

ρ – Density (kg/m^3)

x,y,z – coordinate system

S – Constant (Source term)

u,v,w – velocity variables in the x, y and z direction respectively

p - Pressure

The continuity equation, the momentum equations, and an energy equation are usually referred to as the Navier-Stokes equations.

4.1.1.1   Turbulence model

It is a fact of nature that for sufficiently large Reynolds numbers flows show rapid apparently random fluctuations, even when the controlling factors of the flow, such as body geometry and upstream conditions, are stationary. Such flows are called turbulent. One of the main characteristics of turbulent flow is fluctuating velocity fields. These fluctuations cause mixing of transported quantities like momentum, energy and species concentration and also fluctuations in the transported quantities. Because of the small scales and high frequencies of the fluctuations they are too computationally expensive to simulate directly in practical engineering situations. Instead, the instantaneous governing equations are time-averaged to ignore the small scale fluctuations and the result is a set of less expensive equations containing additional unknown variables. These unknown (turbulence) variables are determined in terms of modelled variables in turbulence models. This process of time-averaging is called Reynolds averaging. When this is done the solution variables in the instantaneous Navier-Stokes equations are decomposed into the mean (time-averaged) and fluctuation components (Reynolds decomposition). Since turbulence is governed by the Navier-Stokes equations, turbulent flow can be computed from first principles by solving the Navier-Stokes equations.

4.1.1.1.1 The RNG k- ε model

For the simulation, the RNG k-ε turbulence model was used. It is similar in form to the standard k-ε model, but includes the following refinements:

• The RNG model has an additional term in its ε equation that significantly improves the accuracy for rapidly varied flows.

• The effect of swirl on turbulence is included in the RNG model, enhancing accuracy for swirling flows.

• The RNG theory provides an analytical formula for turbulent Prandtl numbers, while the standard k-ε model uses user-specified, constant values.

• While the standard k-ε model is a high-Reynolds-number model, the RNG theory provides an analytically-derived differential formula for effective viscosity that accounts for low-Reynolds-number effects. Effective use of this feature does, however, depend on an appropriate treatment of the near-wall region.

These features make the RNG k-ε model more accurate and reliable for a wider class of flows than the standard k-ε model.

4.1.1.1.2 Volume of Fluid (VOF) Model

The VOF model is a surface tracking technique applied to a fixed mesh. It is designed for two or more immiscible fluids where the position of the interface between the fluids is of interest. In the VOF model, a single set of momentum equations is shared by the fluids, and the volume fraction of each of the fluids in each computational cell is tracked throughout the domain. Applications of the VOF model include stratified flows, free-surface flows, filling, sloshing, motion of liquid after a dam break, the prediction of jet breakup (surface tension), and the steady or transient tracking of a liquid-gas interface.

Among the various models that FLUENT uses to solve the equations of the appropriate properties and variables in any simulation, the VOF model is chosen as the most appropriate for the simulation in question. The VOF formulation relies on the fact that two or more fluids (or phases) are not interpenetrating. For each additional phase that is added to the model, a variable is introduced, namely: the volume fraction of the phase in the computational cell. In each control volume, the volume fractions of all phases sum up to unity. The fields for all variables and properties are shared by the phases and represent volume-averaged values, as long as the volume fraction of each of the phases is known at each location. Thus the variables and properties in any given cell are either purely representative of one of the phases, or representative of a mixture of the phases, depending upon the volume fraction values. In other words, if the qth fluid's volume fraction in the cell is denoted as α_q, then the following three conditions are possible (ANSYS Fluent User's Manual, 2009):

- $\alpha_q = 0$: the cell is empty (of the qth fluid)

41

- $\alpha_q = 1$: the cell is full (of the qth fluid)

- $0 < \alpha_q < 1$: the cell contains the interface between the qth fluid and one or more other fluids.

Based on the local value of α_q the appropriate properties and variables will be assigned to each control volume within the domain.

4.2   Numerical Characteristics

4.2.1   Solver

The segregated solver is used with the SIMPLE pressure-velocity coupling scheme. Since the second order discretization for momentum resulted in an unstable solution, the first order scheme was used. For the VOF-method the PRESTO! Scheme is preferable for the pressure interpolation scheme and the modified HRIC scheme for the volume fraction equations in order to improve the sharpness of the interface between the two faces. The first order scheme is used when solving for turbulence.

4.2.2   Computational Domain

From the available two-dimensional AutoCAD drawings that were prepared for the design and used for the construction of the prototype of the Berg River Dam bottom outlet structure a 3-dimensional model domain was developed to create the domain for the numerical model. In order to provide a source of validation and verification of the results from the numerical model, these were compared with the results from the 1:14.066 physical model that was constructed and tested in the Stellenbosch University Hydraulics Laboratory.

The report on the commissioning of the outlet works at the Berg River Dam only provides details for the velocity of air released during the closure of the emergency gate over a certain period of time, until the occurrence of the said incident. Such little detail made it inadequate to effectively compare the results from the numerical model to those for the prototype, for instance, issues regarding pressures in the conduit structure that could have contributed to the sudden air release.

The 3-dimensional CFD model used to investigate the sudden air release problem was run for steady state simulations with static emergency gate openings and the water level in the reservoir maintained at the commissioning water level. This was to determine whether there was a static gate opening for which the aeration demand could not be satisfied by the air vent. This also helped to establish some of the conditions favourable for further CFD research regarding the problem in question.

Hydraulic properties for Perspex were used in the simulation runs for the CFD numerical model, as this was the material from which the physical model was constructed.

Figure 4.2.2-1 below shows a sketch of the generated model.
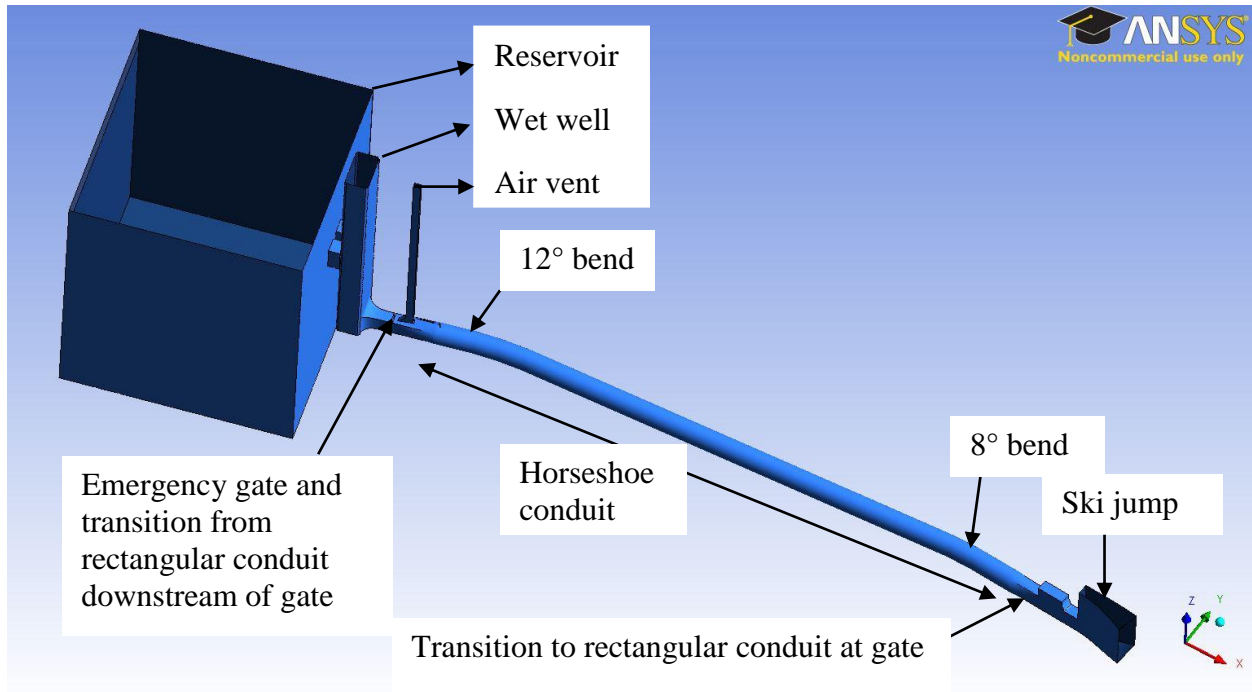
Figure 4.2.2-1: Set-up of the 3-dimensional model domain

As seen in the Figure 4.2.2-1 above, the model domain was constructed with an assumed rectangular reservoir as in the physical model.

The gate structure was constructed with a 60 degree gate lip modification as shown in Figure 4.2.2-2 below. The figure also shows the transition from the rectangular section at the emergency gate to the horseshoe shaped section of the conduit.
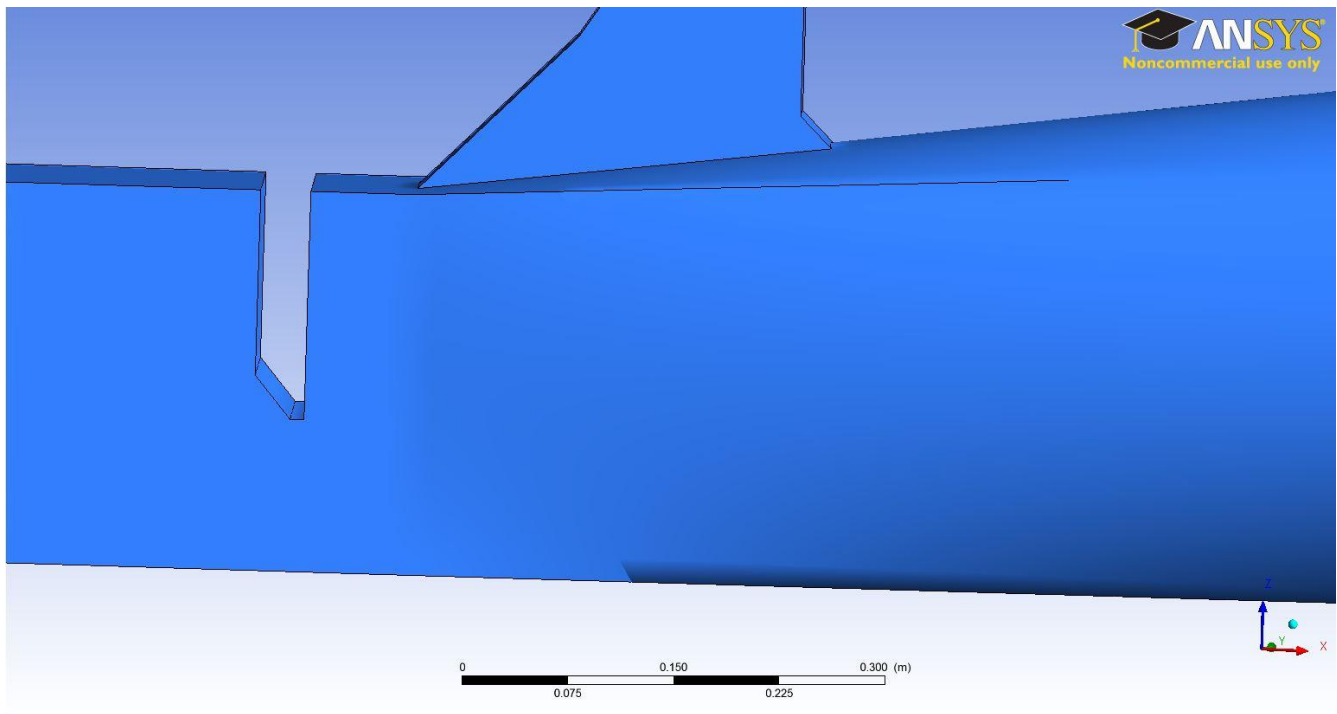
Figure 4.2.2-2: Set-up of the 3-dimensional model domain

4.2.3   Meshing the model domain

Meshing, also known as grid generation, involves the sub-division of the domain into a number of smaller, non-overlapping sub-domains thus forming a grid (or mesh) of cells (or elements, or control volumes) at which solutions are calculated. Refinement and meshing of the domain was done using the ANSYS GAMBIT tool.

Due to the complexity of the geometry, it was difficult to generate a uniform skew-less mesh across the whole domain. A mesh with a lot of skew elements affects the final solution, so this drawback was alleviated through the decomposition of the domain into smaller volumes that could be easily meshed. Different mesh sizes were used for different sections of the geometry but conformity of the meshes at the connections was ensured. The mesh for the domain was created with the TGrid function, which means that the grid is composed primarily of tetrahedral mesh elements but may include hexahedral, pyramidal, and wedge elements where appropriate.

The reservoir was meshed with a size of 60 mm, the intake tower and the rectangular section of the conduit including the emergency gate and the air vent had a 10-20mm mesh. A 40 mm mesh was adapted for the horseshoe shaped conveyance conduit all the way to the ski jump. The finer mesh was

44

adopted in the critical sections of the domain for purposes of accuracy in simulation results and quick convergence but this required more processing time. Overall, approximately 2.5 million elements were generated for the whole domain.

The Figure 4.2.3-1 below shows a screen shot of the meshed model, ready for processing in ANSYS FLUENT.
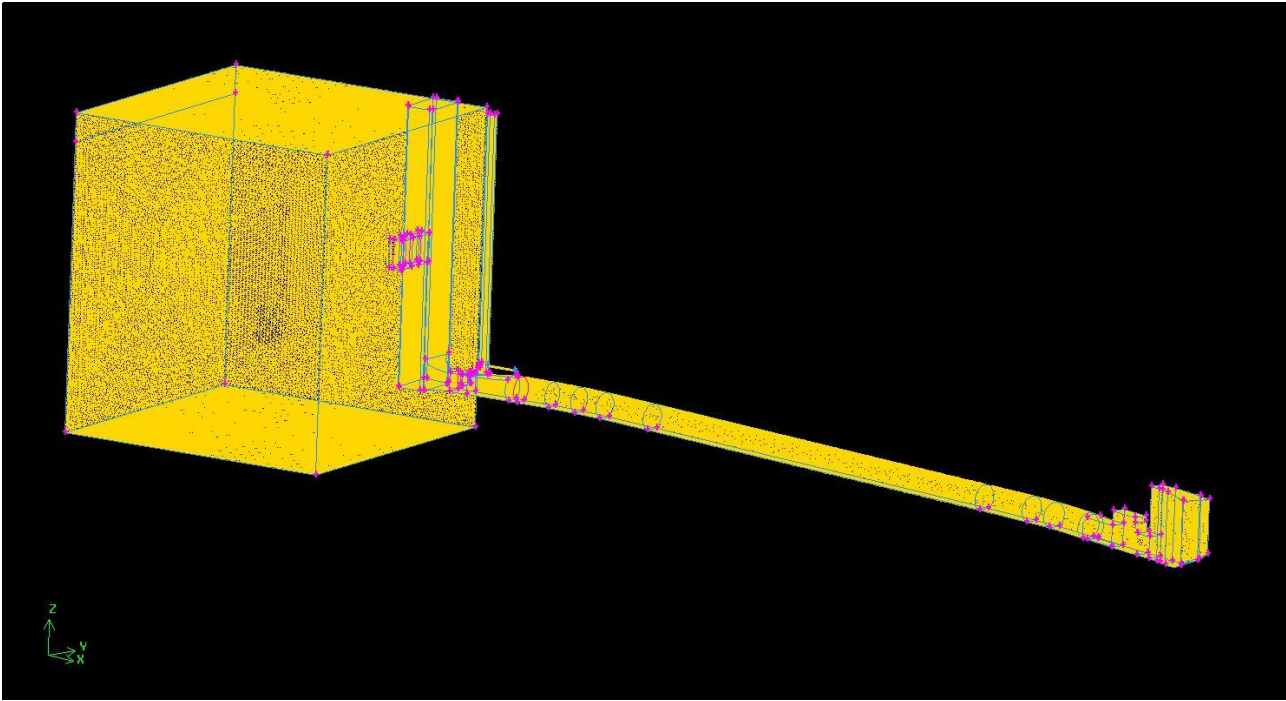
Figure 4.2.3-1: Schematic of the meshed geometry

4.3   Variables used in calculating the model solution

Various parameters in the solver have to be set before the simulations can be started. Scaling and unit setting is done in the solver but there is no provision for unit conversion so all such requirements have to be satisfied before importing the mesh into the solver. The quality of the mesh can be checked in the solver but before the mesh is exported to the solver such conditions as hydraulic boundary surfaces and the hydraulic diameter of such surfaces must be specified.

The hydraulic diameter is defined by the equation,

$$D_h = \frac{4A}{P}$$

45

Where A is the area of surface (m^2) and P is the wetted perimeter of the said surface (m).

Table 4.5-1 below shows the dimensions of the boundary surfaces used in the calculation of the solution for the BRD model.

Table 4.3-1: Hydraulic diameters for the different boundary surfaces

Boundary Surface	Hydraulic Diameter (m)
Reservoir inlet (Bottom)	4.266
Reservoir Surface (Top)	4.266
Reservoir Spillage (Side)	0.775
Wet Well Surface	0.573
Air vent Surface	0.092
Ski jump Surface (Top)	0.565
Ski jump Surface (Side)	0.500

Other initial parameters that need to be defined include: the turbulence models to be used in the solution calculation, the materials and phases in the domain, details of the boundary conditions and cell zone conditions, solution methods, solution controls (relaxation factors), monitors, initialization of the solution, and calculation activities. A gauge pressure of 0 Pa was used.

Table 4.3-1 below summarises other parameters that were defined for the running of the simulations.

Table 4.3-2: Other parameters adopted in the simulations

General conditions	Pressure based solver	Water-Air surface tension coefficient (n/m)		0.0728
	Absolute velocity formulation	Operating pressure (Pa)		101325
	Steady state calculations	Viscocity	Air (kg/m.s)	1.79E-06
	Gravity enabled (9.81 m/s²)		Water(kg/m.s)	0.001003
Models	Viscous model (RNG k-epsilon model)	Density	Air (kg/m³)	1.225
	Standard wall functions		Water (kg/m³)	998.2
	Multi phase model - Volume of Fluid (VOF)	Under-relaxation controls		0.5-0.8
	Implicit volume fraction parameters	Material (Perspex) Hydraulic roughness (mm)		0.003
	Two eulerian fluids (air and water)	Phases	Water	
	Implicit body force formulation		Air	

46

4.4 Model settings

The following six simulation set-ups were investigated for steady state static openings of the emergency gate.

**Table 4.4-1: Simulation set-ups**

Emergency gate opening (%)	Intake gate opening (%)	Radial gate opening (%)
20	100 (middle pair of gates)	100
30	100 (middle pair of gates)	100
40	100 (middle pair of gates)	100
50	100 (middle pair of gates)	100
60	100 (middle pair of gates)	100
70	100 (middle pair of gates)	100

4.5 Initial and Boundary conditions

All CFD problems are defined in terms of initial and boundary conditions. Therefore it is important to specify these correctly and understand their role in the numerical algorithm because it is these conditions that affect the nature of the result. The choice of type and location of open boundaries through which flow enters and leaves the domain is a particular challenge in CFD modelling. Boundary conditions are chosen from a limited set of available boundary types and there must be compatibility between the chosen open boundary condition type and the flow information available for the chosen surface location. In some cases information is partial and as such missing information must be generated on the basis of past experience or assumptions. In other cases, the assumed boundary condition may only be approximately true.

For the BRD model the following boundary conditions were applied:

- In order to reduce the calculation time needed to run the simulations, part of the domain was initially patched with water as shown in Figure 4.5-1 below.

47
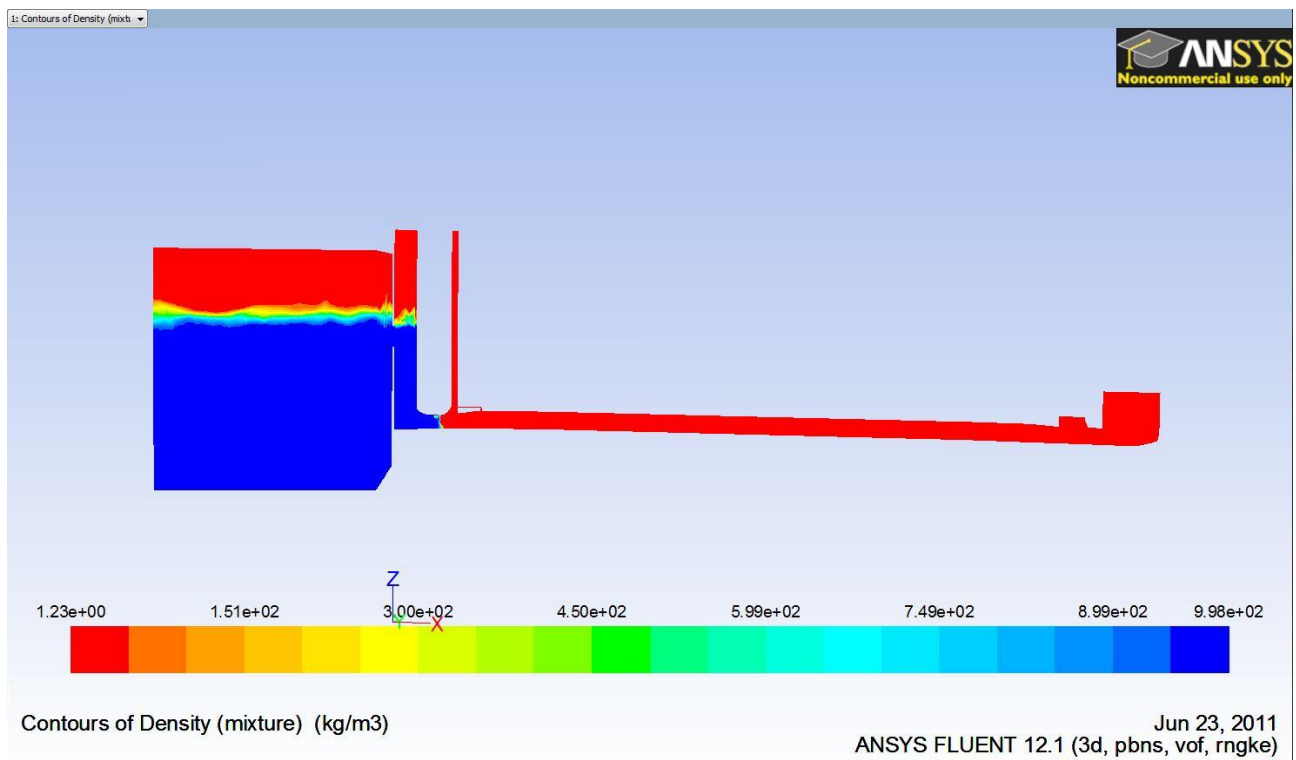
Figure 4.5-1: Initially patched domain

- The water level in the reservoir (shown in blue) was maintained at the required level by allowing excess to spill out of the domain through a face at the front of the reservoir. The red colour represents air.

- The reservoir was allowed to gradually fill up from the bottom because this prevented disturbance of the flow as it entered the wet well. Another option would be to model an extremely large reservoir that filled up from the side allowing the water to gradually flow towards the intake tower. However, this would call for more calculation time and storage space due to the increased domain.

- Flow into the wet well was allowed by means of the two middle selector gates ignoring the top and bottom paired selector gates with the assumption that these were closed and that there was no contribution of flow into the wet well from them as was the case during the commissioning of the bottom outlet structure.

- The surface of the reservoir was assumed to be open to the atmosphere and the pressure there was set to atmospheric pressure. An opening was also left on the side of the reservoir to allow spillage so as to maintain the water level as required.

- No boundary condition was applied to the intake selector gates since they were directly connected to the reservoir and the water could freely flow into the intake tower.
- The top of the wet well was left open to the atmosphere as well. This provided another possible source of aeration to the flow from the reservoir.
- The top of the air vent was set to allow aeration from the atmosphere which would be required to balance out the negative pressure that would develop behind the emergency gate.
- The vertical face and top face at the end of the ski jump were set as openings to the atmosphere with an outflow boundary condition, implying that unless the fluid escaped through any other opening, this was the only outlet to the domain.
- The radial gate just before the ski jump was ignored in this simulation because it was fully open at all times during the commissioning,
- The rest of the domain was taken as the wall structure containing the conveyed fluid and no-slip conditions were applied to this wall structure.
- The conveyed fluid was an air-water mixture. The reservoir filled up from the bottom at an assumed rate of 0.03m/s. Higher fill-up rates caused divergence of the solutions.

4.6   Limitations of numerical model

Like any other experimental, physical or computational procedures, a few problems were encountered in the running of the simulations.

- Getting the model to stabilise and converge was a major task because there were many varying parameters that had to be adjusted specific to the said simulation. This required experience with the use of the software.
- The only way to tell that steady state has been achieved in a steady state simulation is by stopping the simulation and manually checking the mass flow rate at the inlet and outlet. There is no way to program FLUENT to stop when equilibrium has been reached. The program continues running until it diverges. Therefore, case and data files have to be saved for smaller iterations in case the equilibrium point is achieved. Otherwise if saving is done over large iterations then data is missed between the saved files. The disadvantage of saving data over small iterations is that it takes up a lot more memory per simulation.
- It is difficult to visually monitor the direction of air in the air vent during every step of the simulation process because the model is only able to save data over the specified period of

calculation time. Therefore, one cannot easily tell whether there has been a spike or gust of air in the air vent. This can only be remedied by creating an animation video at the end of the whole simulation process.

- Processing is time consuming given the various tasks that the program has to process for every given element. There is no assurance in the behaviour at the beginning of the simulation (whether there will be divergence later in the simulation process or not) so one has to wait until it has run to completion to determine whether the results are realistic and usable or not. If not, then the whole set up has to be redone, parameters readjusted, and the simulation rerun until usable results are obtained.

- If the given parameters need to be monitored against a time variance then the simulations must be run as transient and it should be noted that the simulation time is not the same as the real time. Transient simulations take a lot more time to run although they give results similar to steady state simulations.

- The more complex the geometry, the poorer the meshing output and thus the more divergence in simulations due to the highly skewed elements generated in the model.

- The nature of the results given at the end of any simulation is greatly affected by the type of initial and boundary conditions.

- The software requires that there is constant connection to the network server for the licence to be usable otherwise simulations get interrupted.

- With experience comes the skill to use the software, otherwise divergence of the solution will occur if specified parameters such as relaxation factors are not correctly used. Expert use of the package requires repeated use as parameters vary from one model to another, whether 2 dimensional or 3 dimensional.

- Depending on the amount of information that needs to be processed, a considerable memory is required to construct, mesh and run simulations. Over 2 million elements had to be processed and files with over 500 gigabytes needed to be stored for each model set up.

- During the prototype commissioning, the outlet structure was fully open and the conduit was flowing full before the testing began. In the CFD numerical model, however, patching up the whole domain with the fluid to simulate the prototype flow caused divergence; the model drained.

- After steady state was achieved, the simulation had to be stopped manually and results taken as required. If the simulation was continued, divergence eventually occurred. For this reason, it was difficult to continuously monitor the simulation after steady state to determine what happens to the velocities in the air vent.

- The commissioning report mentioned suction noises at the radial gate during emergency gate closure but since it was not possible to simulate noise levels in the CFD numerical model, this aspect could not be analysed.

- Assumptions must be made of what happens outside the model since one cannot visibly or numerically monitor what goes on beyond the limits of the domain. For this reason, whatever water isn't held up in the reservoir beyond the required level is spilled in order to simulate the reservoir water level during the commissioning test.

- Getting the model to stabilise and converge especially for the transient simulations was a major task because there were many time varying parameters that had to be adjusted specific to the said simulation. This required vast experience in the use of the software.

- It was necessary to compromise between storage and simulation data. With the data files so large, it was demanding to have to save data very frequently.

- Animations of the simulation could only be created at the end of the whole simulation process and all case and data files generated during the simulation had to be kept in order to create the animation. This required more storage space.

CHAPTER 5

5. SIMULATION RESULTS

All simulations carried out on the 3-dimensional model were steady state for fixed gate openings. The reservoir was filled at a constant rate of 0.03 m/s and any inflows excess of the releases overflowed the front side of the reservoir. The open surface flow through the selector gates into the wet well was simulated as well as the pressurised flow underneath the emergency gate. The CFD simulation of the flow underneath the emergency gate showed higher velocities than those measured in the physical model. These CFD simulations are compared with the physical model results in Section 5.2 below.

Depending on the emergency gate opening, steady state was achieved after approximately 5000 iterations. Simulation results were only extracted from files for which equilibrium was established. Turbulence upstream of the emergency gate was attributed to the circulation of flow as it dropped down into the intake tower and that downstream of the emergency gate was attributed to the occurrence of highly aerated flow in the conduit.

The layout of this chapter shows the pictorial results of the CFD modelling which provides a visual representation of the simulation output. Then results for discharge, velocity and pressure are also compared with the calculated results and the results of the hydraulic modelling.

5.1   Pictorial representation of results

5.1.1   Density Contours

The density contours aided in the visualisation of the flow pattern in the domain. The flow pattern exhibited by the numerical model was quite similar to that observed in the physical model for all gate openings save for the 70% gate opening for which the emergency gate was fully submerged.

Figures 5.1.1-1A to 5.1.1-6A below show contours of density in the domain for emergency gate openings of 20%, 30%, 40%, 50%, 60%, and 70%.

A study by Nafaji et al. (2010) on flow patterns in gated tunnels showed that the flow pattern in transition tunnels could exhibit rooster tail (cross) wave formation. The study attributed such behaviour to flow conditions and geometry of the tunnel. This flow pattern is observed in the CFD numerical solutions downstream of the 12° bend as the flow progresses from pressurised to free surface flow.
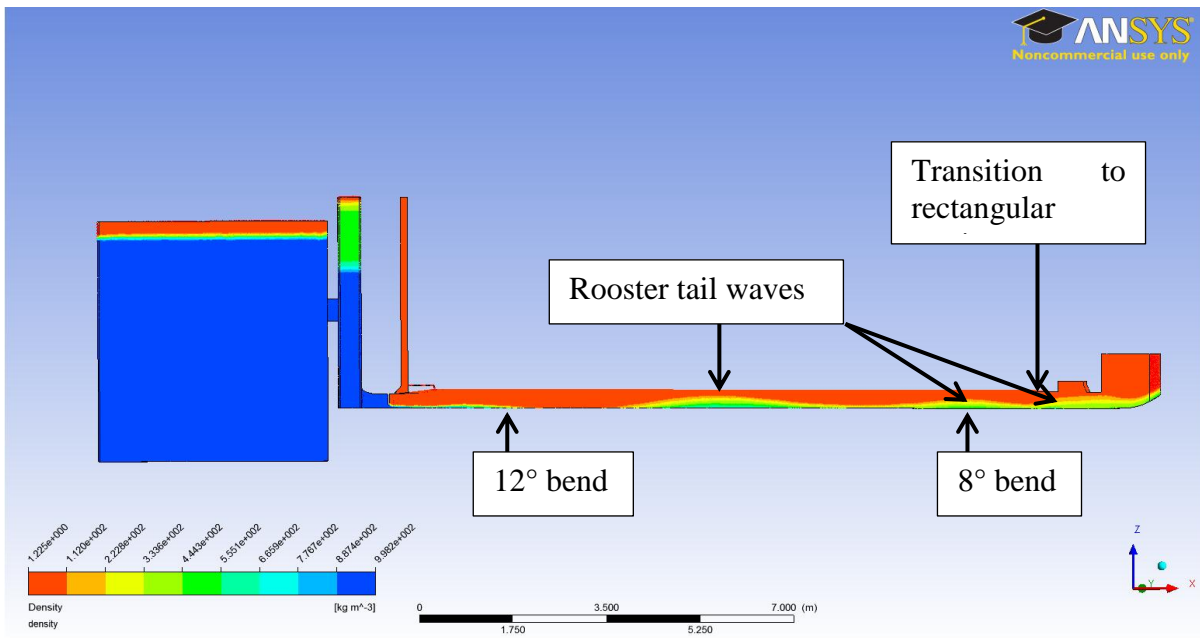
Figure 5.1.1-1A: Density contours for 20% emergency gate opening
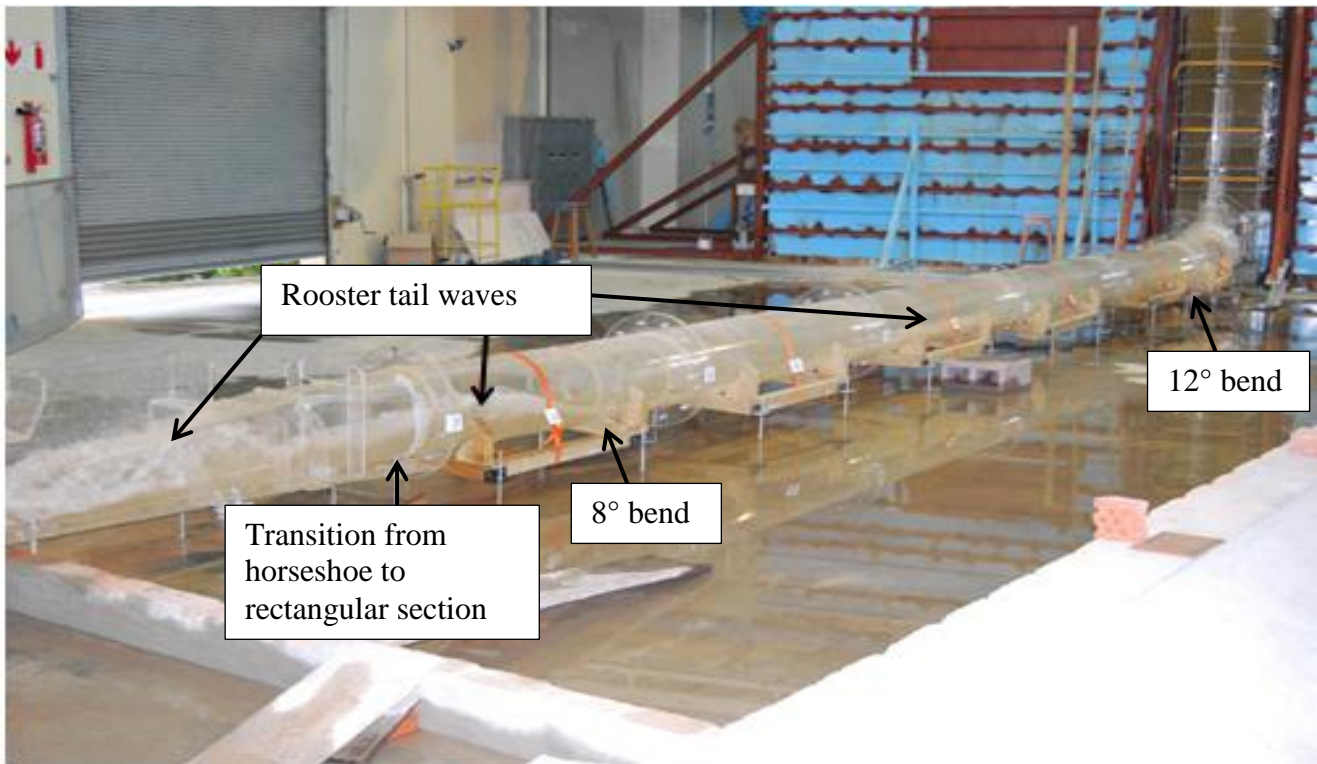
Figure 5.1.1-1B: Flow pattern in physical model for 20% emergency gate opening

53

Figure 5.1.1-1A shows the following:

- Water (shown in dark blue) with a density of 998.2 kg/m^3 occurs in the reservoir and wet well upstream of the emergency gate.
- Air (shown in red) with a density of 1.225 kg/m^3 is drawn down the air vent and downstream in the conduit.
- The jet under the gate becomes more aerated with densities varying between 200 kg/m^3 and 400 kg/m^3 (shown in colours orange, yellow and green).

Figure 5.1.1-1B shows the flow pattern in the conduit section of the physical model for 20% emergency gate opening. As similar flow pattern is observed as in the CFD numerical model with the formation of rooster tail waves in the conduit.

Figure 5.1.1-2A shows the following:

- The jet issuing underneath the emergency gate is less aerated than that for the 20% gate opening.
- The fluid in the conduit has densities ranging between 200 kg/m^3 (shown in orange) and 550 kg/m^3 (shown in light green).
- The cross waves appear deeper than in the 20% emergency gate setting. This may be attributed due to the increased discharge.

Figure 5.1.1-2B shows a section of the conduit upstream of the 8 degree bend, on the physical model at 30% emergency gate opening.

As in the CFD numerical model, the aerated flow exhibits rooster tail wave formation in the conduit due to reduced flow velocities. In Nafaji's study, rooster tail wave formation in tunnels caused the blockage of air passages above free surface flows and therefore prevented the circulation of air from the tunnel outlet.

In Figures 5.1.1-2A and 5.1.1-3A, the flow in the conduit increases with increasing emergency gate opening, and aeration is adequately provided by the air vent. Air is allowed to flow downstream from the air vent into the conduit but the formation of cross waves at the transition from the horseshoe to the rectangular section of the radial gate block up-flow of air into the conduit.
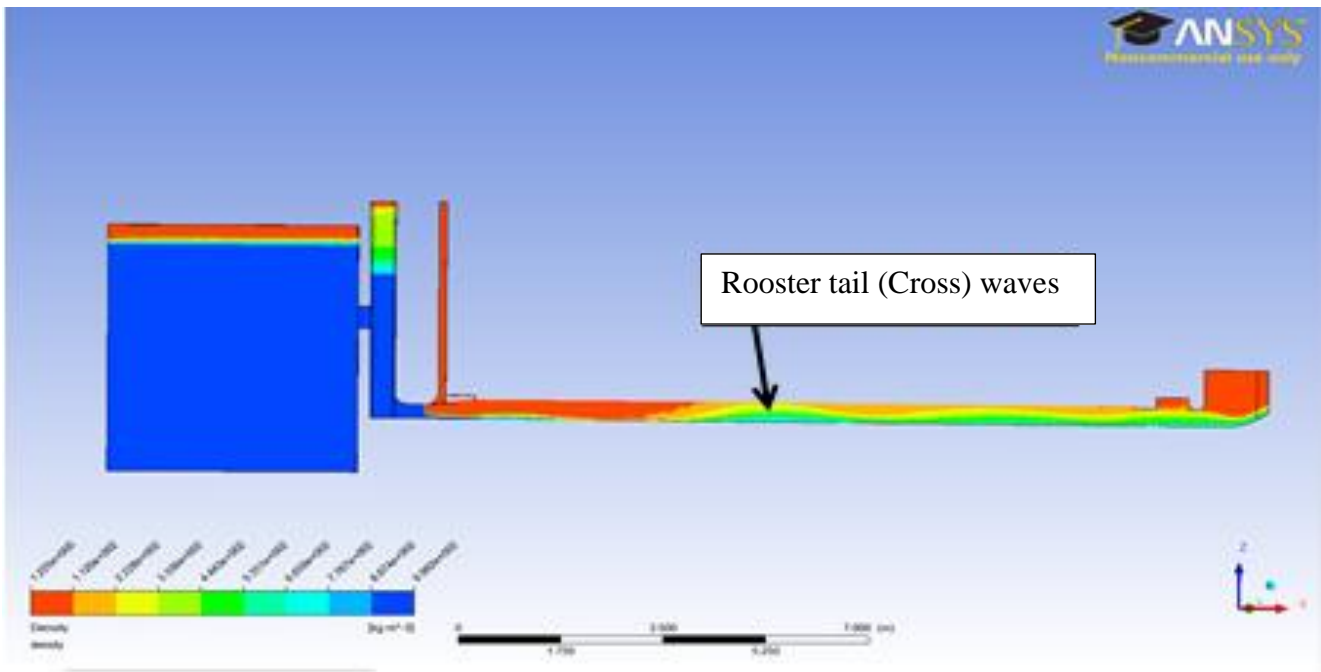
Figure 5.1.1-2A: Density contours for 30% emergency gate opening (Numerical)
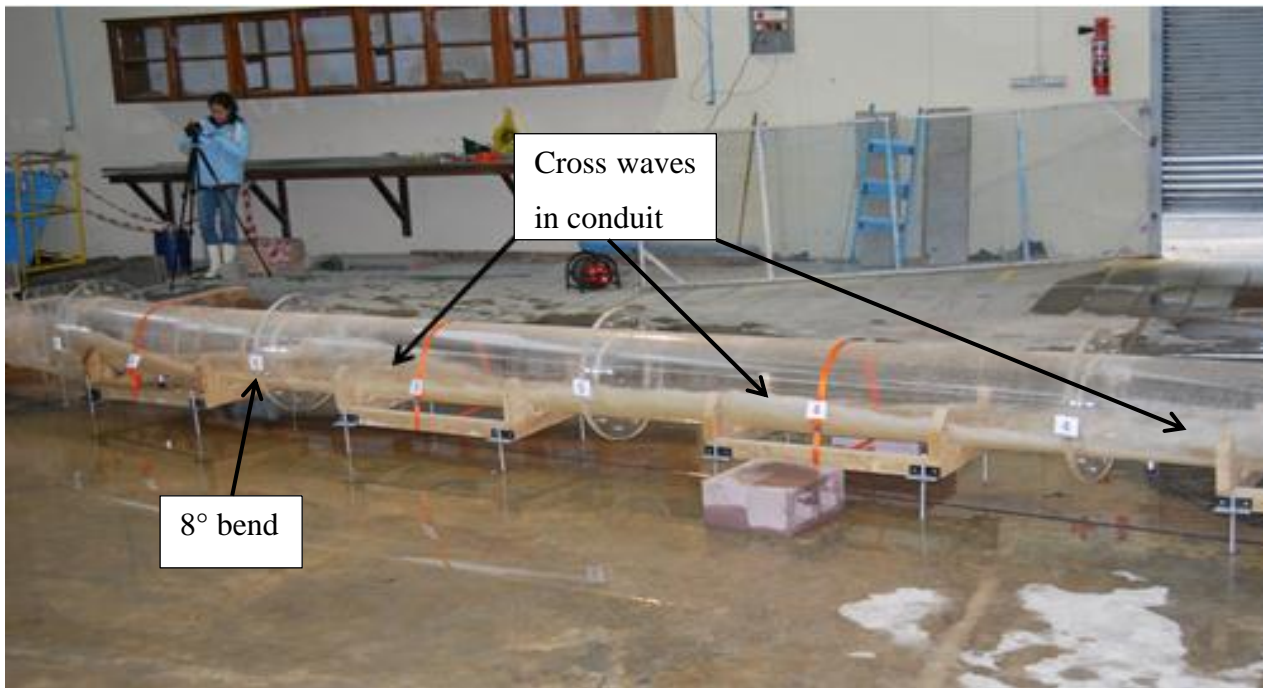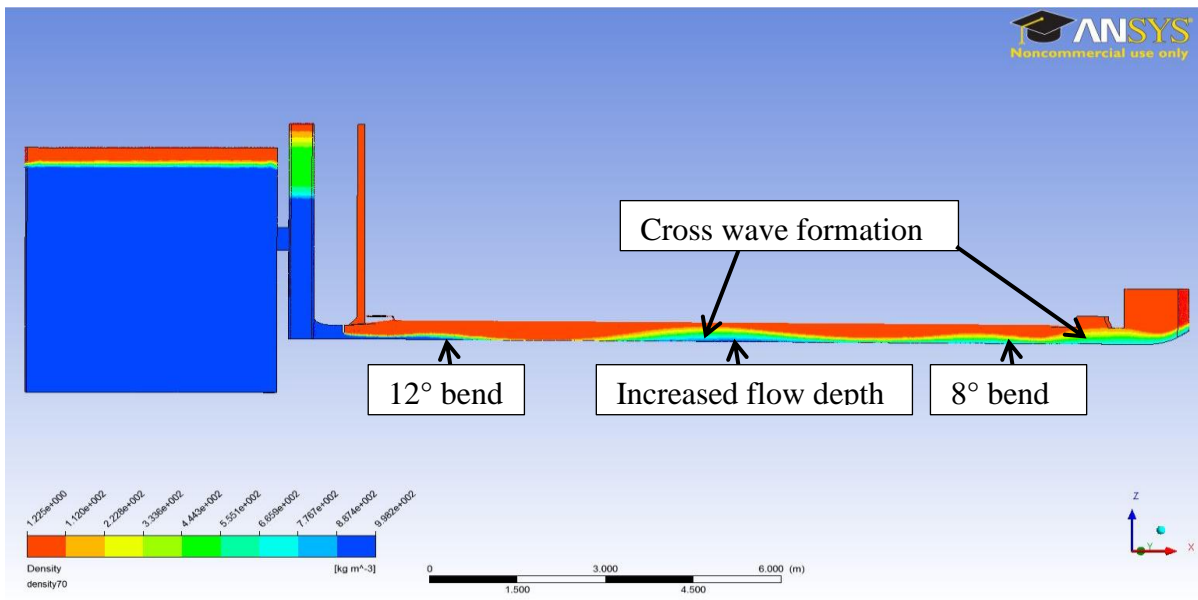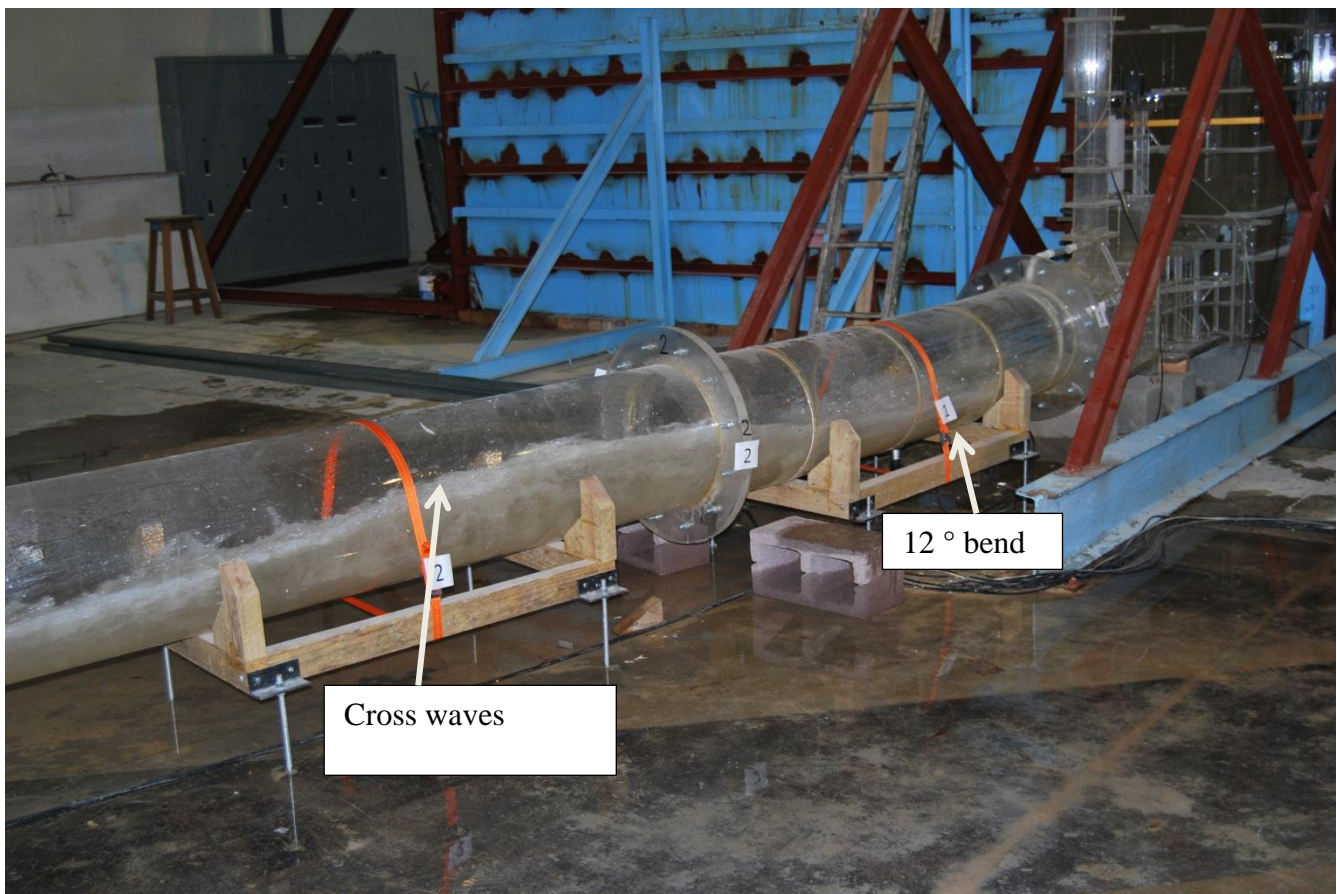

Figure 5.1.1-2B: Flow pattern in physical model for 30% emergency gate opening

Figure 5.1.1-3A: Density contours for 40% emergency gate opening

Figure 5.1.1-3B: Flow pattern in physical model for 40% emergency gate opening

For the 40% emergency gate opening, Figure 5.1.1-3A indicates that:

- Upstream of the emergency gate the flow is aerated by the open surfaces of the wet well and the reservoir.
- The jet underneath the gate is less aerated than that for the 20% and 30% emergency gate opening with densities ranging from 300 kg/m^3 (shown in yellow) and 998.2 kg/m^3 (shown in dark blue).
- The amount of air entrained in the flow throughout the conduit due to the formation of cross waves reduces.
- The increased depth of flow downstream of the emergency gate is evident and this aerated flow appears to fill the conduit upstream of the ski jump at the constriction where the conduit area reduces.

Figure 5.1.1-3B shows a section of the conduit from the physical model at 40% emergency gate opening.

The flow pattern exhibited in the physical model is similar to that of the CFD numerical model. Air is entrained in the surface of the flow as it moves downstream in the conduit. The increase in water depth further downstream in the conduit appears to result from reduced velocities on account of friction losses with some evidence that cross waves may occur.

In Figure 5.1.1-4A the following is observed:

- The jet issuing underneath the gate begins to fill up the conduit with densities of the fluid ranging from 200 kg/m^3 (shown in orange in the air pockets) and 998.2 kg/m^3 (shown in dark blue).
- Air pockets begin to form downstream of the 12 degree bend where the flow is almost full.
- At the position of the radial gate the conduit appears to be blocked by the flow, preventing free air release downstream as the flow enters the ski jump.
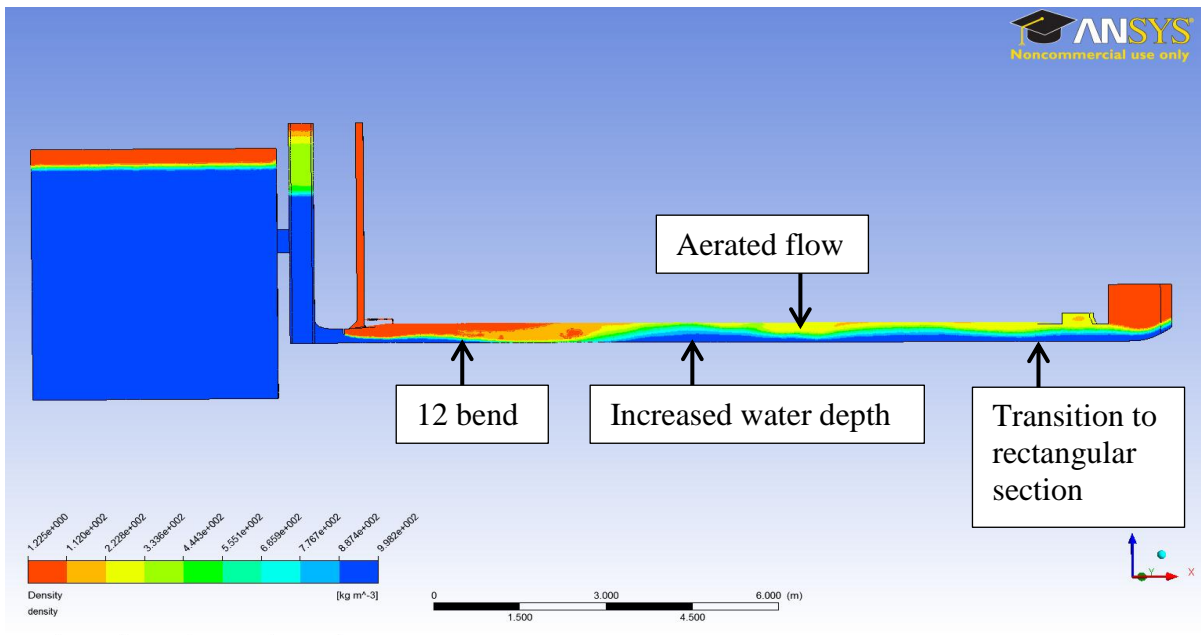
Figure 5.1.1-4B shows a section of the conduit from the physical model at 50% emergency gate opening. The flow pattern is similar to that from the CFD numerical model in Figure 5.1.1-4A.
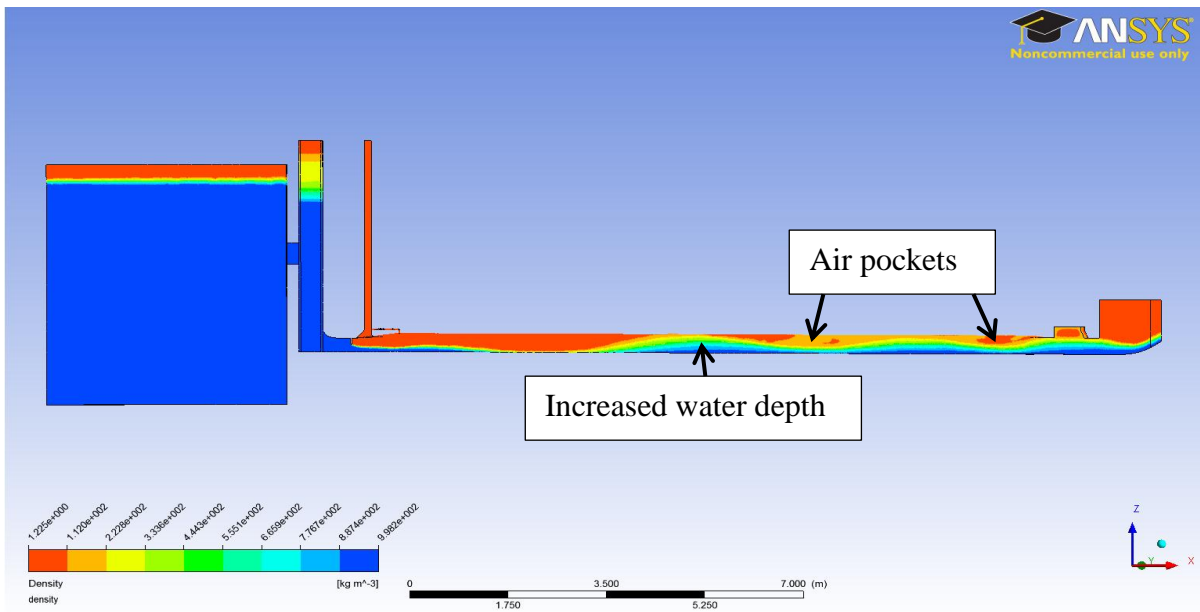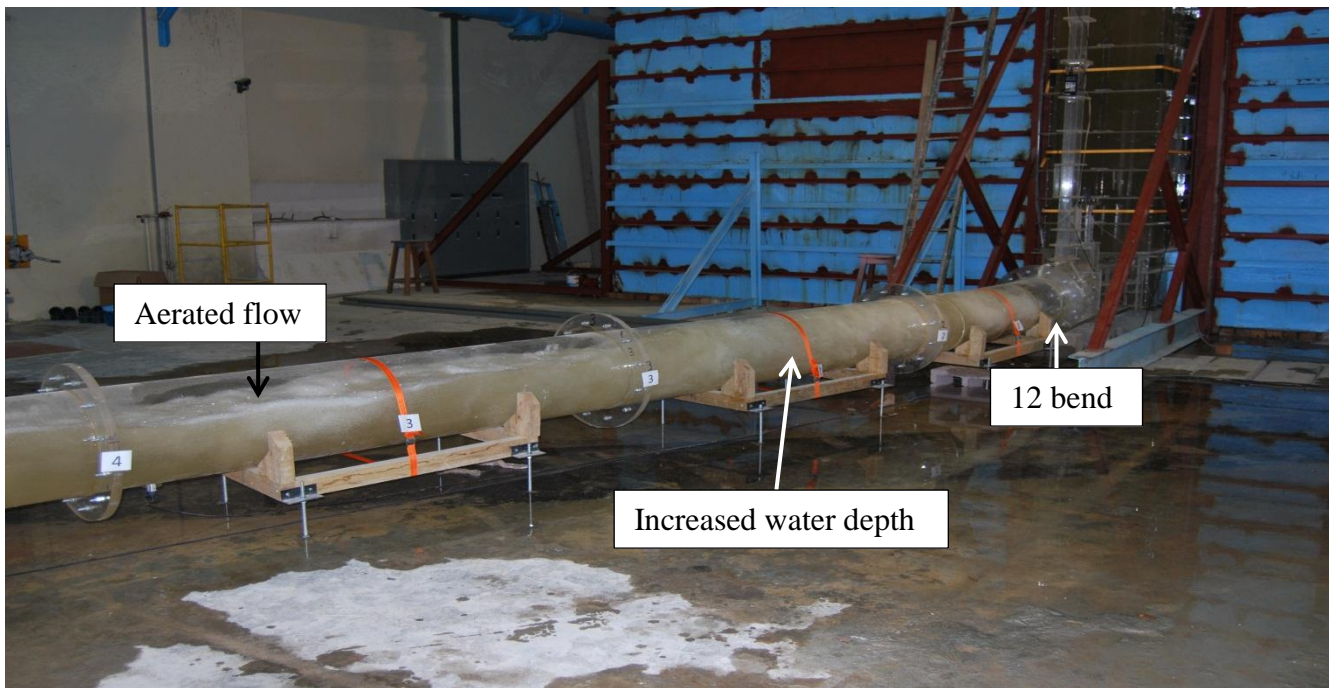
Figure 5.1.1-4A: Density contours for 50% emergency gate opening (Numerical)
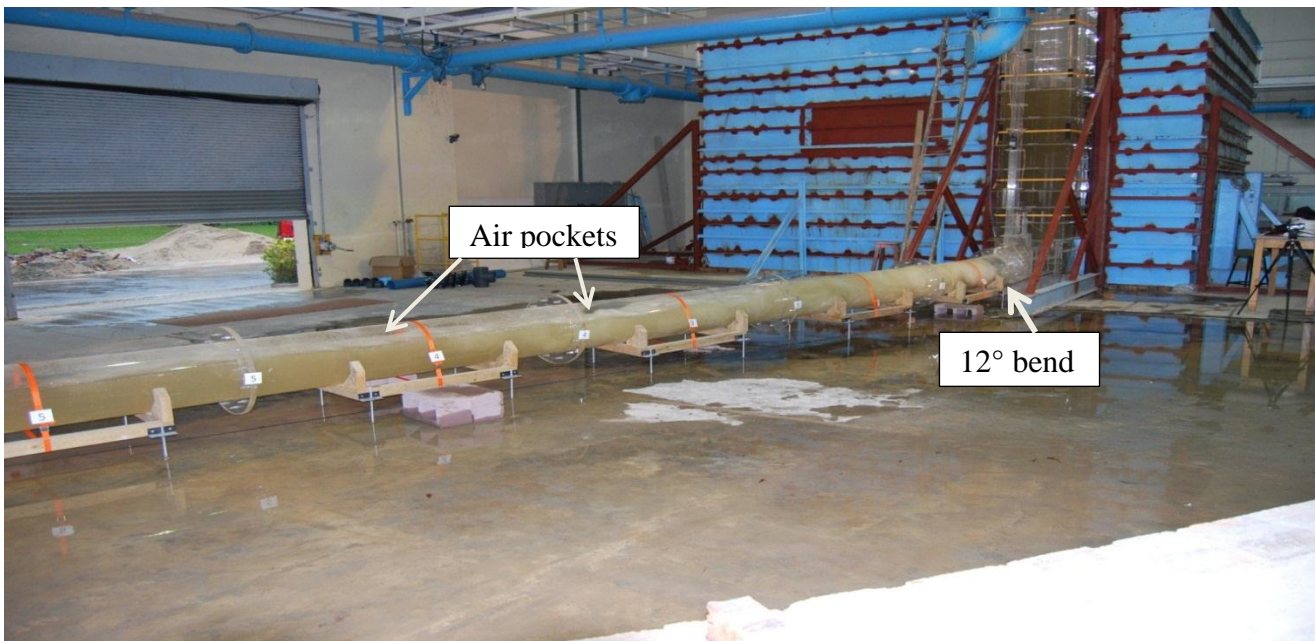
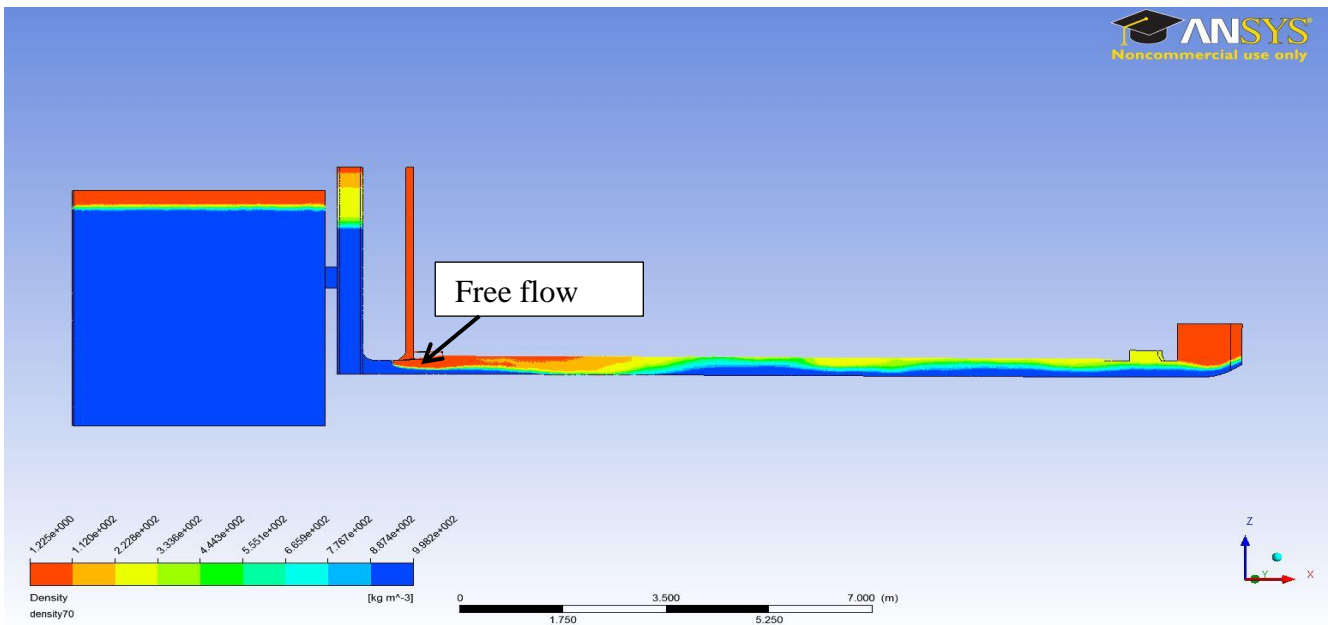**Figure 5.1.1-4B: 50% emergency gate opening (Physical)**

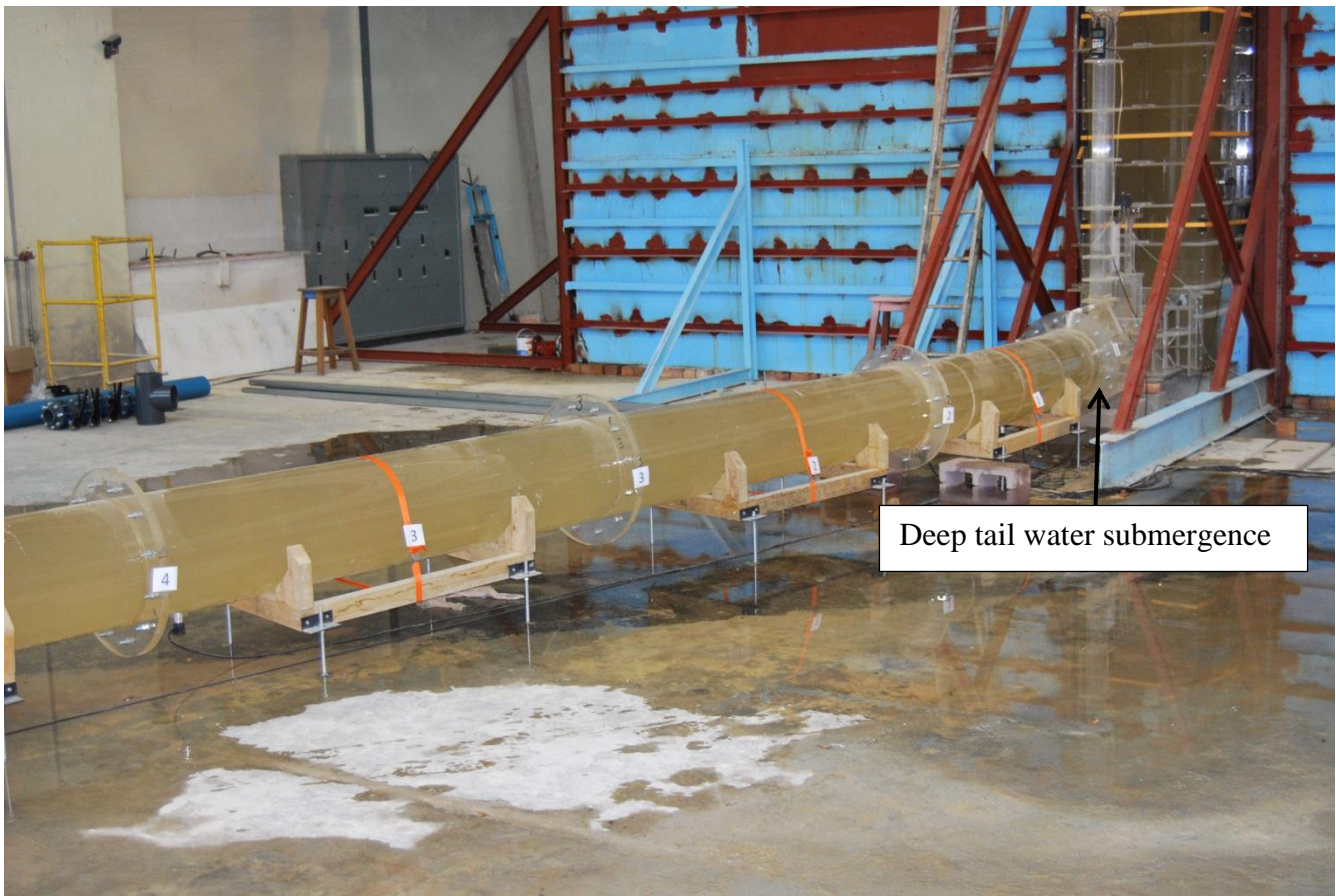**Figure 5.1.1-5A: Density contours for 60% emergency gate opening**

Figure 5.1.1-5B: Emergency gate region on physical model for 60% emergency gate opening

Figure 5.1.1-6A: Density contours for 70% emergency gate opening

Figure 5.1.1-6B: Emergency gate region on physical model for 70% emergency gate opening

At 60% emergency gate opening, Figure 5.1.1-5A and Figure 5.1.1-5B below the following:

- The conduit is flowing full after the 12 degree bend and the flow density ranges between 200 kg/m^3 (shown in orange) and 998.2 kg/m^3 (shown in dark blue).

- The sudden increase in water depth after the 12 degree bend may imply the formation of a hydraulic jump but after determining the Froude number at various sections along the conduit, it was established that the flow was supercritical throughout. With the flow being supercritical and still entraining air in the air pockets formed at the top of the conduit, the air vent should be able to provide enough aeration to satisfy the entrainment.

- There is circulation of air from the air vent immediately downstream of the emergency gate above the issuing jet, which causes aeration for the flow.

- The top of the wet well and the reservoir provide aeration for the flow upstream of the emergency gate.

Figure 5.1.1-6A shows the following:

- The flow in the conduit downstream of the emergency gate is full and the density of the fluid varies between 300 kg/m^3 (shown in green and 998.2kg/m^3 (shown in dark blue).

- There is no submergence of emergency gate as was experienced in the hydraulic model (Figure 5.1.1-6B).

- There are no air pockets formed on the surface of the flow in the conduit.

The conduit flowed partially full for gate openings of 20%, 30% and 40%. At 50%, 60% and 70% the conduit started to flow full, with an air-water mixture at the surface as shown in Figure 5.1.1-6A and 6B.

Continuous damming of the flow upstream of the ski jump was observed at the position of the radial gate. When this damming blocked air from being pushed out of the domain it led to oscillation of the flow in the conduit.

Both the numerical and physical model results for all tested emergency gate openings provided no release of air up the air vent as in the prototype commissioning test.

5.1.2   Velocity vectors in the wet well tower

The figures below show the velocity vectors, coloured by density of the flow into the wet well tower for emergency gate openings of 20%, 30%, 40%, 50%, 60% and 70%. As for the contours above, red represents air and blue represents water.
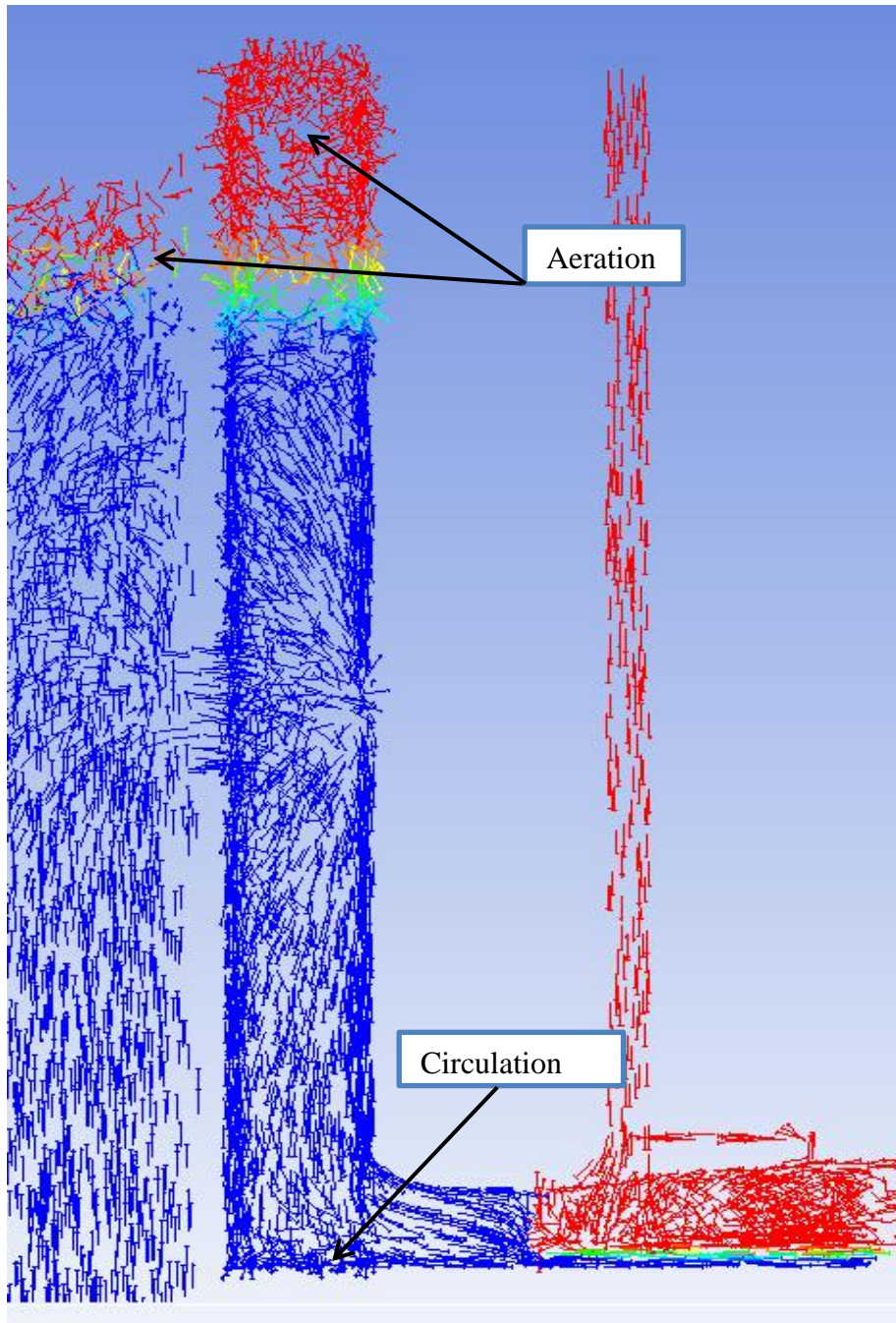
Figure 5.1.2-1: Wet well velocity vectors for 20% emergency gate opening

Figure 5.1.2-1 shows the following:

- As the flow leaves the reservoir into the wet well tower, the main potential sources of aeration are the top of the wet well upstream of the emergency gate and the air vent at the outlet downstream of the emergency gate.
- There appears to be rotational flow at the bottom of the wet well tower. As the wet well fills up, the flow area is constricted at the emergency gate and there appears to be a contra flow at the top of the conduit immediately upstream of the gate.
- Air is drawn down the air vent to the downstream of the emergency gate and there is air circulating above the issuing jet.

Rotational flow

Contracted flow
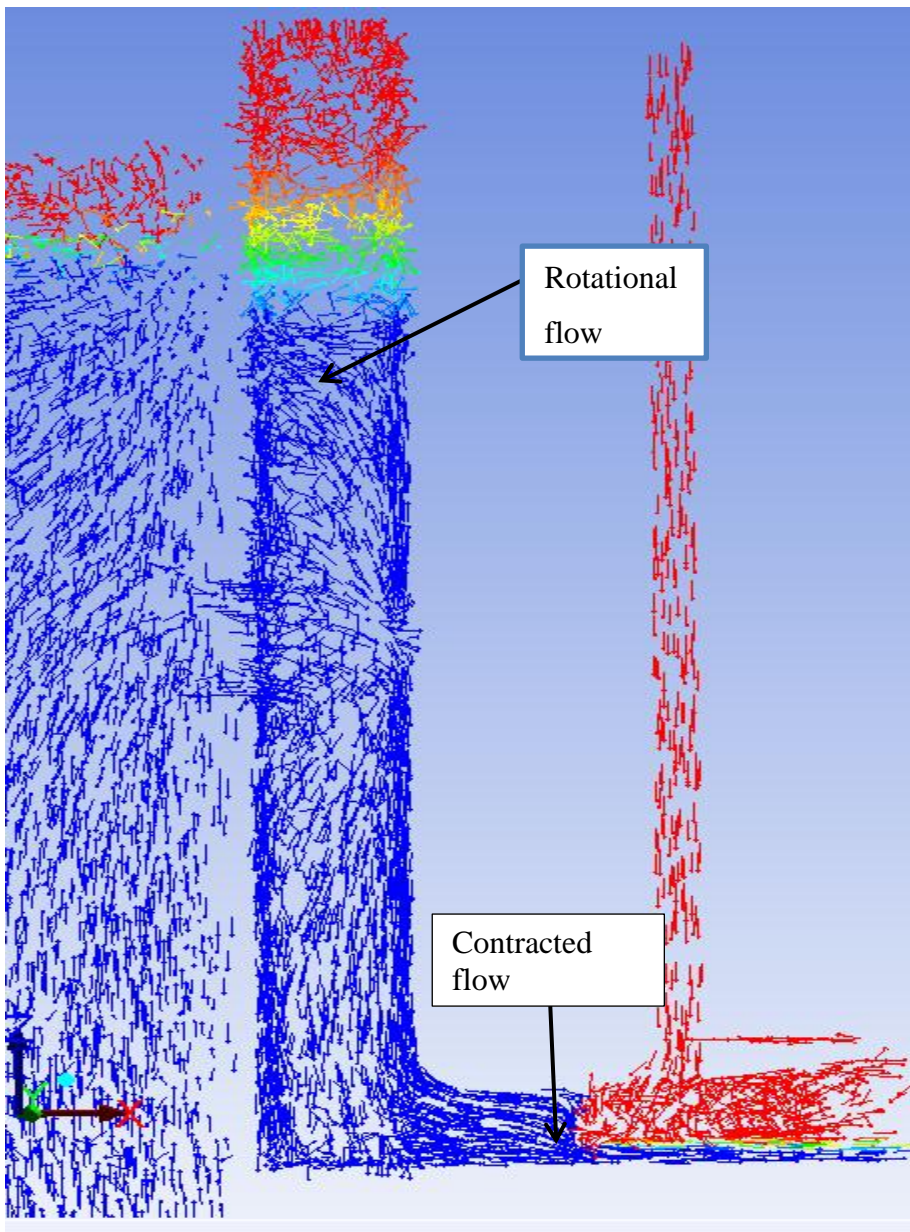
Figure 5.1.2-2: Wet well velocity vectors for 30% emergency gate opening

From the 30% gate opening (Figure 5.1.2-2) and onwards, horizontal rotational flow is observed on the surface of the water in the wet well tower, above the selector gates. Such rotational flow was also observed in the wet well in the physical model. This could lead to the formation of vortices that entrap air upstream of the emergency gate (Sharma, 1976) but no vortices were observed in the numerical model.
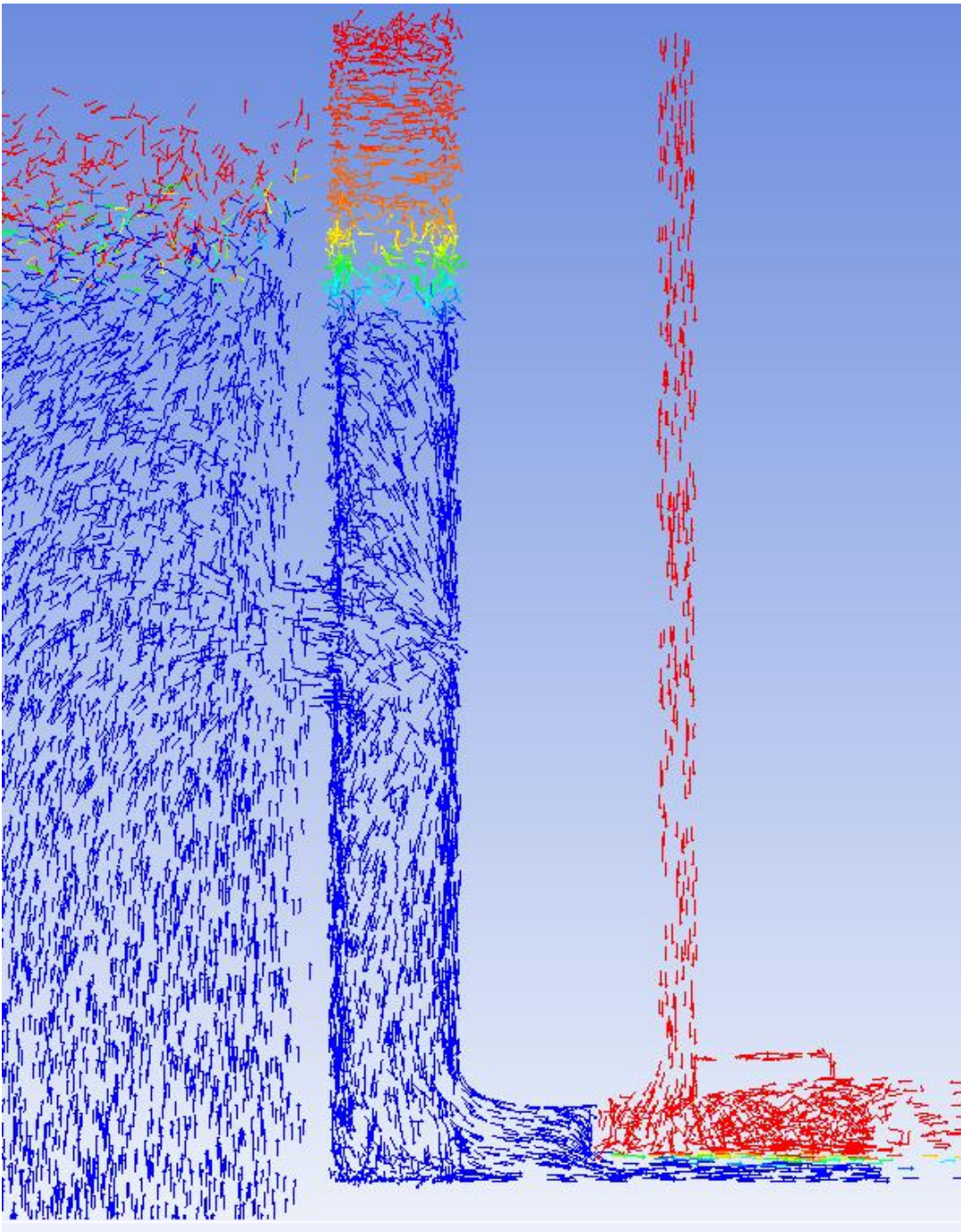
Figure 5.1.2-3: Wet well velocity vectors for 40% emergency gate opening

The fluid at the surface of the tower (Figure 5.1.2-1 to Figure 5.1.2-6), above the intake gates, appears to be entrapped with air; aeration being provided by the top of the wet well. The air, however, does not appear to go down further into the wet well and therefore is not considered a source of air downstream of the emergency gate. This phenomenon was not evident in the physical model.

The rotational flow at the surface of the water in the wet well tower is expected due to the horizontal flow into the wet well the intake gates.
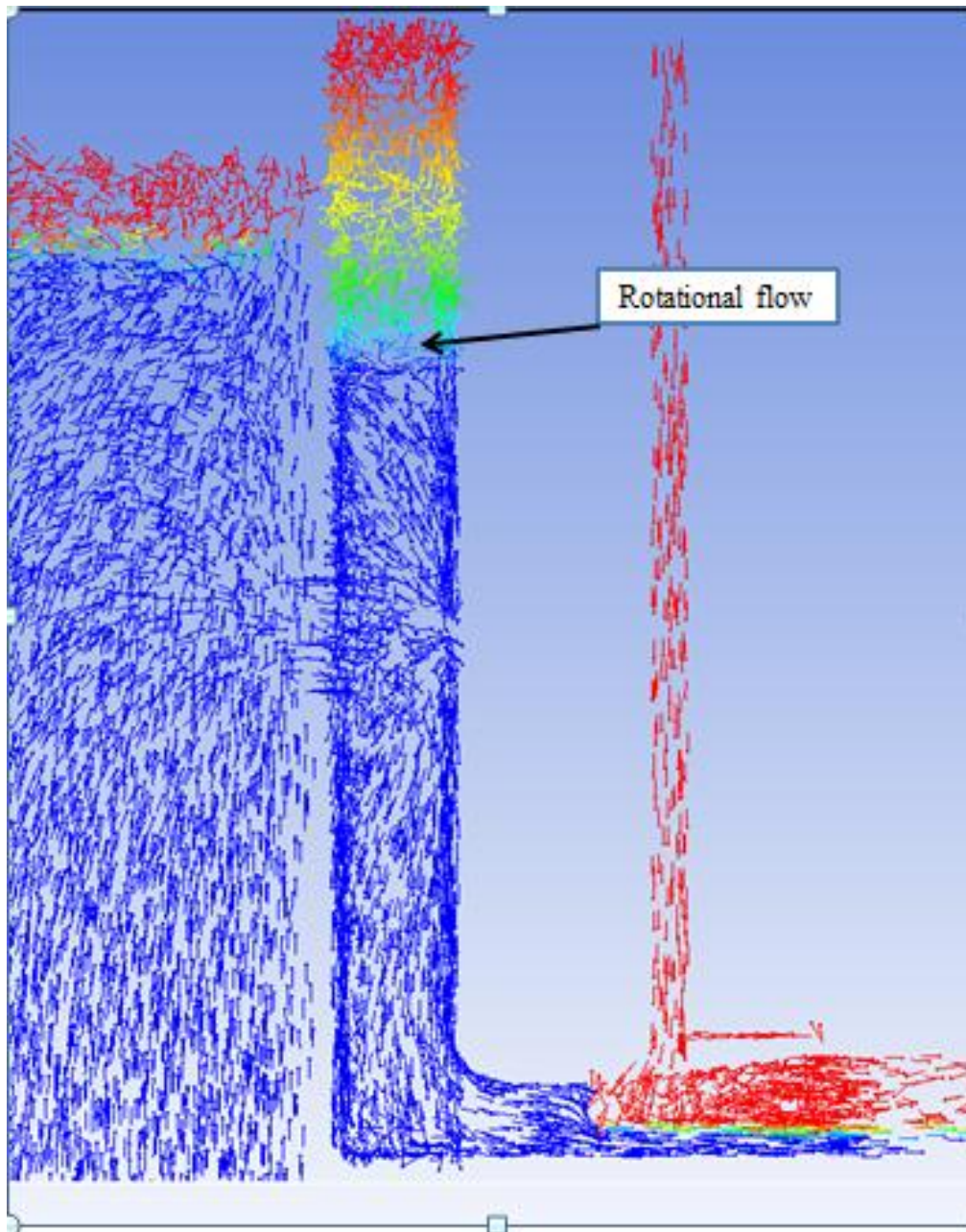
Figure 5.1.2-4: Wet well velocity vectors for 50% emergency gate opening

For the 50% emergency gate opening shown in the Figure 5.1.2-4 above and the 60% emergency gate opening shown in the Figure 5.1.2-5 below, there is not as much circulation observed in the wet well tower as in previous settings. As the flow area at the emergency gate increases, the velocity of flow decreases. However, the discharge through the emergency gate also increases.
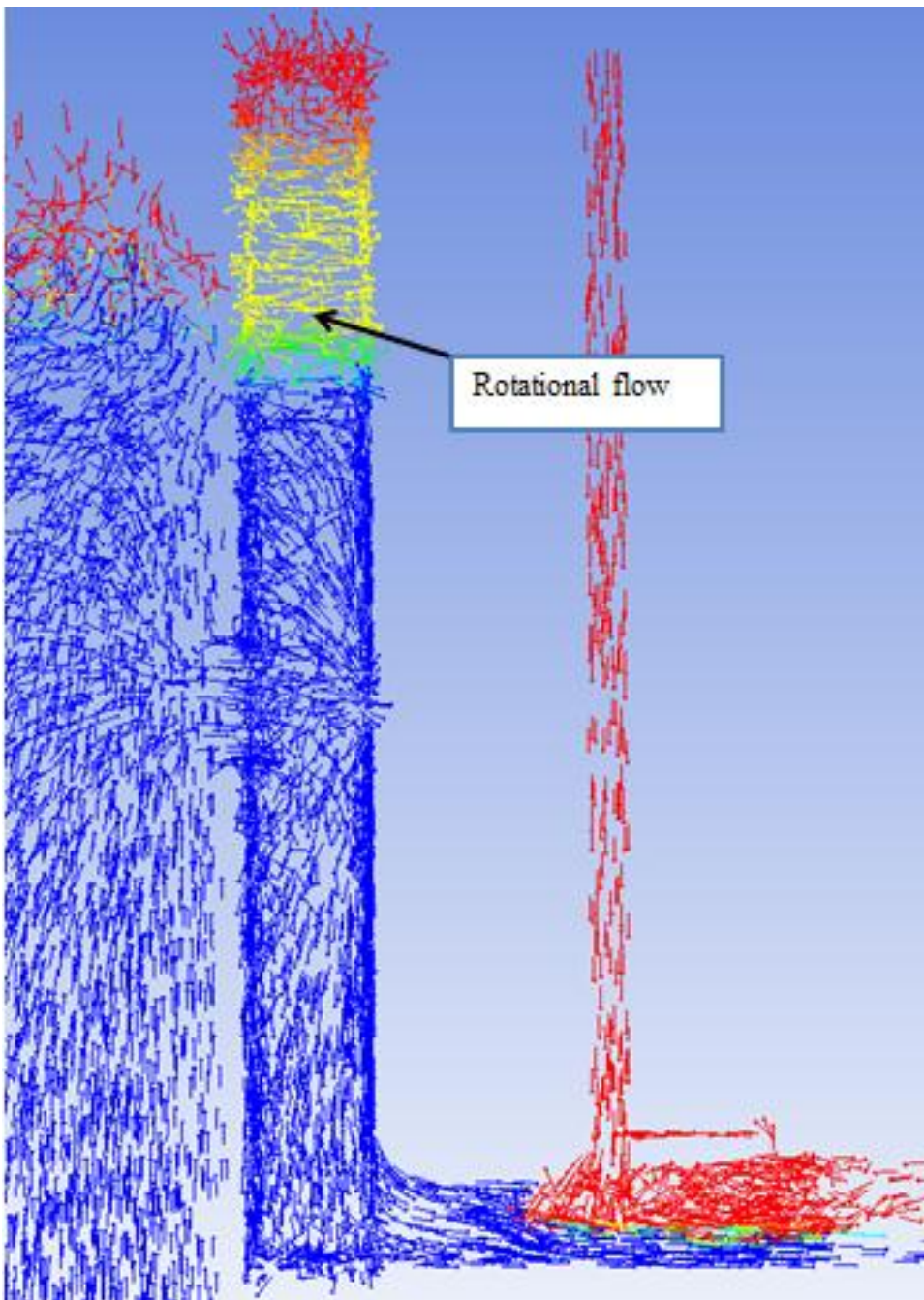
Figure 5.1.2-5: Wet well velocity vectors for 60% emergency gate opening
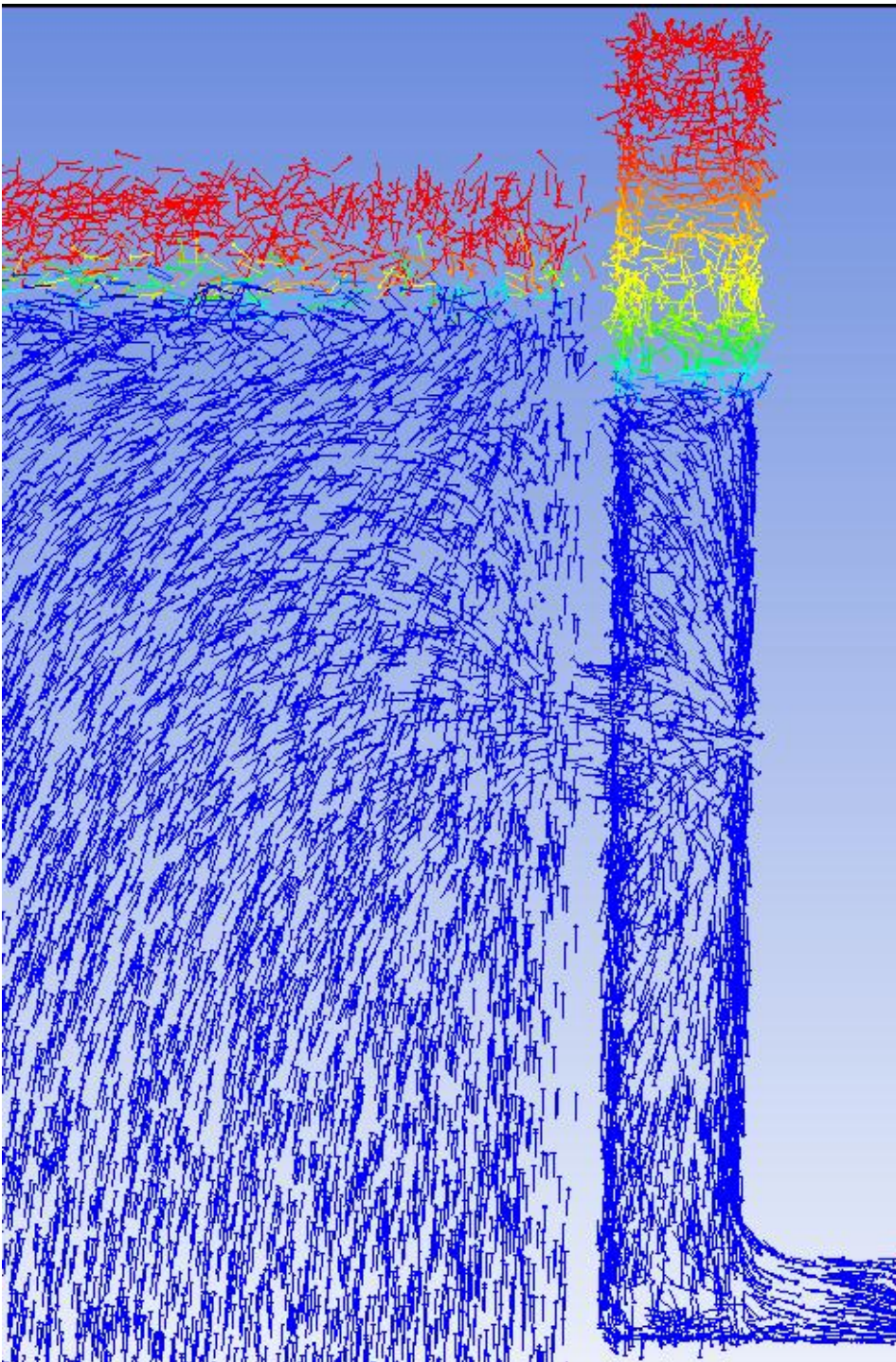
Figure 5.1.2-6: Wet well velocity vectors for 70% emergency gate opening

For all scenarios where rotational flow in the wet well tower was observed, it is possible that such flow could entrain large amounts of air. However, it was not established whether aeration at the top of the wet well contributed to the air downstream of the emergency gate.

5.1.3   Velocity vectors in gate and air vent region

The figures below show the velocity vectors of the flow, coloured by density (Blue representing water and red representing air), as it approaches the emergency gate and proceeds into the conduit, for emergency gate openings of 20%, 30%, 40%, 50%, 60% and 70%.

The mesh at the gate was set up as in the physical model with modifications made to the gate lip but the side grooves for the gate were not incorporated in the numerical model geometry. The exclusion of the side grooves should not affect the results of the simulation and their introduction would mean extra unnecessary cells.

Because of the highly pressurized flow upstream of the emergency gate (Figure 5.1.3-1A) and the small flow area of the gate, the water issues from the gate in the form of a spray jet and the water depth of highly aerated flow increases further downstream in the conduit.

The 20% emergency gate opening setting results in the greatest aeration to the flow on account of the highly pressurised jet issuing from underneath the gate. There is high circulation of air just below the air vent, immediately downstream of the emergency gate, as the vent provides the required aeration demand.

Figure 5.1.3-1B shows the similarity of the flow patterns for the numerical and physical models. Air is continuously sucked into the model through the air vent.

The discharge underneath the gate increases with increasing gate opening and for 30% and 40% gate openings as seen in Figures 5.1.3-2A/2B and 5.1.3-3A/3B below, the jet issuing is free flow. No submergence of the emergency gate is observed but continued aeration is provided by the air vent.
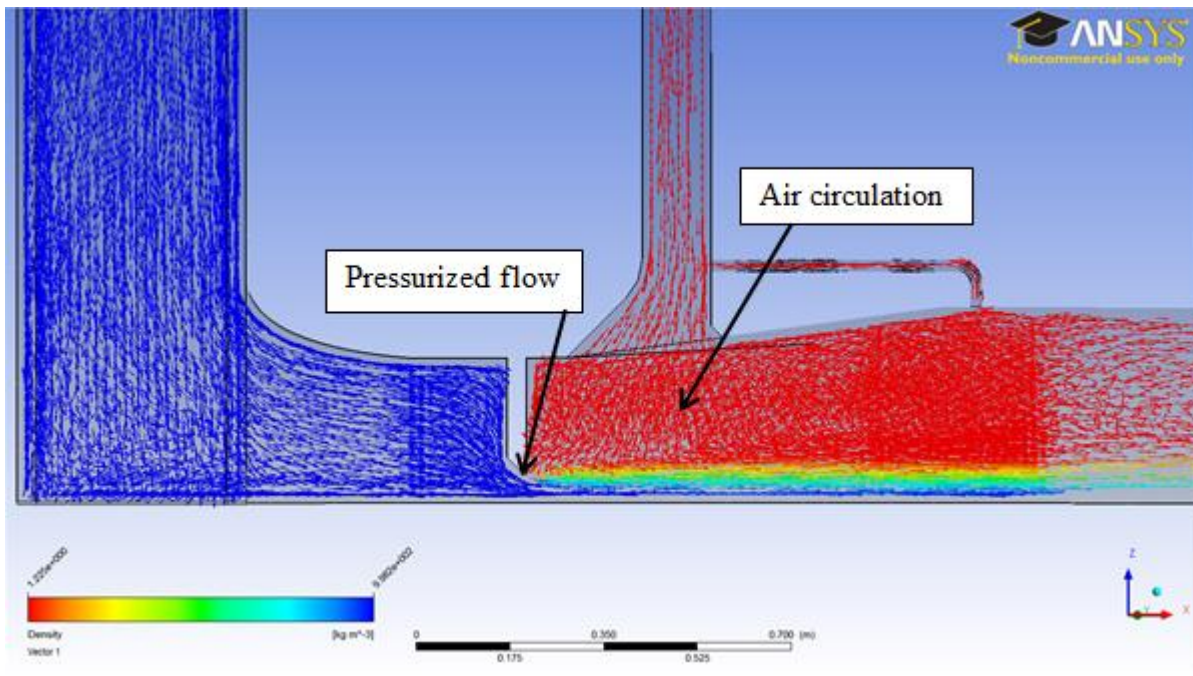
Figure 5.1.3-1A: Velocity vectors in emergency gate and air vent region for 20% emergency gate opening

Figure 5.1.3-1B: Flow pattern in emergency gate and air vent region for 20% emergency gate opening (Physical)

70
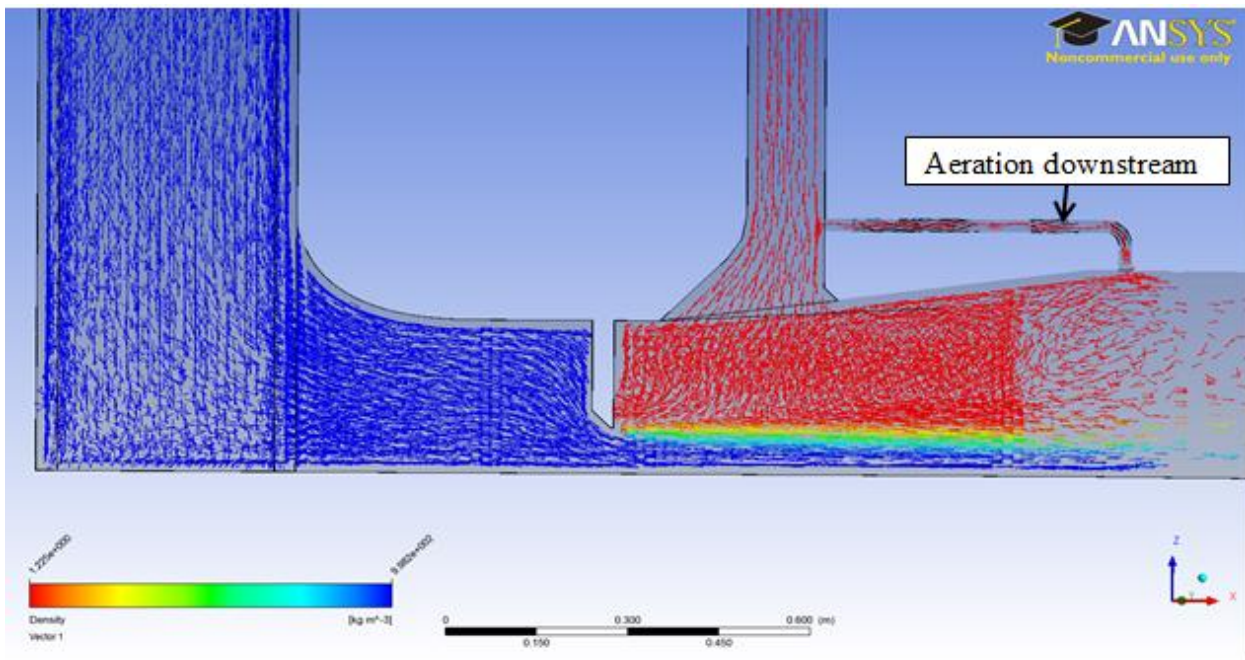
Figure 5.1.3-2A: Velocity vectors in emergency gate and air vent region for 30% emergency gate opening

Figure 5.1.3-2B: Flow pattern in emergency gate and air vent region for 30% emergency gate opening (Physical)

Figure 5.1.3-2A above shows the small pipe attached to the air vent providing aeration downstream of the emergency gate, at the beginning of the conduit.

On account of a short coming of the software used for post processing, it was not possible to develop uniform vectors across the whole domain. This was because of the complexity of the geometry and because during the meshing, the domain had to be partitioned into smaller components that had different mesh sizes. Smaller mesh sizes were used in the critical sections of the model such as the gate lip and the air vent region. Therefore, the density of the plotted vectors in the various sections of the domain has no relation to nature of the result. This is a post processing drawback.

Figure 5.1.3-2B shows the flow pattern at emergency gate and air vent region for 30% emergency gate opening in the physical model.

Considering the shape of the gate lip structure as shown in Section 4.2.2 above and the velocities at which the flow emerges through the gate, the flow does not contract greatly. For the 40% emergency gate opening shown in Figure 5.1.3-3A and 5.1.3-3B for the CFD and physical model, the upstream angle on the gate lip allows the flow to be directed smoothly underneath the gate and also reduces the pressure on the upstream side of the emergency gate.
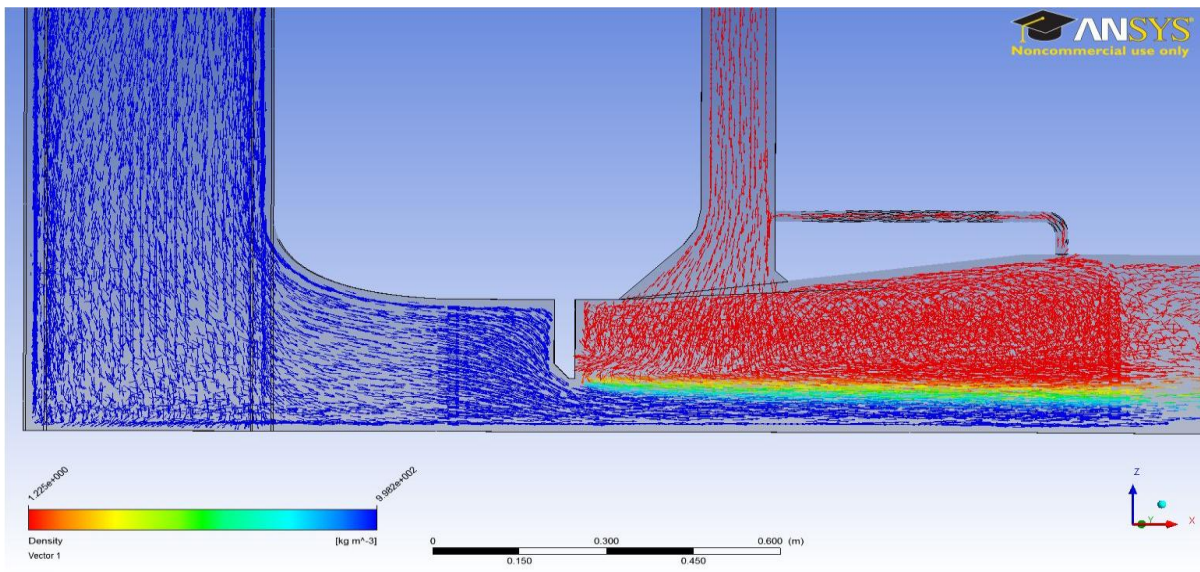
Figure 5.1.3-3A: Velocity vectors in emergency gate and air vent region for 40% emergency gate opening

Figure 5.1.3-3B: Flow pattern in emergency gate and air vent region for 40% emergency gate opening (Physical)

73
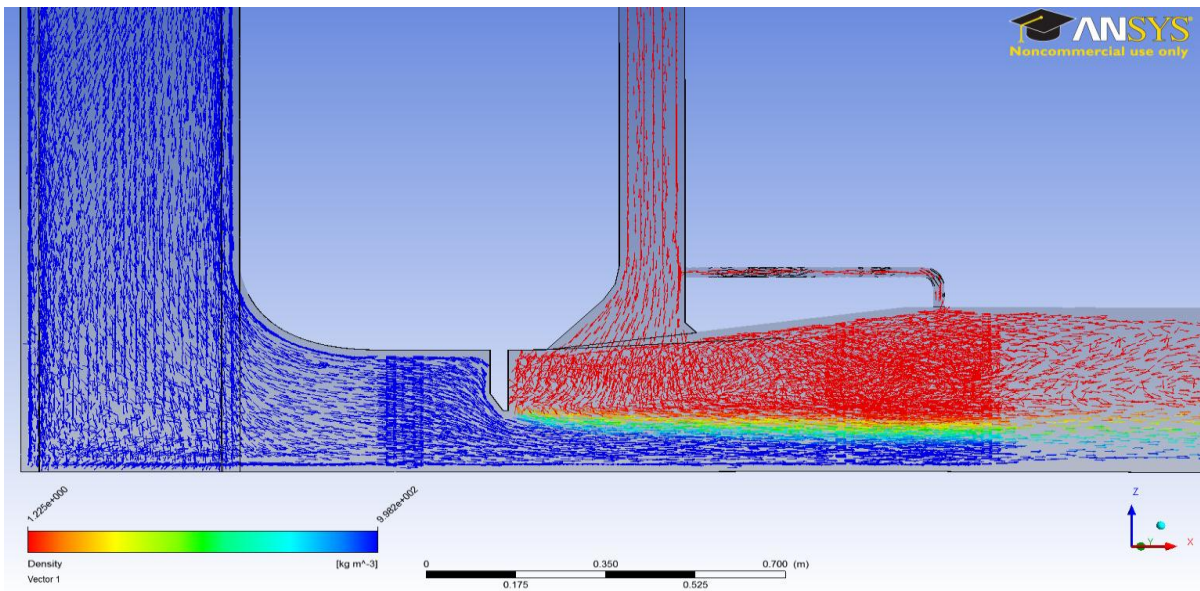
Figure 5.1.3-4A: Velocity vectors in emergency gate and air vent region for 50% emergency gate opening

Figure 5.1.3-4B: Flow pattern in emergency gate and air vent region for 50% emergency gate opening (Physical)

74

For the 50% emergency gate opening shown in the Figure 5.1.3-4A and the 60% emergency gate opening as shown in the Figure 5.1.3-5A, there is minimal rotational flow upstream of the emergency gate, at the bottom of the wet well. The rotation reduces as the flow area at the emergency gate increases.

There is no deep tail-water submergence in the numerical and physical models as free flow occurs downstream of the emergency gate. The conduit flows partially full downstream of the emergency gate and further downstream the conduit begins to flow full as discussed in Section 5.1.1 with aeration being efficiently provided by the air vent.

Except for the 60% and 70% gate openings, the flow pattern immediately downstream of the emergency gate for all other simulated gate openings was similar to that of the physical model. At the 60% and 70% emergency gate openings, the physical model exhibited deep tail-water submergence of the flow immediately downstream of the emergency gate (Figures 5.1.3-5B and 5.1.3-6B) where there was increased water depth. The flow appeared fully pressurized with the conduit flowing full all the way from the emergency gate down to the ski jump whereas the CFD model showed aerated flow.
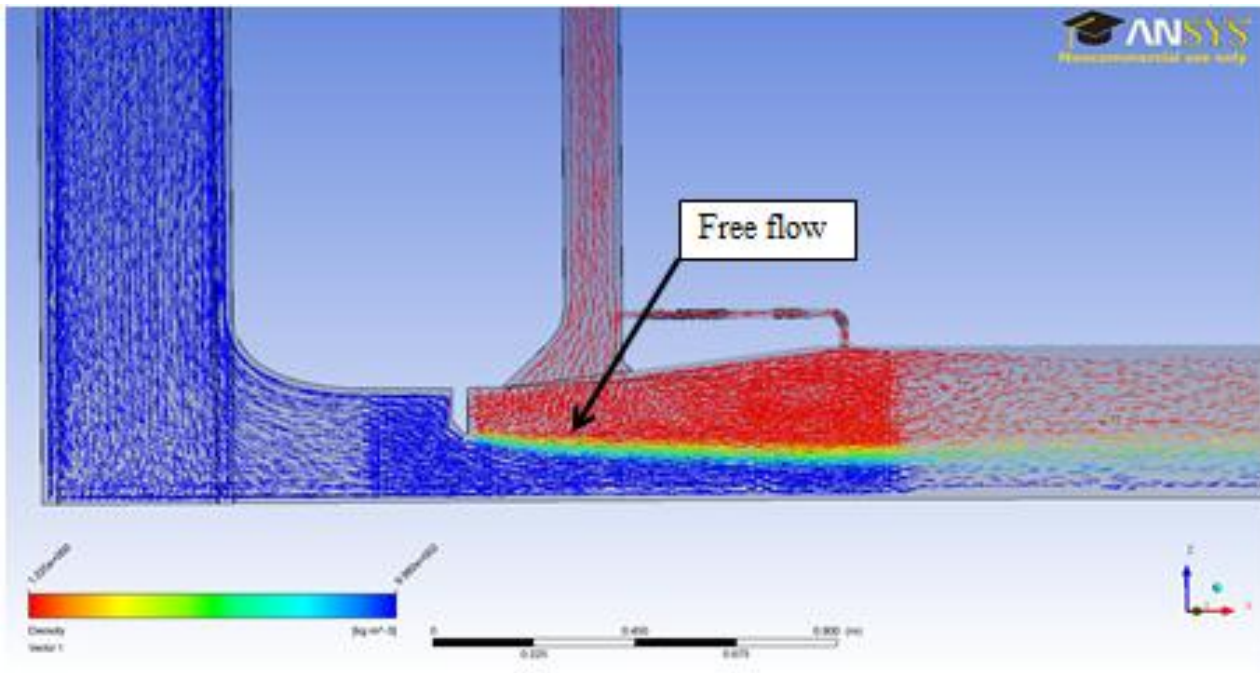
Figure 5.1.3-5A: Velocity vectors in emergency gate and air vent region for 60% emergency gate opening

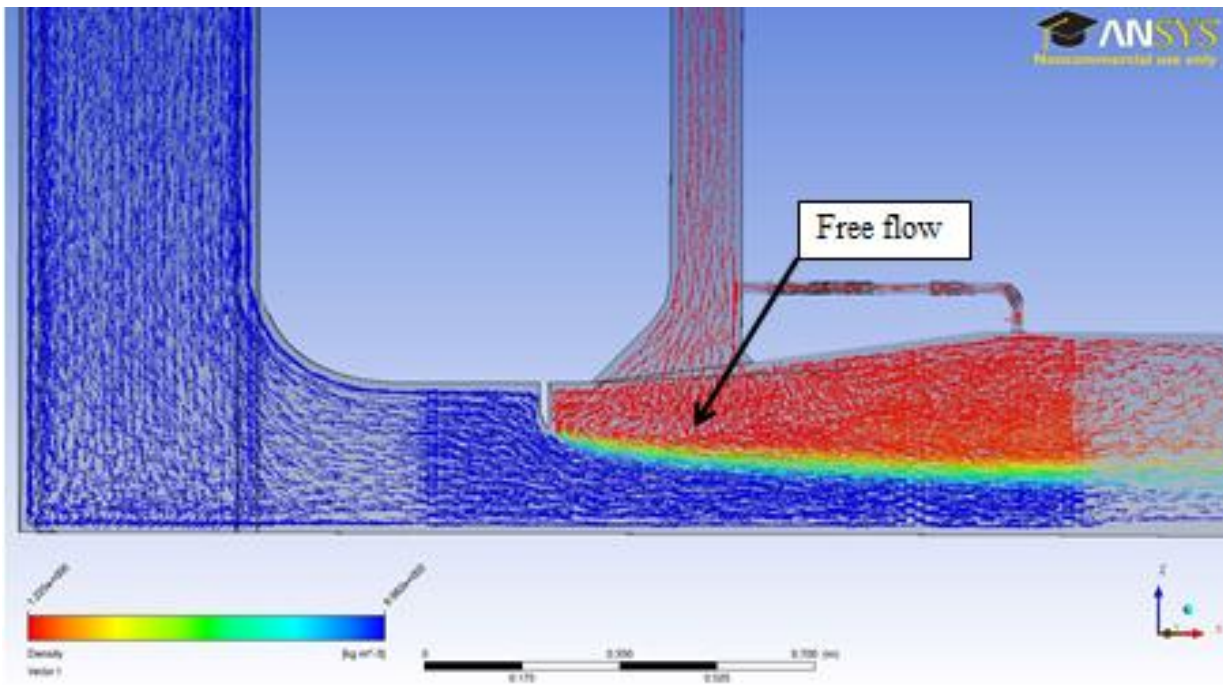**Figure 5.1.3-5B: Flow pattern in emergency gate and air vent region for 60% emergency gate opening (Physical)**

76

Figure 5.1.3-6A: Velocity vectors in emergency gate and air vent region for 70% emergency gate opening

Figure 5.1.3-6B: Emergency gate region on physical model for 70% emergency gate opening

5.1.4   Velocity vectors at the end box and ski jump

The flow pattern at the ski jump was monitored as well to determine its possible influence on the occurrence of full flow which resembles a hydraulic jump. Blue represents water, red represents air and colours in between (such as orange, yellow and green) represent aerated flow.

The following figures display the flow pattern at the ski jump in the form of velocity vectors coloured by density for emergency gate openings of 20%, 30%, 40%, 50%, 60% and 70%.
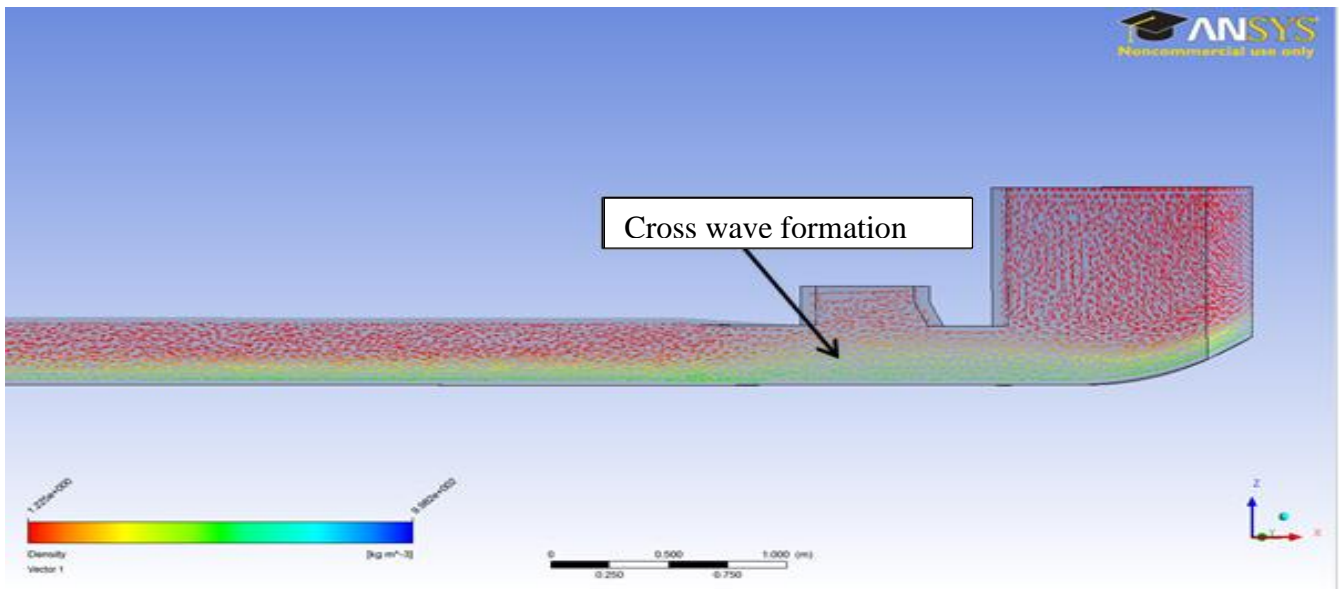
For the 20% emergency gate opening (Figure 5.1.4-1A and 5.1.4-1B) there is formation of cross waves upstream of the ski jump. The conduit flows partially full and the density of the flow is low with a lot of air entrained. There is circulation of air above the flow especially in the area of the 8 degree bend where the conduit begins to constrict and at the end box where the radial gate is located.

For the 30% opening, Figure 5.1.4-2A indicates that the flow has air entrained in it with the density ranging between 300 kg/m^3 and 600kg/m^3.

Figure 5.1.4-2B shows the flow pattern in the physical model for the 30% gate opening.

At 40% as seen in Figure 5.1.4-3A/3B, there is damming of flow upstream from the ski jump and the density of the water still varies between 400 kg/m^3 and 800 kg/m^3 meaning that there is still a significant amount of air entrapped in the flow. This damming is not a hydraulic jump since the flow was found to be supercritical throughout the conduit. The pressurized flow issues from the emergency gate at high velocities and the velocities decrease due to friction losses as the flow goes down the conduit with increased flow area. At the end of the horseshoe conduit, the conduit area reduces causing the flow depth to increase before the flow is discharged at the ski jump. This situation causes damming upstream of the ski jump.

For gate openings of 30% and for larger openings, there is minimal circulation of air at the 8 degree (second) bend however there is some circulation above the ski jump. For larger openings the conduit flows fuller and less air is entrained in the flow.

Figure 5.1.4-1A: Velocity vectors at the ski jump for 20% emergency gate opening
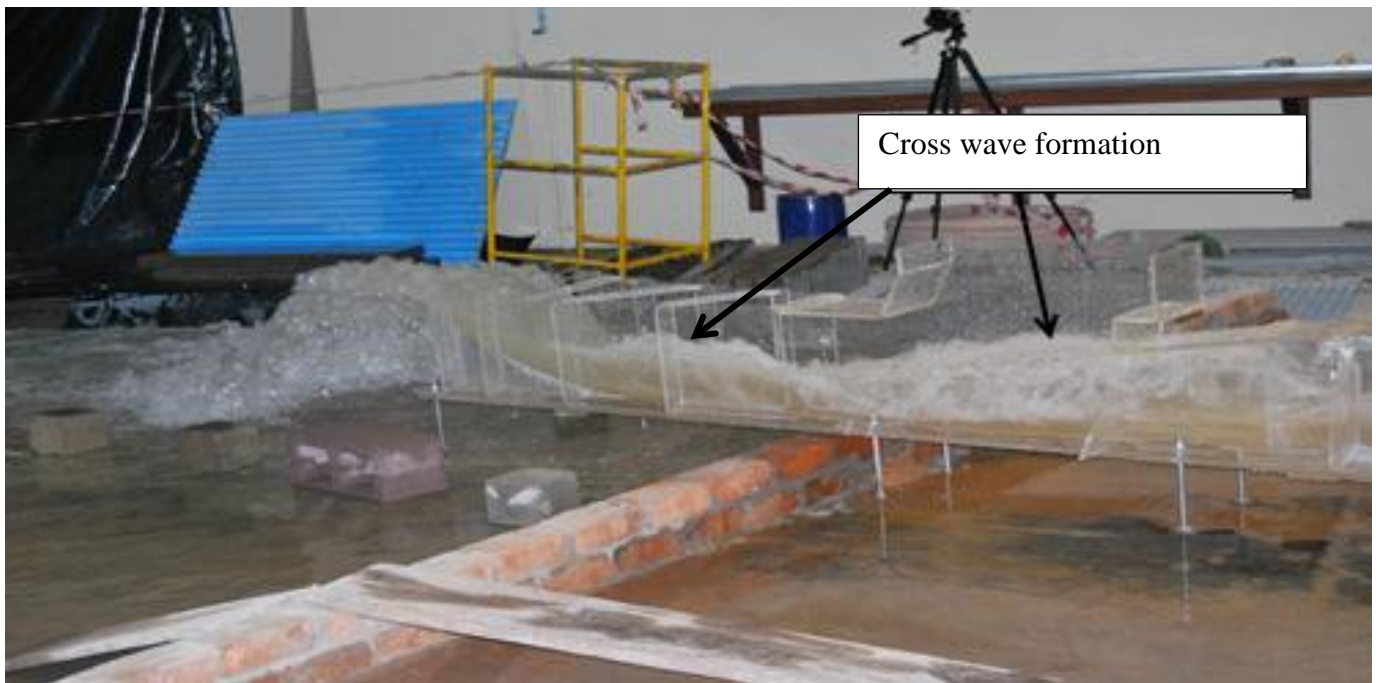
Figure 5.1.4-1B: Flow pattern at ski jump and end box for 20% emergency gate opening
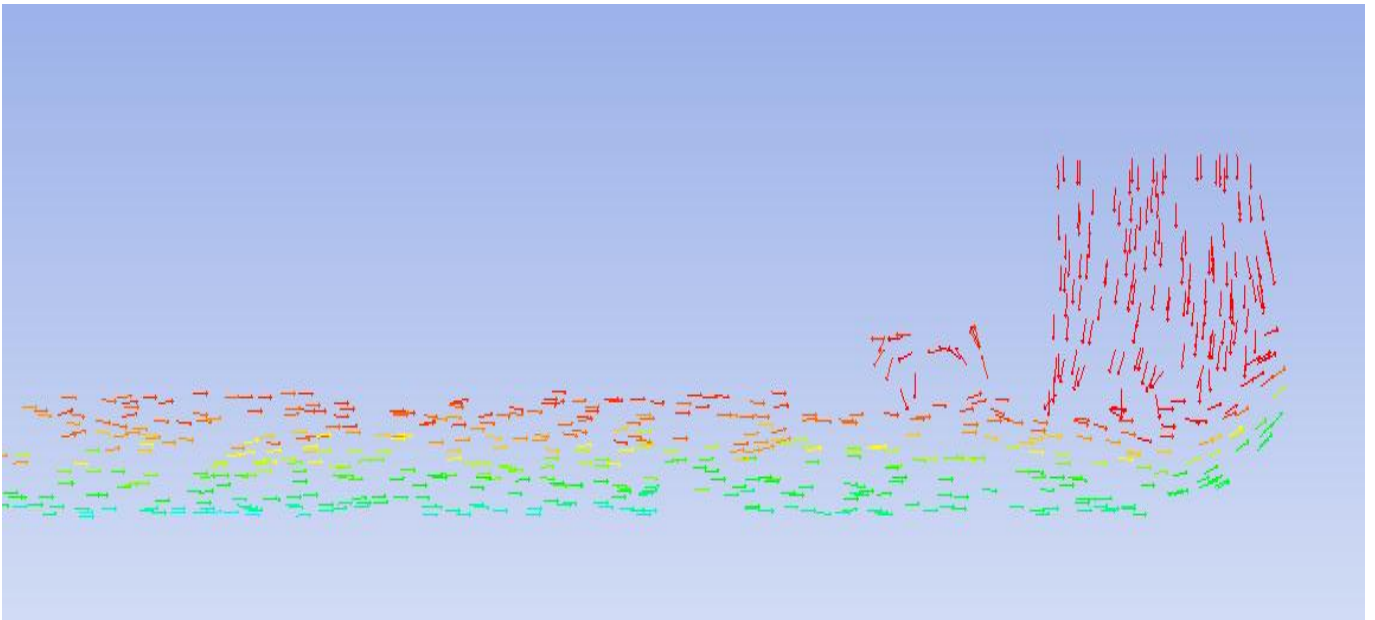
Figure 5.1.4-2A: Velocity vectors at the ski jump for 30% emergency gate opening

Cross waves

 Figure 5.1.4-2B: Flow pattern at ski jump and end box for 30% emergency gate opening
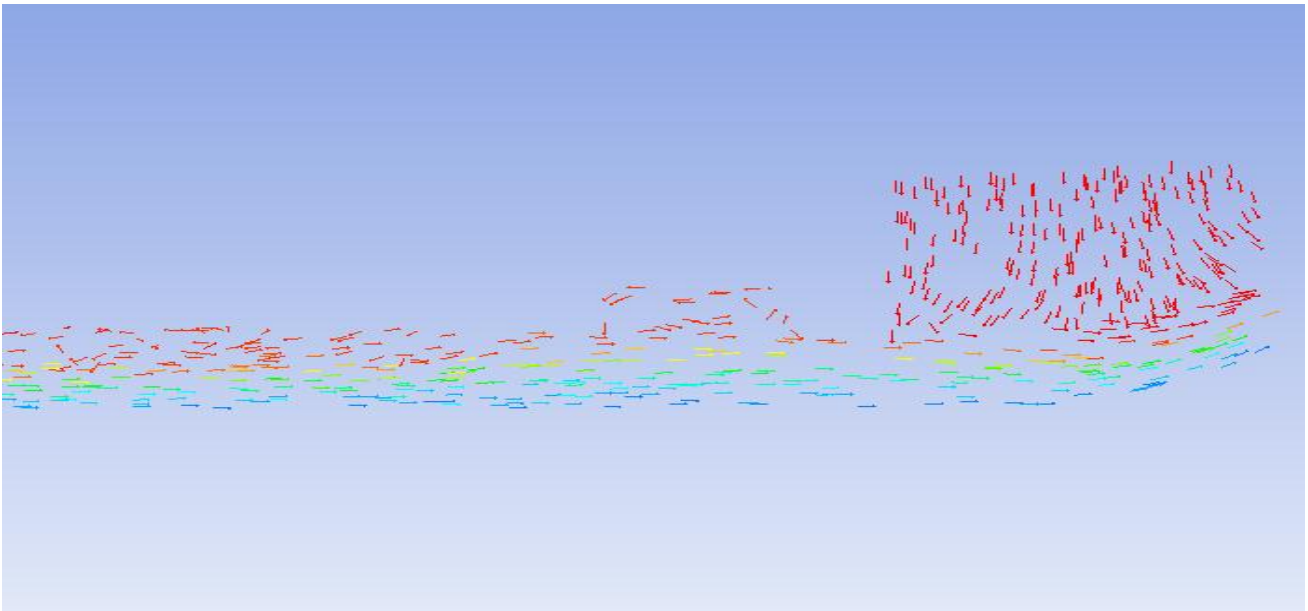
Figure 5.1.4-3A: Velocity vectors at the ski jump for 40% emergency gate opening

Figure 5.1.4-3B: Flow pattern at ski jump and end box for 40% emergency gate opening
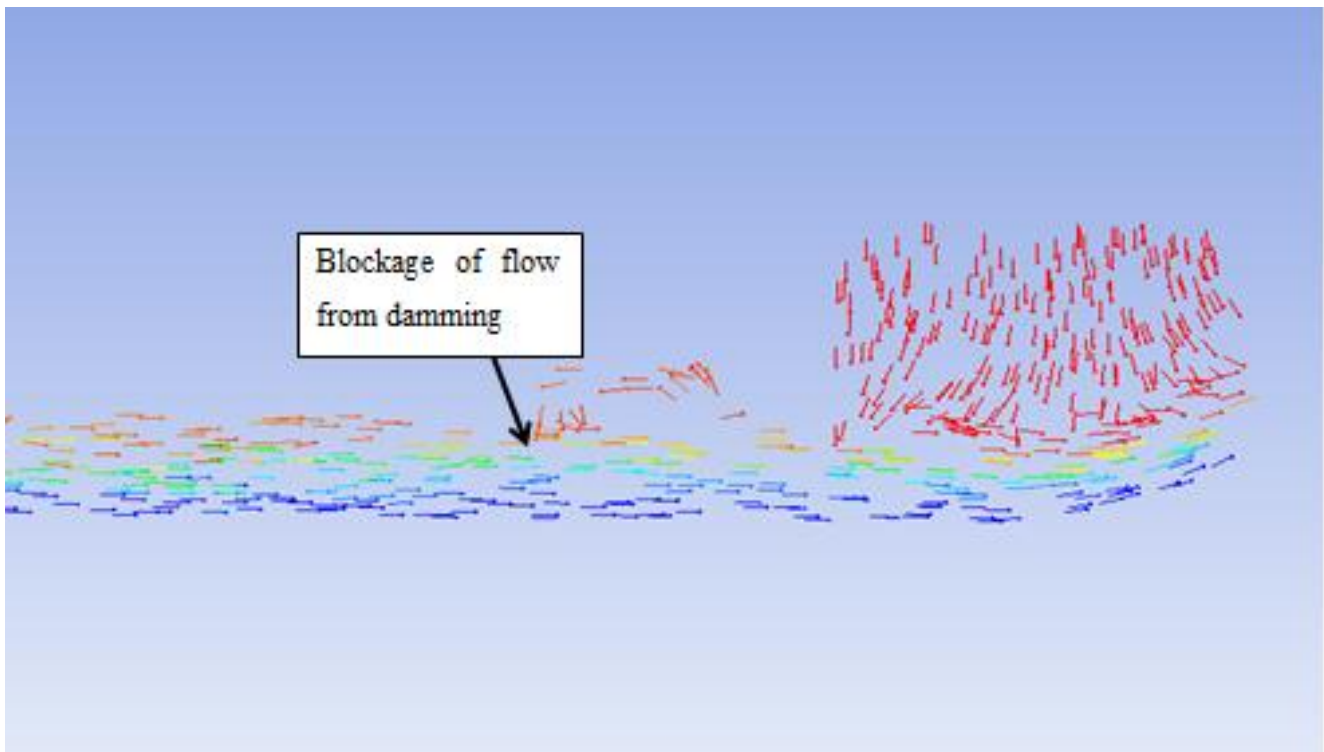
Figure 5.1.4-4A: Velocity vectors at the ski jump for 50% emergency gate opening

Figure 5.1.4-4B: The ski jump for 50% emergency gate opening (Physical)

Figure 5.1.4-5A: Velocity vectors at the ski jump for 60% emergency gate opening (numerical)

Figure 5.1.4-5B: The ski jump for 60% emergency gate opening (Physical)
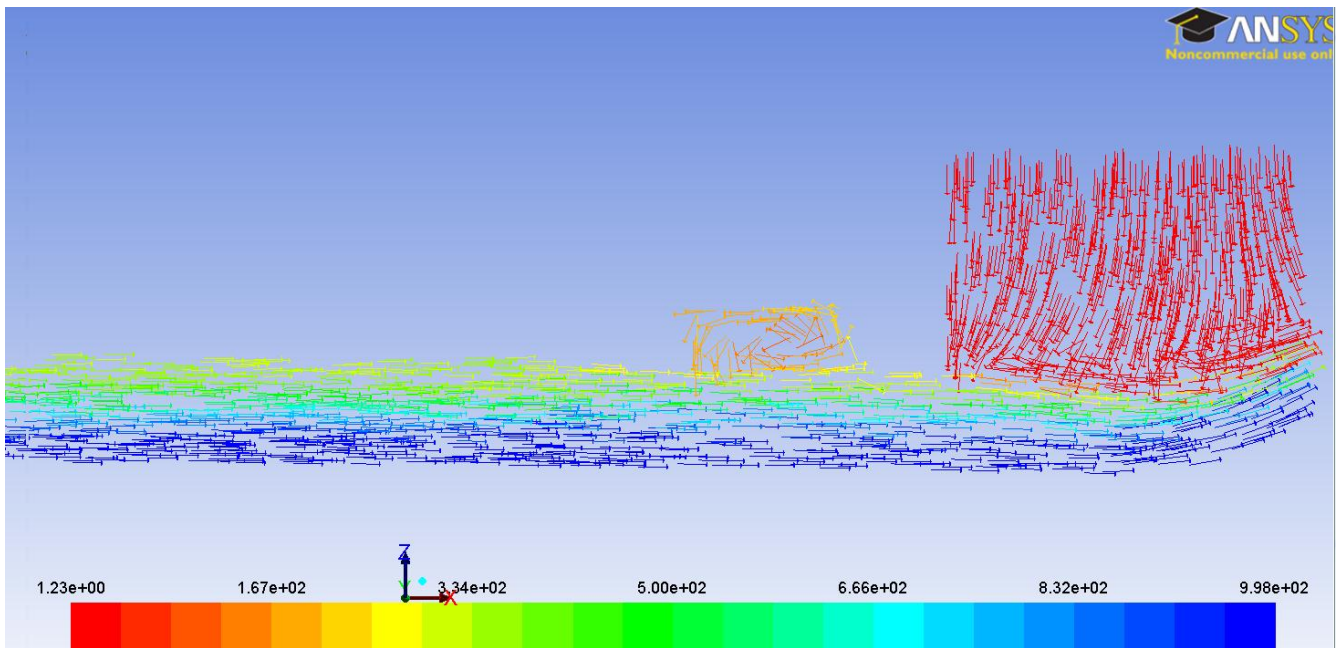
Figure 5.1.4-6A: Velocity vectors at the ski jump for 70% emergency gate opening

Figure 5.1.4-6B: The ski jump for 70% emergency gate opening (Physical)

84

Visually, from the colour coding, for the 50% gate opening (Figure 5.1.4-4A) and onwards, the flow appears to have less air entrained in 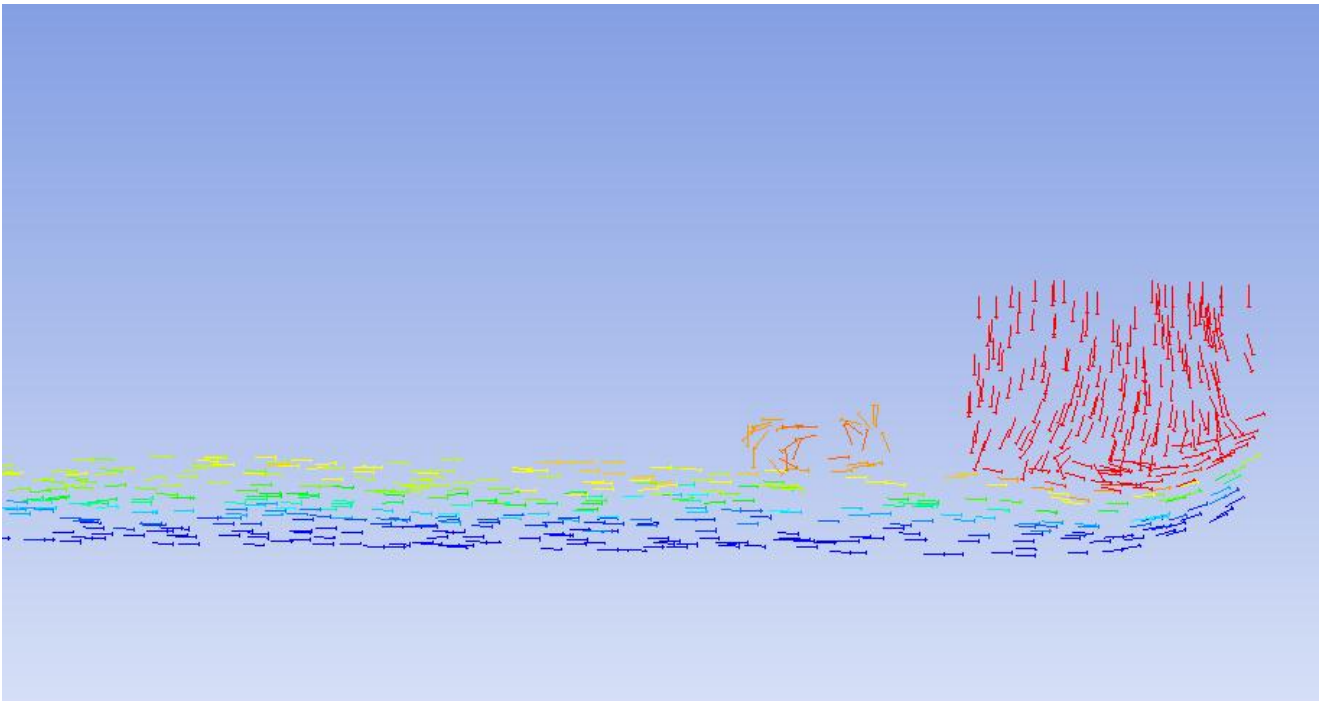it and the pipe still appears to be flowing partially full with the most air trapped at the surface of the flow. The flow seems to block the smaller cross-section after the last bend and upstream of the ski jump, at the beginning of the end box due to the narrowing of the pipe (Figure 5.1.4-4A/4B) which causes a contraction to the flow of air and water.

For 60% and 70% emergency gate openings (Figure 5.1.4-5A and 5.1.4-6A), the pipe appears to be flowing full downstream of the emergency gate, with densities ranging from 500 kg/m^3 to 998.2 kg/m^3. There is, however, still air entrained in the flow as can be seen from the varying densities (yellow and green representing the air-water mix and blue representing water). The conduit is flowing full and there is circulation of air above the flow on the ski jump.

5.1.5 Pressure contours in domain

Figure 5.1.5-1 below shows the contours of pressures developed in the domain for the 20% emergency gate opening. Other figures for the different gate openings have not been included because they look exactly the same as the one below but the differences are in the values of the results generated.

The pressure varies from 4m of water at the bottom of the reservoir (represented by red) and 0.2m of water at the top of the reservoir (represented by light green).
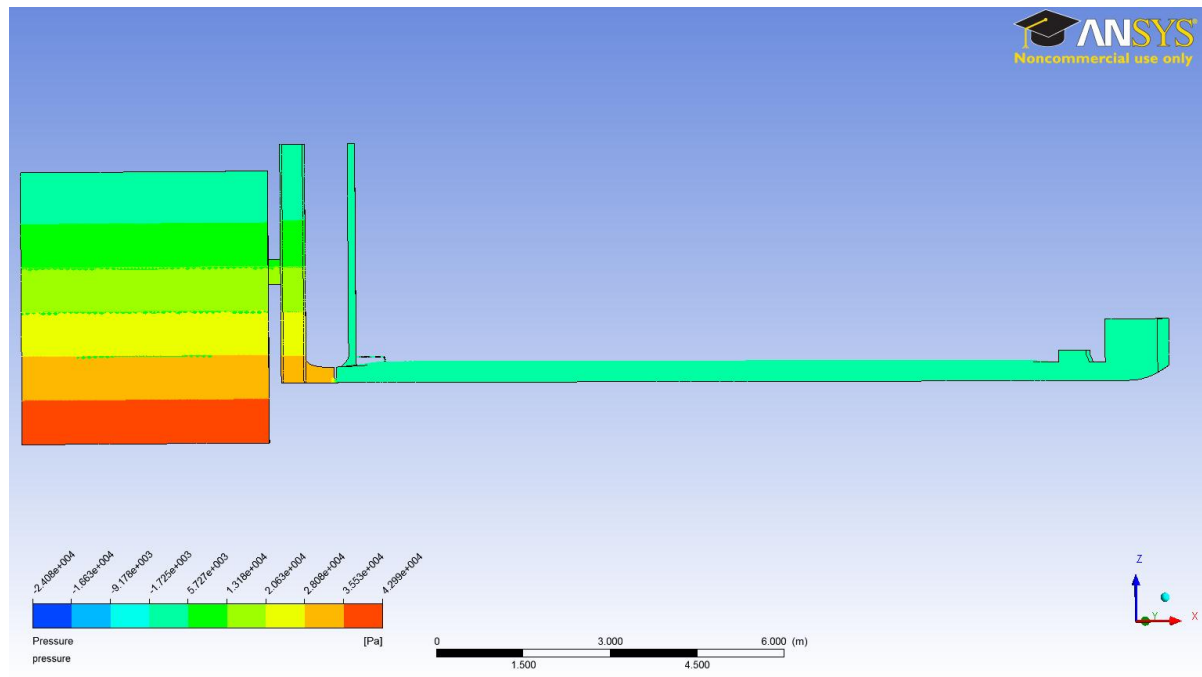
Figure 5.1.5-1: Static pressure contours for 20% emergency gate opening

85

These very coarse pressure contours (Figure 5.1.5-1) indicate that the pressures in the reservoir and the wet well are the same, the highest pressure being experienced at the bottom of the reservoir. However, as the flow issued underneath the emergency gate, the pressures began to vary further on in the conduit although this is not evident in the caption because the contours are too coarse.

At 20% emergency gate opening, downstream of the emergency gate, along the length of the conduit, pressures vary between 0.176m below and 1.346m above gauge pressure (numerical model values). Since the initial condition for pressure in the model was set to atmospheric pressure, values of pressure below zero were taken as being below atmospheric pressure.

At 30% emergency gate opening, the pressures in the conduit vary between 0.517m below and 1.116m above gauge pressure (numerical model values), with the negative pressures being experienced mainly downstream of the emergency gate and at the floor of the ski jump.

At 40% emergency gate opening, negative pressures in the order of 0.26m below gauge pressure (numerical model values) were modelled downstream of the emergency gate and 1.059m above gauge pressure (numerical model values) further on in the conduit up to the ski jump for the given conditions.

At 50% emergency gate opening the pressures downstream on the floor of the conduit vary between 0.38m below and 0.976 above gauge pressure (numerical values). Negative pressures are also shown on the floor of the ski jump which is surprising as this is a concave surface.

For the 60% emergency gate opening the pressures on the floor of the conduit vary between 0.328m below and 1.01 m above gauge pressure(numerical model values) and for the 70% emergency gate opening the pressures vary between 0.325m below and 2m above atmospheric pressure (numerical model values).

5.1.6   Pressure contours at the emergency gate and air vent region

The following figures display the pressure contours in the region of the emergency gate at the the base of the air vent where connects to the conduit for gate openings of 20%, 30%, 40%, 50%, 60% and 70%. It should be noted that the colour scales for the pressures shown in Figures 5.1.6-1 to 5.1.6-6 below are not consistent.
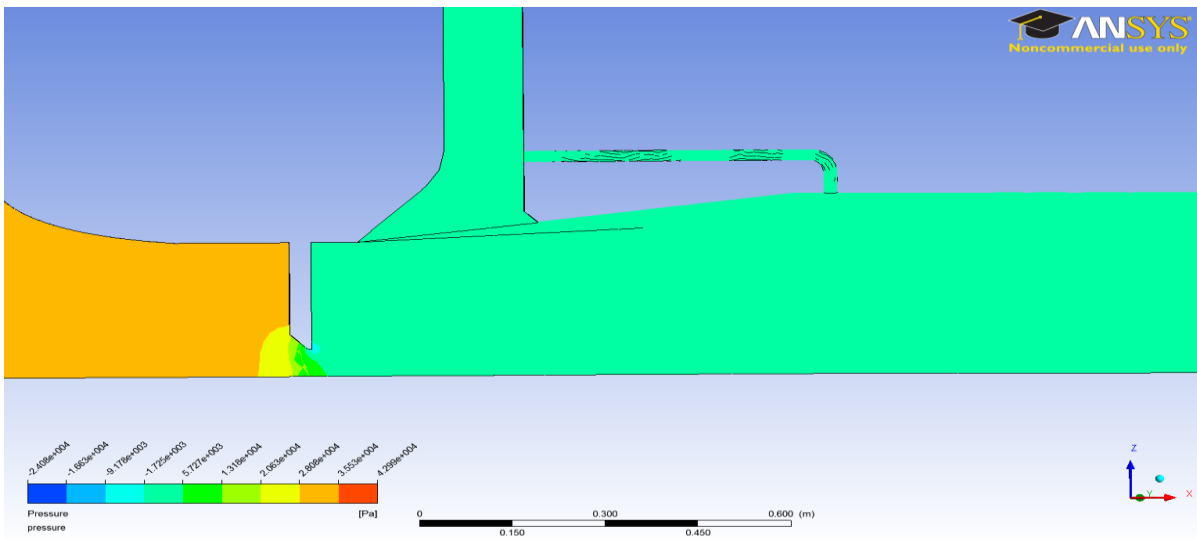
Figure 5.1.6-1: Static pressure contours at emergency gate and air vent region for 20% emergency gate opening

The numerical results of the simulation showed that negative pressures develop at the downstream side of the gate lip.

For the 20% emergency gate opening, shown in Figure 5.1.6-1, pressures of up to 0.176m below gauge pressure (numerical model values) were observed on the gate lip.
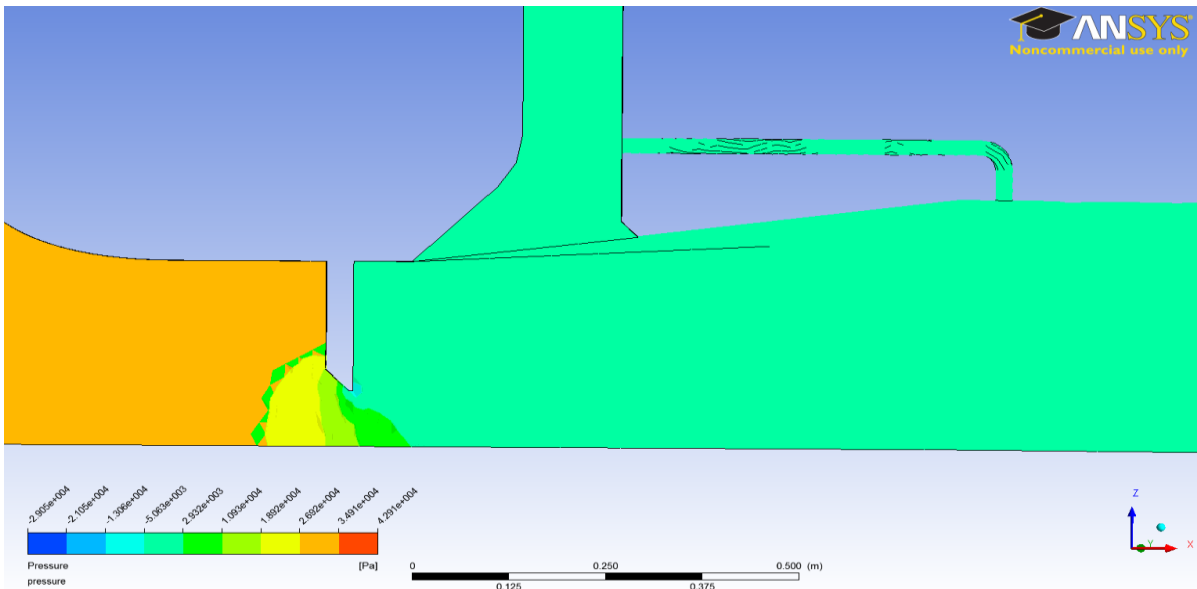
Figure 5.1.6-2: Static pressure contours at emergency gate and air vent region for 30% emergency gate opening

87

At 30% emergency gate opening, shown in Figure 5.1.6-2, there were no negative pressures shown upstream of the emergency gate but pressures of up to 0.52m below gauge pressure were shown on the downstream side of the gate lip.

At 40% emergency gate opening, as seen in Figure 5.1.6-3 below, pressures of up to 0.267m below gauge pressure were shown on the downstream side of the gate lip.

At 50% emergency gate opening, as seen in Figure 5.1.6-4 below, pressures of up to 0.38m below gauge pressure were observed on the downstream side of the gate lip.

Figure 5.1.6-3: Static pressure contours at emergency gate and air vent region for 40% emergency gate opening

The pressure contours shown in Figure 5.1.6-1 to 5.1.6-6 show how the pressures reduce from the upstream to the downstream of the emergency gate.
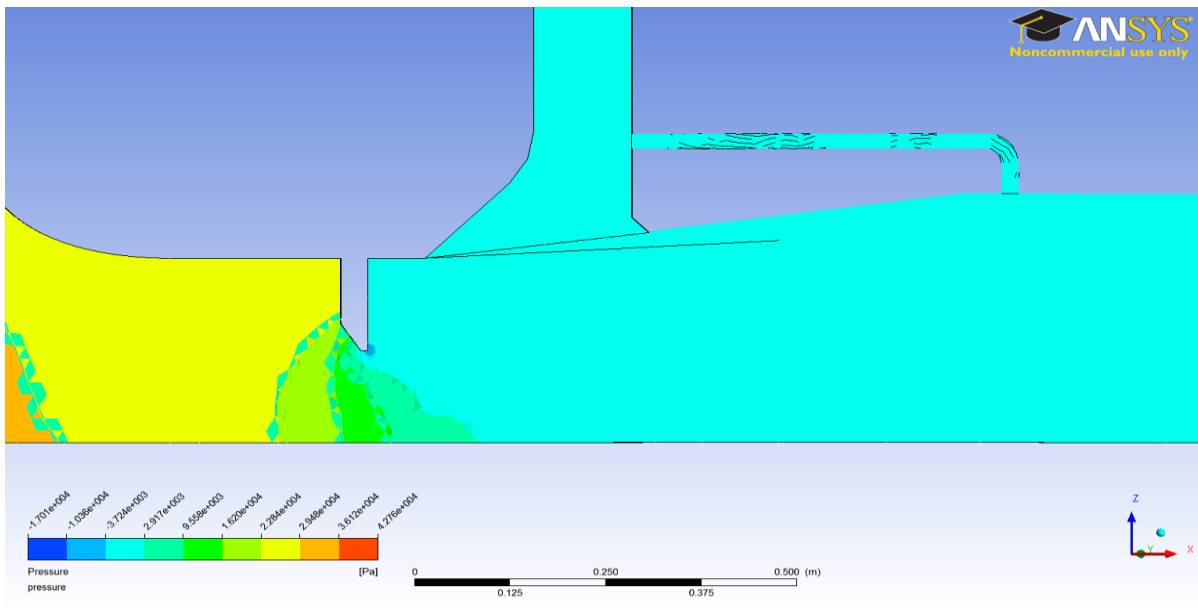
Figure 5.1.6-4: Static pressure contours at emergency gate and air vent region for 50% emergency gate opening
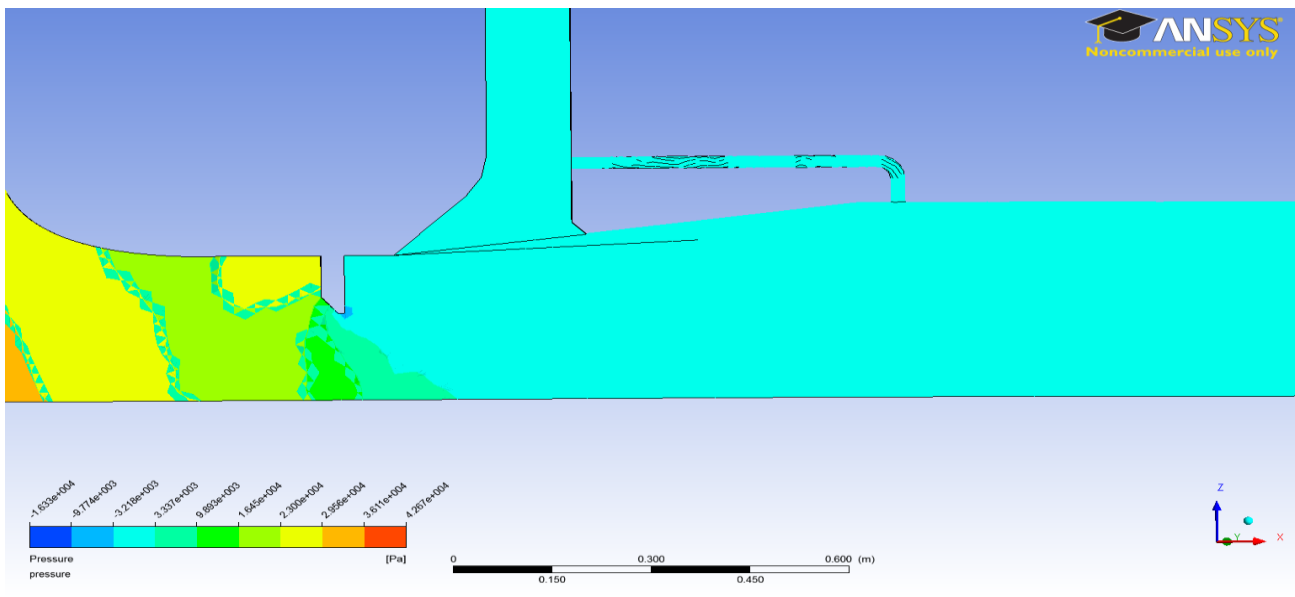
Figure 5.1.6-5: Static pressure contours at emergency gate and air vent region for 60% emergency gate opening

At 60% emergency gate opening, as seen Figure 5.1.6-5 above, pressures of 0.33m below gauge pressure were shown on the downstream side of the gate lip and as mentioned in Section 5.1.5, negative pressures were shown to occur further downstream in the conduit.
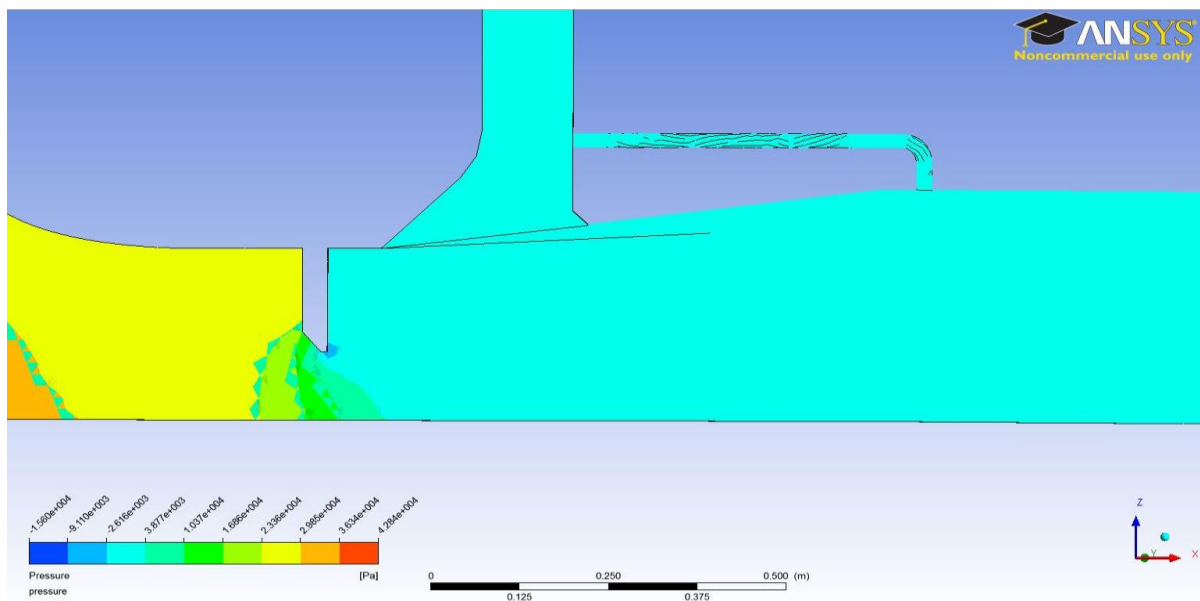
89
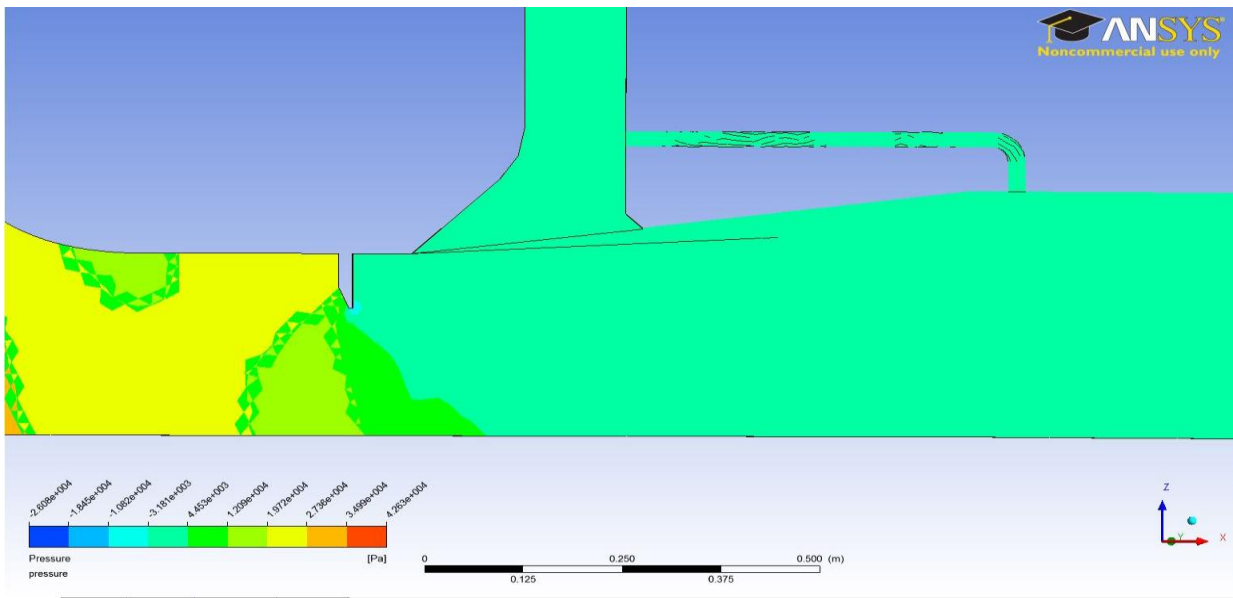
Figure 5.1.6-6: Static pressure contours at emergency gate and air vent region for 70% emergency gate opening

At 70% emergency gate opening, negative pressures up to 0.325m below atmospheric pressure (numerical values) were determined at the downstream end of the gate lip although these are not shown on Figure 5.1.6-6.

Table 5.1.6-1 below summarises the gate lip pressures determined for the various emergency gate openings.

Table 5.1.6-1: Simulated negative pressures at the emergency gate lip

Emergency gate opening (%)	Pressure at gate lip (m)
20	-0.176
30	-0.520
40	-0.467
50	-0.380
60	-0.330
70	-0.325

Figure 5.1.6-7 below graphs the negative pressures for the various gate openings.
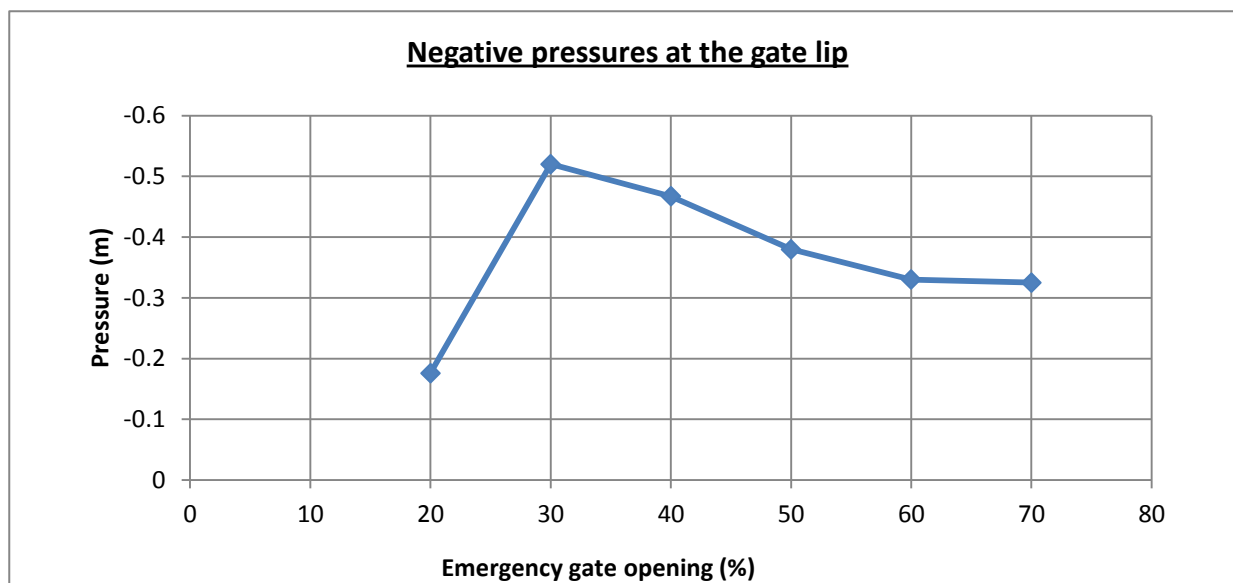
Figure 5.1.6-7: Plot of negative pressures at the emergency gate lip for different gate openings (Note: Magnitude of negative pressures is considered)

Borodina (Borodina, 1969) suggests that negative pressures lips reduce with increasing gate opening since the amount of air entrained in the water decreases as the discharge increases. The conduit begins tof low full. Figure 5.1.6-7 above, indicates that this is the case but however, the negative pressure for the 20% emergency gate opening is not consistent with Borodina's hypothesis. There is no explanation for the inconsistent pressure for the 20% emergency gate opening but it might be safe to conclude that emergency gate openings below 30% are critical. Such pressures at the gate lip might cause adverse cavitation effects if they are less than atmospheric pressure, however, this would not be the case for the prototype.

Gate openings less than 20% could not be tested on the physical model for fear of damage to the model, as had been experienced before in previous tests of the model.

5.1.7   Streamlines

The following figures display the velocity streamlines for static gate openings of 20%, 30%, 40%, 50%, 60% and 70%. The streamlines show the progression of the flow in the domain.
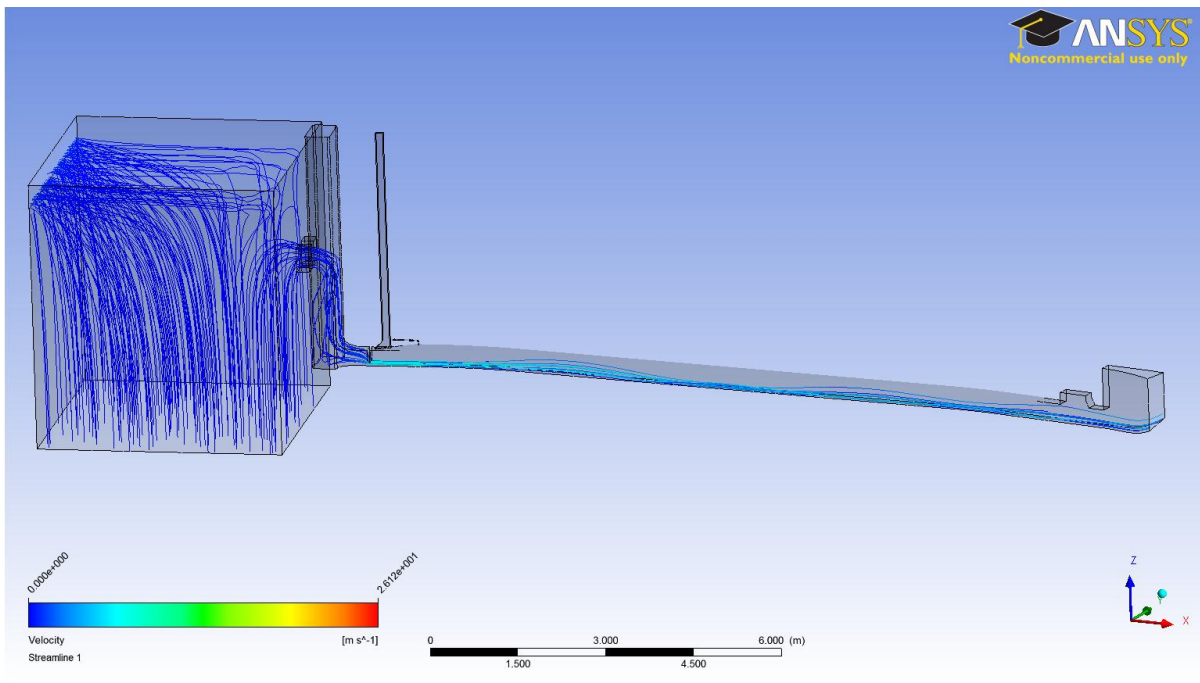
Figure 5.1.7-1: Velocity streamlines for 20% emergency gate opening

The streamlines originating from the bottom of the reservoir upward show how the reservoir fills up from the bottom.
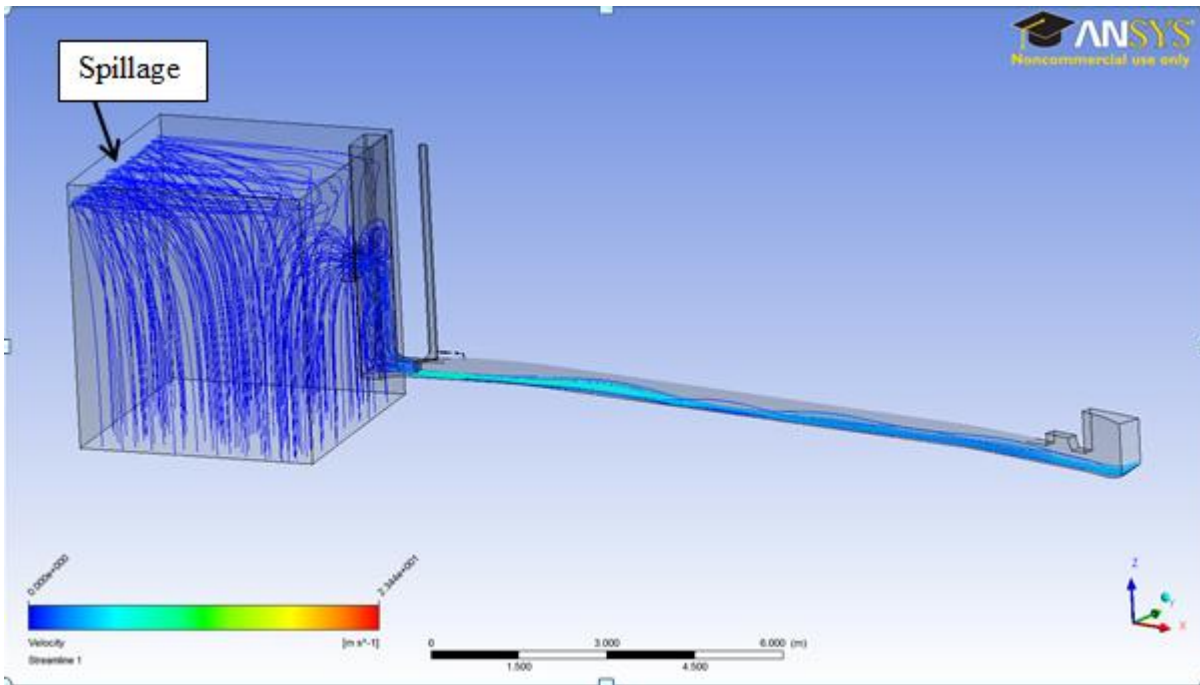
Figure 5.1.7-2: Velocity streamlines for 30% emergency gate opening

92

As expected (Figures 5.1.7-1 to 5.1.7-6), the number of streamlines increases with increasing emergency gate openings due to the increase in discharge. Also, there is increased swirling flow as the flow fills up in the wet well tower due to the increase in flow through the selector gates.
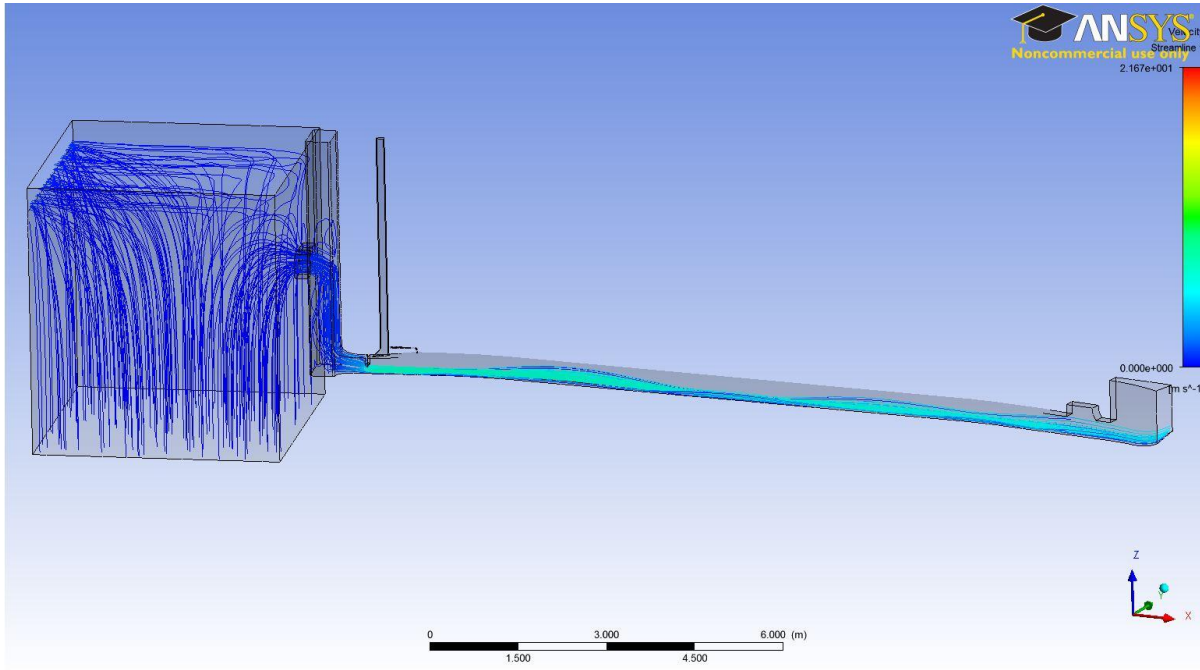
Figure 5.1.7-3: Velocity streamlines for 40% emergency gate opening
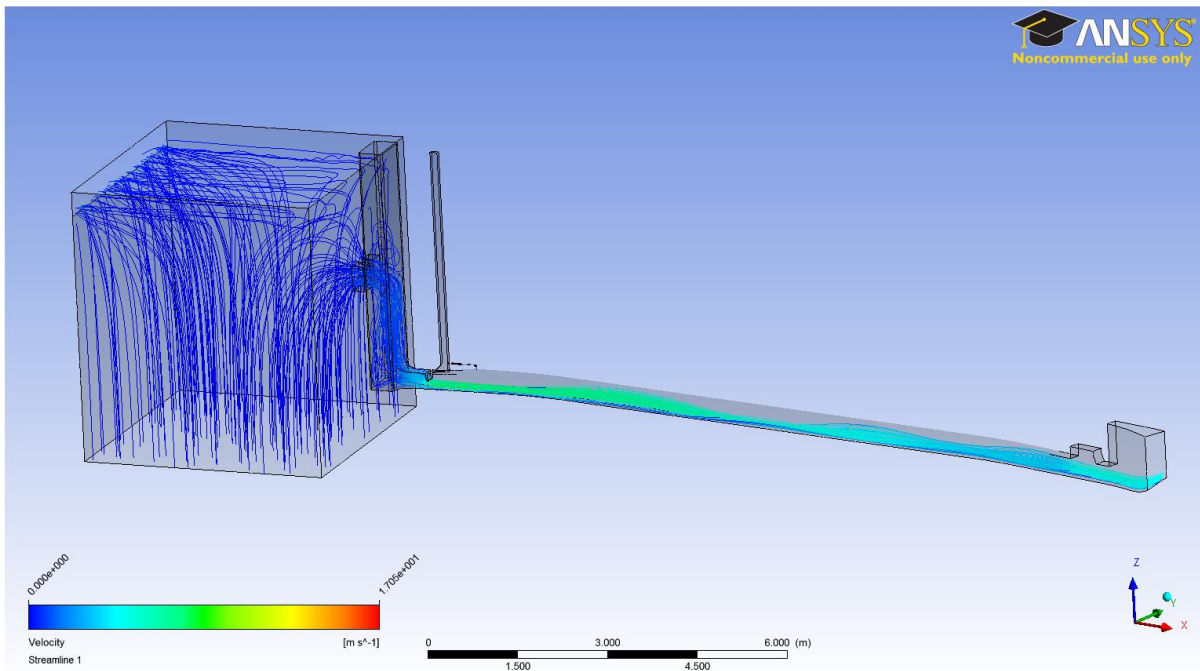
Figure 5.1.7-4: Velocity streamlines for 50% emergency gate opening

The figures also show the high velocities of the water at the emergency gate and the reduced velocities as it flows through the conduit. This may be attributed to the variation in flow area.
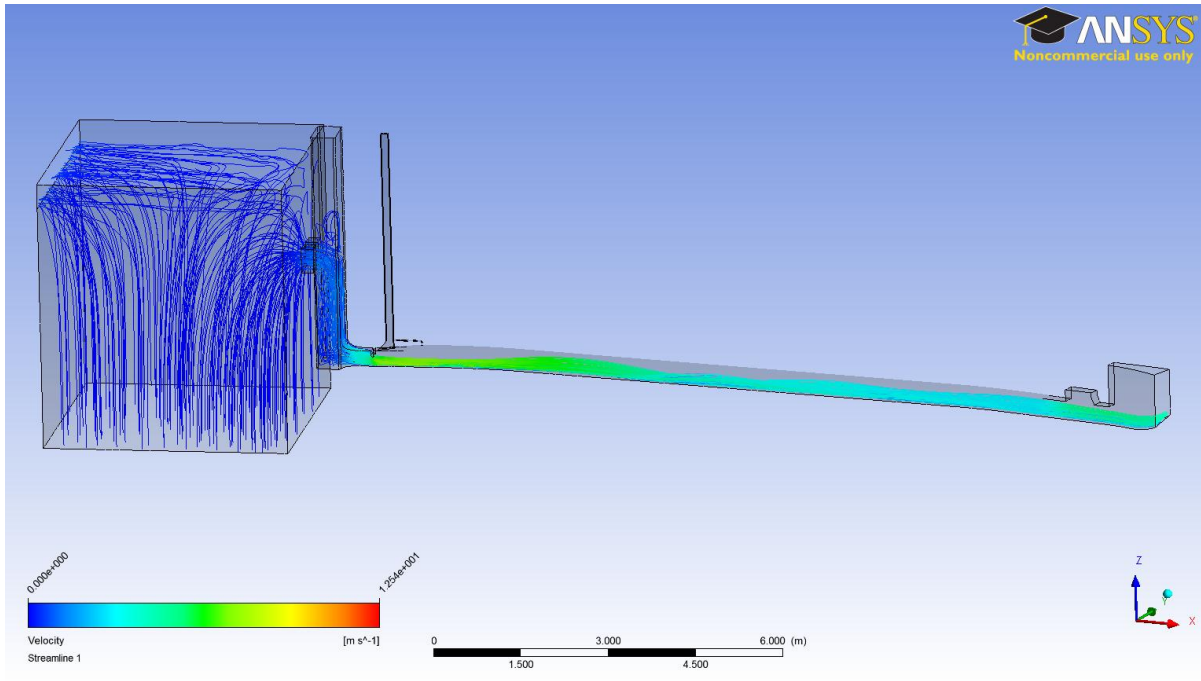
Figure 5.1.7-5: Velocity streamlines for 60% emergency gate opening
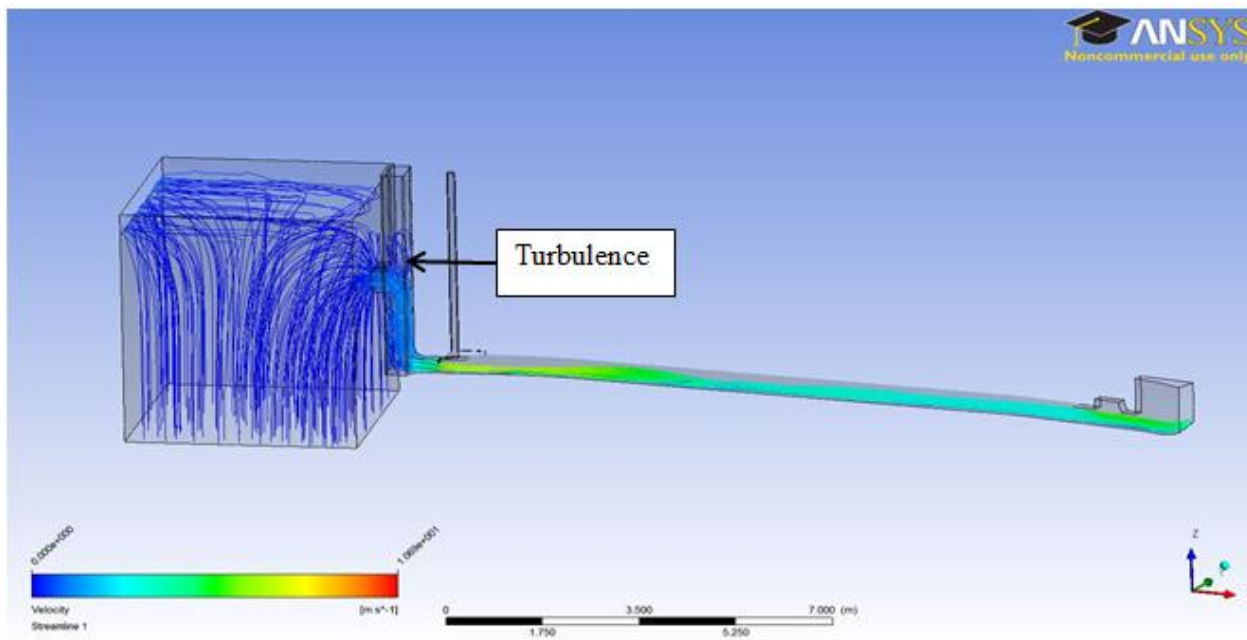
Figure 5.1.7-6: Velocity streamlines for 70% emergency gate opening

5.1.8   Flow patterns at the bends

The figures below show the velocity vectors, coloured by density, at the first bend (12 degrees) downstream of the emergency gate and at the second bend (8 degrees) upstream of the radial gate housing for the various emergency gate openings.

The figures also show the nature of flow in the wet well tower above. For some gate openings it was possible to see the swirling effect of the flow in the tower.
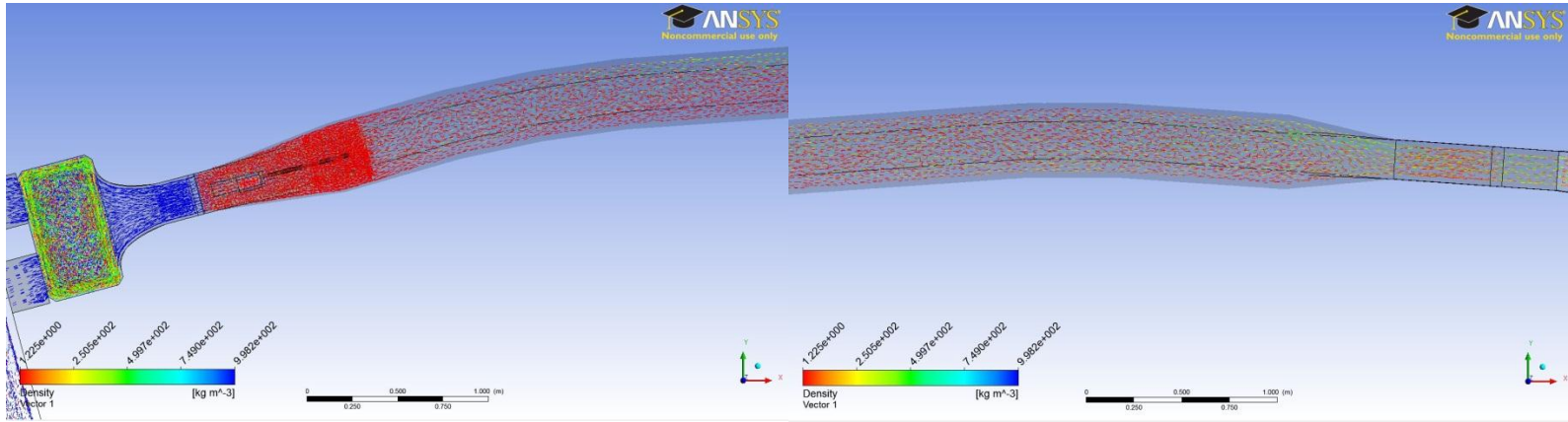
Figure 5.1.8-1: Plan view of velocity vectors at bends and wet well for 20% emergency gate opening
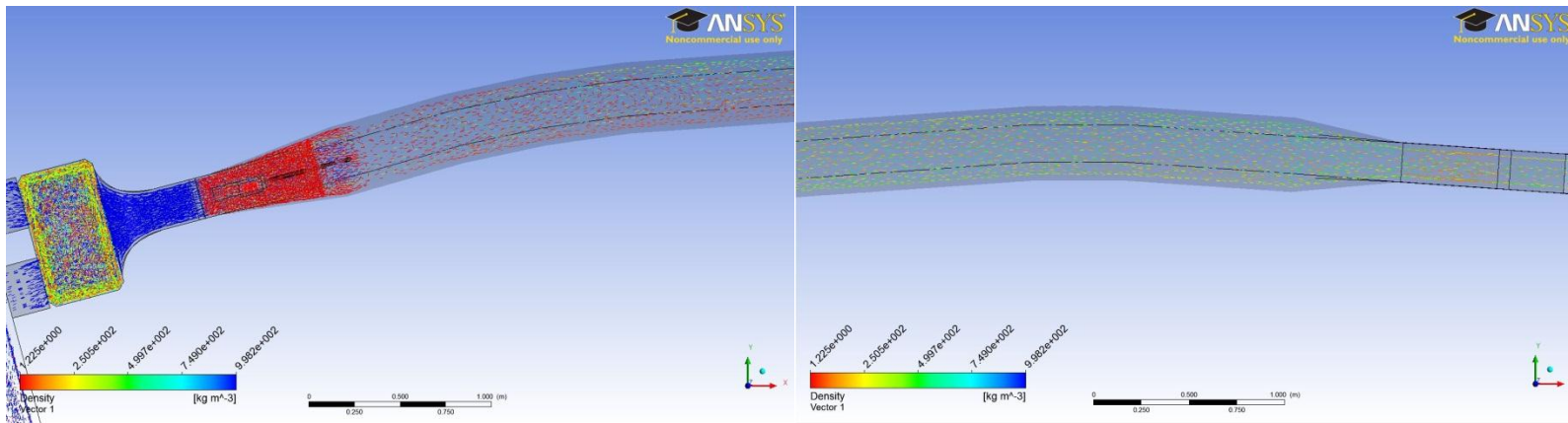
Figure 5.1.8-2: Plan view of velocity vectors at bends and wet well for 30% emergency gate opening
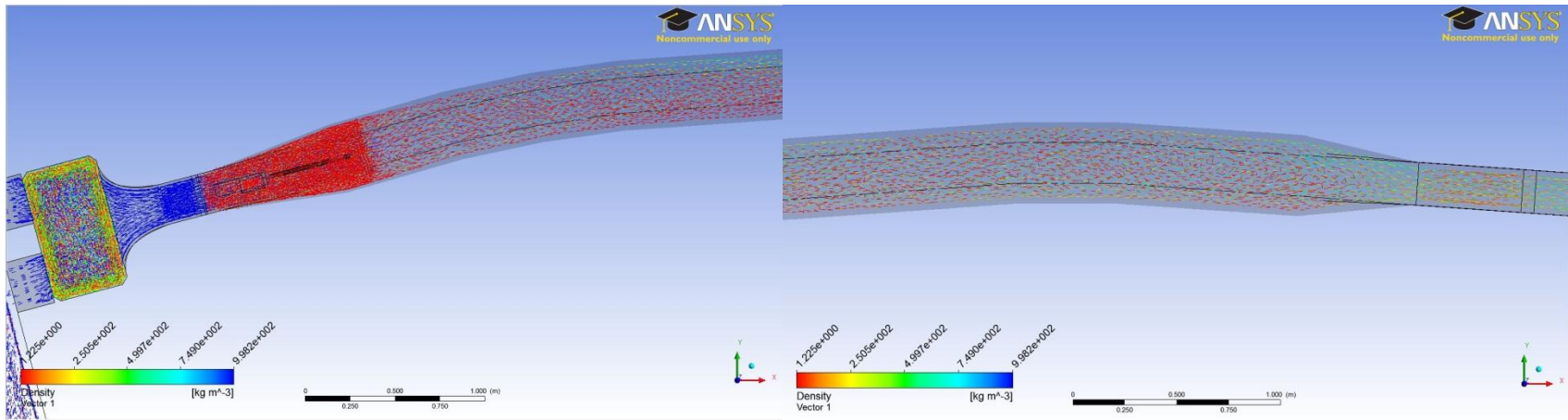
Figure 5.1.8-3: Plan view of velocity vectors at bends and wet well for 40% emergency gate opening
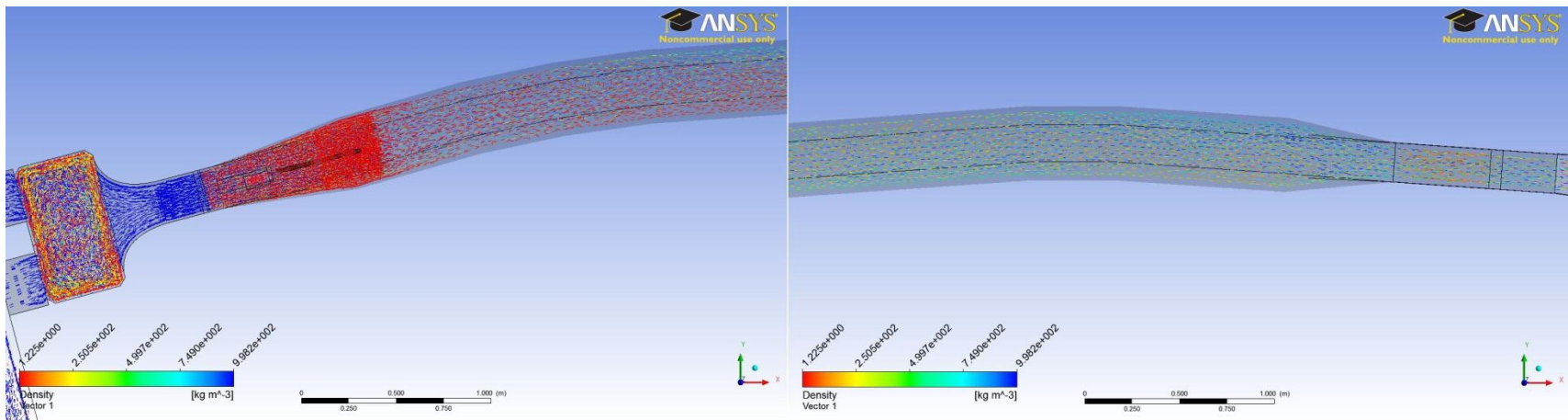
Figure 5.1.8-4: Plan view of velocity vectors at bends and wet well for 50% emergency gate opening

97
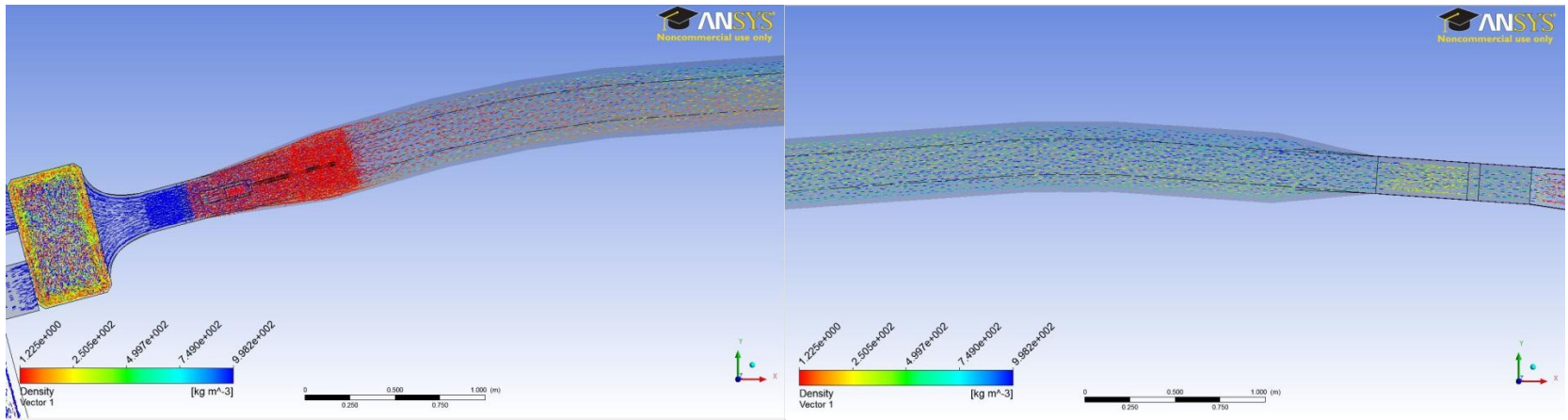
Figure 5.1.8-5: Plan view of velocity vectors at bends and wet well for 60% emergency gate opening
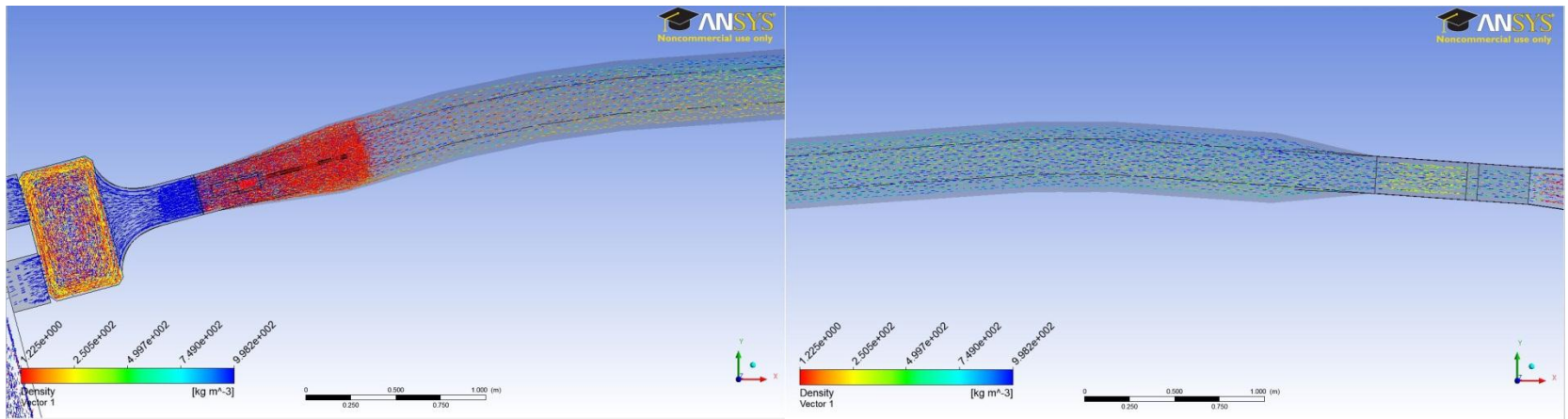
Figure 5.1.8-6: Plan view of velocity vectors at bends and wet well for 70% emergency gate opening

The purpose of showing the flow at the bends was to establish whether they influenced the nature of the flow in the conduit.

At 20% and 30% emergency gate openings, Figures 5.1.8-1 and 5.1.8-2, the results showed that the first and second bends introduced slight changes in flow density possibly on account of the super elevation and cross waves that would occur.

For gate openings of 40% and more (Figures 5.1.8-3 to 5.1.8-6), the flow across the bends appeared undisturbed. There was damming of highly aerated flow at different parts of the conduit that could be mistaken for a hydraulic jump it was established that the flow in the outlet structure was supercritical. The fluid in the wet well was shown to be rotational and swirly. Such behaviour of the flow could contribute to the formation of vortices that are known to entrap a lot of air (Borodina, 1969). From the animations created of the simulations, no vortices were observed in the wet well but there was horizontal rotational flow on the surface of the water in the tower.

5.2 Graphical and tabulated results

5.2.1 Discharge

For the CFD numerical model, the discharge into the wet well from the reservoir was determined by placing three velocity point monitors at the selector gates at the entrance to the wet well and the average of these results used to determine the discharge. The same method was also used to determine the discharge at the emergency gate. Results showed that there were unexpected differences in the obtained values although steady state had been attained. The results are shown in Table 5.2.1-1 below and graphically represented in Figure 5.2.1-1.

Table 5.2.1-1: Comparison of discharges from the numerical and the physical model

CFD Numerical model results								(1)	(2)
Emergency gate opening (%)	Emergency gate velocity (m/s)	Emergency gate area (m²)	Emergency gate discharge (m³/s)	Selector gate velocity (m/s)	Selector gate area (m²)	Selector gate discharge (m³/s)	Physical model discharge (m³/s)	Percentage discharge error at Emergency gate (%)	Percentage discharge error at selector gates (%)
20	8.13	0.01	0.10	0.50	0.24	0.12	0.070	30	42
30	7.56	0.02	0.14	0.75	0.24	0.18	0.107	23	41
40	7.99	0.02	0.20	0.90	0.24	0.22	0.141	28	35
50	6.49	0.03	0.20	1.05	0.24	0.25	0.170	15	33
60	6	0.04	0.22	1.50	0.24	0.36	0.203	8	44
70	5.79	0.04	0.25	1.74	0.24	0.42	0.240	4	43

(1) CFD Emergency gate discharge and Measured Physical model discharge:

$$100 \times \left(\frac{CFD\ Emergency\ gate\ discharge - Measured\ Physical\ model\ discharge}{CFD\ Emergency\ gate\ discharge} \right)$$

(2) CFD Selector gates discharge and Measured Physical model discharge:

$$100 \times \left(\frac{CFD\ Selector\ gates\ discharge - Measured\ Physical\ model\ discharge}{CFD\ Selector\ gates\ discharge} \right)$$
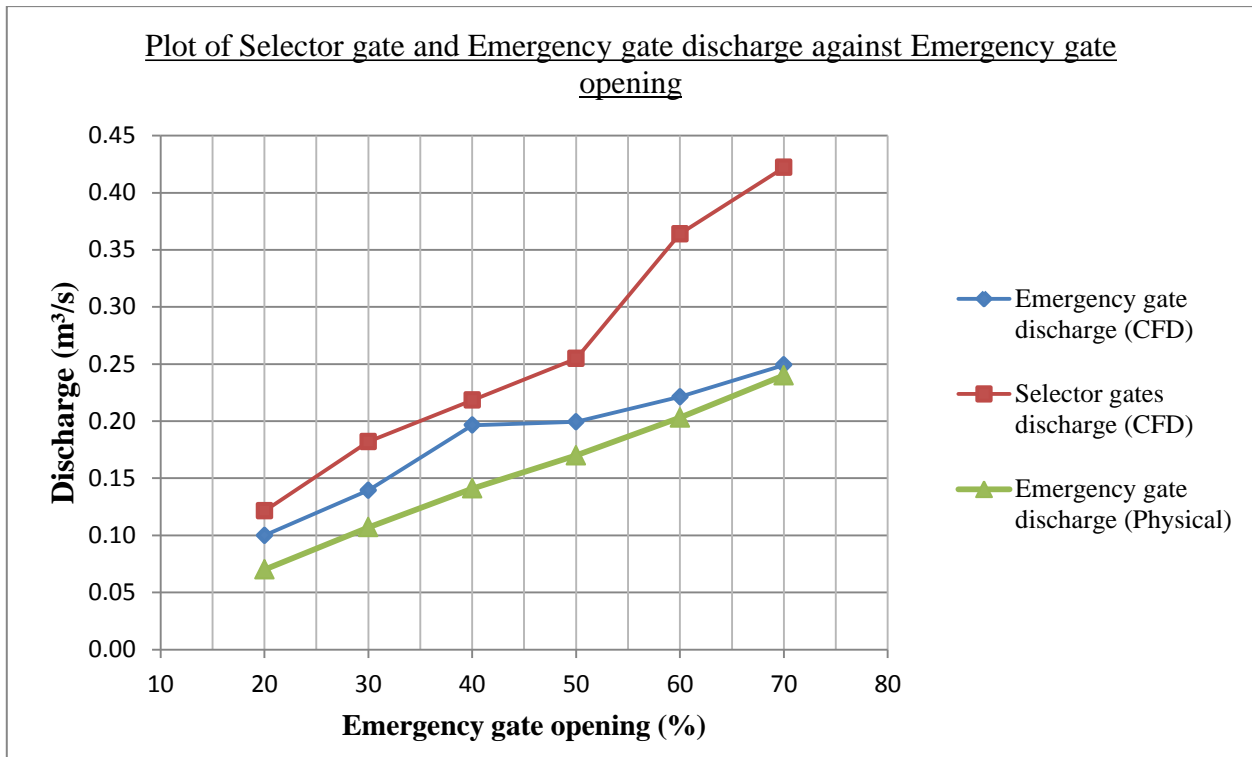
Figure 5.2.1-1: Discharge through selector and emergency gate

Whereas as the trend in results is similar (Figure 5.2.1-1), there are significant differences in discharge results especially for the CFD selector gate discharge and the measured emergency gate discharge. It is not certain why there are such large differences in the CFD discharge results at the selector gates and the emergency gate of the CFD model since mass balance was attained before results were extracted from the simulations. A viable excuse would be the errors and uncertainties of CFD modelling as explained in Section 1.2.1 (Veersteg et. al., 2007). The CFD results also differ from the measured discharge results probably due to errors in measurement of the flows in the physical model. However, the numerical results for the emergency gate discharge are closer to those from the physical model.

The CFD emergency gate discharge results were chosen for comparison to the physical and empirical calculated results because they were closer to those for the physical model which was used as a validation instrument in the research. Also, flow discharge underneath the gate directly affected the air discharge downstream of the emergency gate.

5.2.2   Air Entrainment

Results for the discharge, air velocity in the air vent, and aeration demand, from the CFD model were compared to those from the physical model and also to those generated from the empirical formulae for gate openings in bottom outlet structures based on the literature review cited above. Tables 5.2.2-1 and 5.2.2-2 show the air velocities determined for the CFD model and the physical model respectively.

In the empirical calculation of the contraction depth at the emergency gate, a contraction coefficient of 0.61 was assumed as recommended by Chadwick et. al., (2004) for free flow underneath sluice gates (Section 3.1.4.1). Also, in the empirical calculations, the gate discharge equation (Section 3.1.4.1) was used to determine the discharge of the outlet structure and Wisner's equation (Wisner, 1965) was used in calculating the aeration ratio as cited in the literature review (Section 3.1.4.2.1).

Table 5.2.2-1: Air velocities in the air vent from the CFD model

Emergency gate opening (%)	Emergency gate discharge (m³/s)	Emergency gate velocity (m/s)	Emergency gate discharge (m³/s)	Air vent velocity (m/s)	Air vent area (m²)	Air vent discharge (m³/s)	Aeration ratio (β)	Contracted flow depth (m)	Froude number, Fr
20	0.0999	8.13	0.0999	23.4100	0.0091	0.2130	2.1312	0.0330	14.2978
30	0.1394	7.56	0.1394	21.5600	0.0091	0.1961	1.4072	0.0494	10.8556
40	0.1964	7.99	0.1964	20.1500	0.0091	0.1833	0.9333	0.0659	9.9360
50	0.1994	6.49	0.1994	15.7800	0.0091	0.1436	0.7198	0.0824	7.2186
60	0.2213	6	0.2213	11.5300	0.0091	0.1049	0.4741	0.0989	6.0921
70	0.2491	5.79	0.2491	9.9200	0.0091	0.0902	0.3623	0.1154	5.4428

Table 5.2.2-2: Air velocities in the air vent from the physical model

Emergency gate opening (%)	Emergency gate discharge (m³/s)	Emergency gate velocity (m/s)	Air vent velocity (m/s)	Air vent area (m²)	Air vent discharge (m³/s)	Aeration ratio (β)	Contracted flow depth (m)	Froude number, Fr
20	0.070	5.6948	4.2550	0.0091	0.0387	0.5530	0.0330	10.0151
30	0.107	5.8032	5.5050	0.0091	0.0501	0.4681	0.0494	8.3330
40	0.141	5.7354	1.8770	0.0091	0.0171	0.1211	0.0659	7.1323
50	0.170	5.5321	3.1160	0.0091	0.0283	0.1668	0.0824	6.1531
60	0.203	5.5049	1.2500	0.0091	0.0114	0.0560	0.0989	5.5895
70	0.240	5.5785	0.2000	0.0091	0.0018	0.0076	0.1154	5.2440

In the empirical calculation, the discharge had to be determined first and then used to establish the air velocities in the air vent unlike in the numerical and physical models where the discharge was known. Table 5.2.2-3 shows the empirical calculations described before.

Table 5.2.2-3: Air velocities in the air vent from empirical calculations

Emergency gate opening (%)	Prototype emergency gate opening (m)	Scaled head on emergency gate (m)	Scaled gate opening (m)	Emergency gate discharge (m³/s)	Emergency gate velocity (m/s)	Contracted flow depth (m)	Froude number (F)	Aeration ratio (β)	Air vent velocity (m/s)
20	0.76	2.825	0.054	0.055	4.515	0.033	7.940	0.362	2.205
30	1.14	2.798	0.081	0.083	4.480	0.049	6.433	0.257	2.329
40	1.52	2.771	0.108	0.109	4.444	0.066	5.527	0.199	2.387
50	1.9	2.744	0.135	0.135	4.408	0.082	4.903	0.162	2.405
60	2.28	2.717	0.162	0.161	4.372	0.099	4.439	0.135	2.398
70	2.66	2.690	0.189	0.187	4.336	0.115	4.076	0.116	2.372

The CFD model results, the measured physical model results and the empirical results are compared in the figures below. Figure 5.2.2-1 plots the discharge through the emergency gate, Figure 5.2.2-2 plots the velocity in the air vent and Figure 5.2.2-3 plots the aeration ratios.
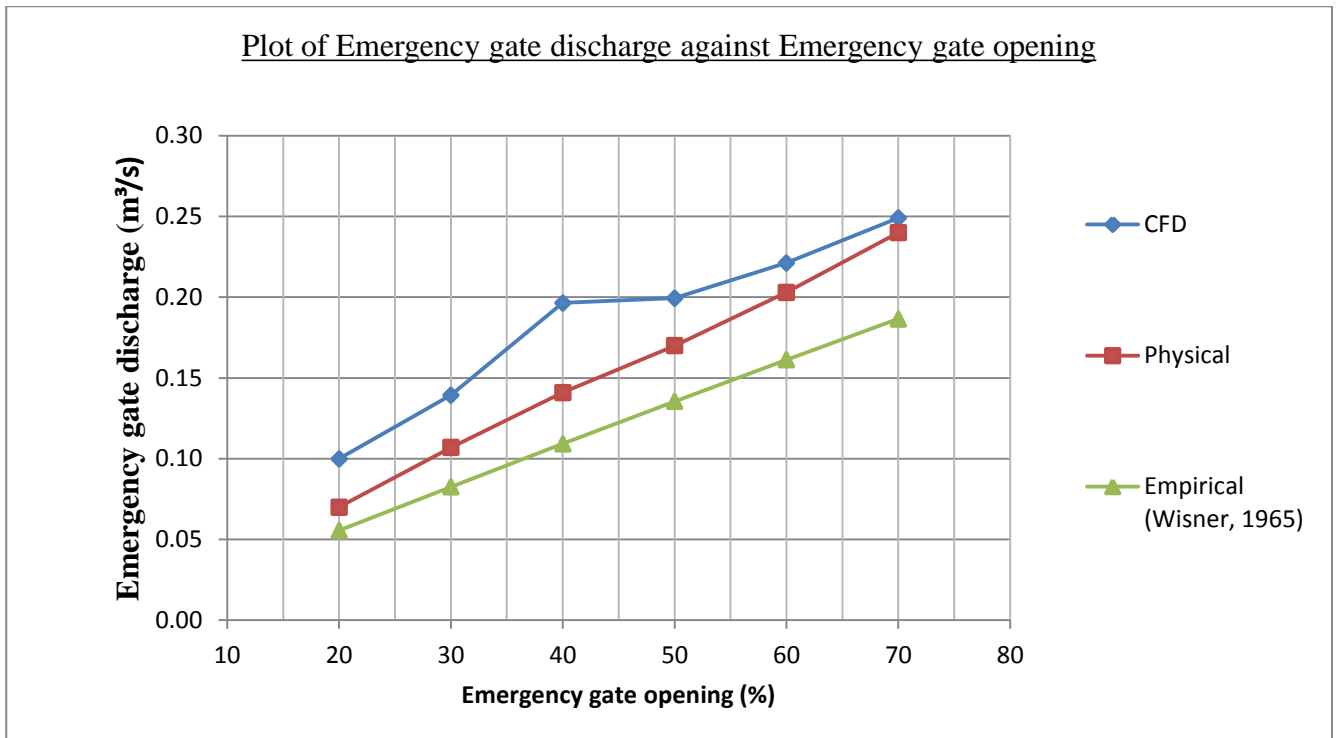
Figure 5.2.2-1: Discharge of the flow for different emergency gate openings

Figure 5.2.2-1 shows that the trend in results of the CFD model is similar to that for the physical model and the empirical calculations. However, the CFD model indicates higher results. These variations may be attributed to the errors and uncertainties common to most CFD models (Veersteg et. al., 2007).

Figure 5.2.2-1 also shows that he discharge increases with increasing emergency gate opening, but did not vary with time since simulations were for steady state. The CFD discharge results compared more closely with the physical model results for emergency gate openings larger than 50% whereas the empirical results compared better for gate openings less than 50%.

Figure 5.2.2-2 compares air flows in the air vent as determined with the CFD model, measured in the physical model and calculated empirically.

For the CFD model air flows in the air vent were determined from the velocity calculated at three locations in the mid-section of the air vent. The average of these velocities results was used for comparison with those from the physical model and calculated empirical.

The air velocity in the physical model was determined by placing an anemometer in the mid-section of the air vent which digitally sensed and recorded the air velocities. However, the anemometer was not able to record the direction of air flow so this was monitored by placing a piece of plastic sheet

106

in the mid-section of the air vent which blew upward or downward depending on the direction of air flow.

Figure 5.2.2-2 below shows the air velocities in the air vent for the CFD model, the physical model and the empirical calculations.
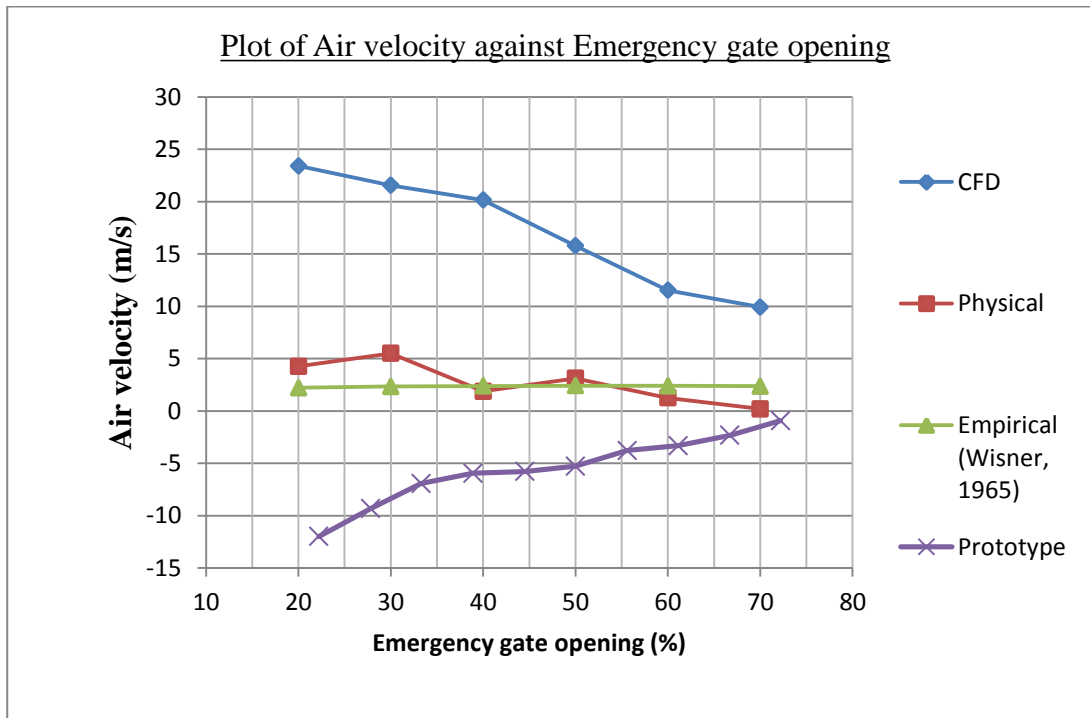
Figure 5.2.2-2: Air velocity in air vent for different emergency gate openings (Note: Positive velocity indicates air flow into the model)

In Figure 5.2.2-2, it can be seen that there is great variation in the air velocity values from the numerical model and those from the physical model despite the similar trend. The variation in values is probably partially due to the higher discharges from the numerical model. The air velocity decreases with increasing gate opening which implies that the aeration demand decreases with increasing gate opening. This is understandable because as the emergency gate openings increase, the pipe begins to flow full and there is less air entrained in the flow. It should be noted that in all cases (CFD and physical models), air was sucked into the air vent and not blown out as was the case with the prototype. The release of air from the prototype occurred under dynamic gate closure conditions when the reservoir was not full. The prototype results adjusted by scale factor for the physical model as also plotted on Figure 5.2.2-2.

Based on cited literature that quotes an air velocity limitation of 45m/s for prototype values, the CFD model would render the air vent inadequate for all emergency gate openings below 50%, since the prototype velocities would be quite higher than the said values for these gate openings.

The graph below shows the aeration demand of the flow for the CFD model, physical model and empirical calculations (Wisner, 1965).
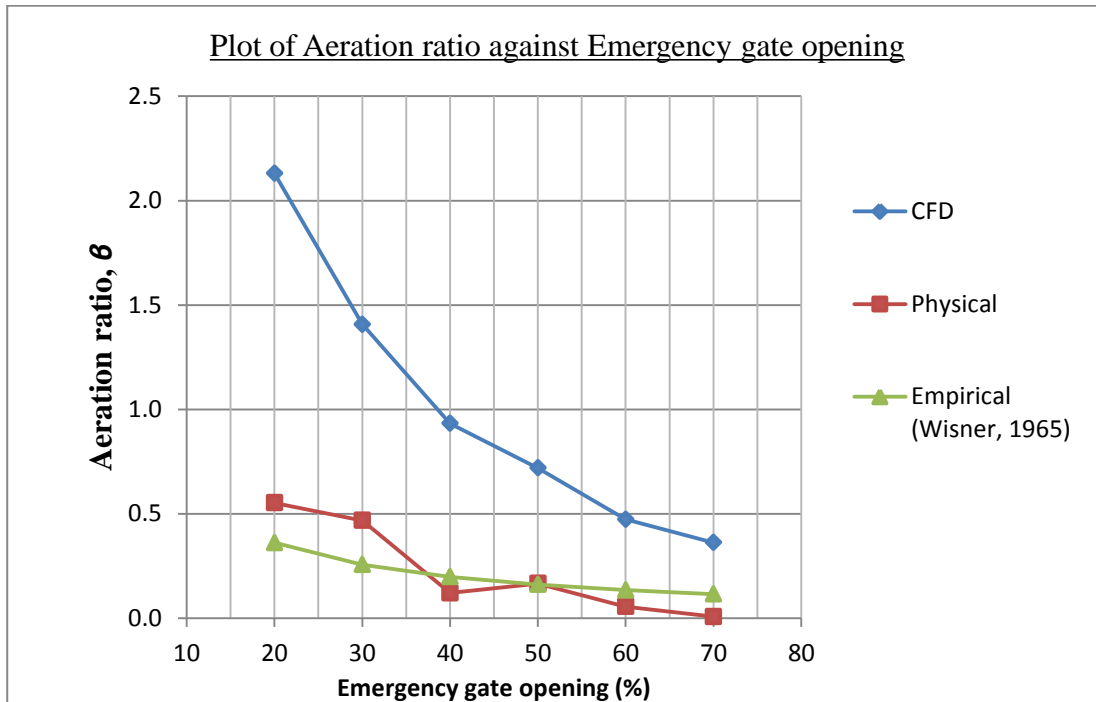
Figure 5.2.2-3: Aeration demand for the different emergency gate openings (Note: $\beta = Q_a/Q_w$ where Q_a is the air discharge and Q_w is the water discharge at the emergency gate)

The aeration demands determined from the CFD model are much higher than those measured in the physical model and those determined by the empirical calculations. However, they all appear to follow the same trend with the demand decreasing with increasing emergency gate openings. Thus, the smaller the gate opening the greater the amount of air sucked into the conduit downstream of the emergency gate.

The results from the CFD model where compared to those from a previous research project by Najafi et. al. (2007) on the numerical simulation of air-water flow in gated tunnels. Figure 5.2-5 below shows a graph extracted from the research paper.
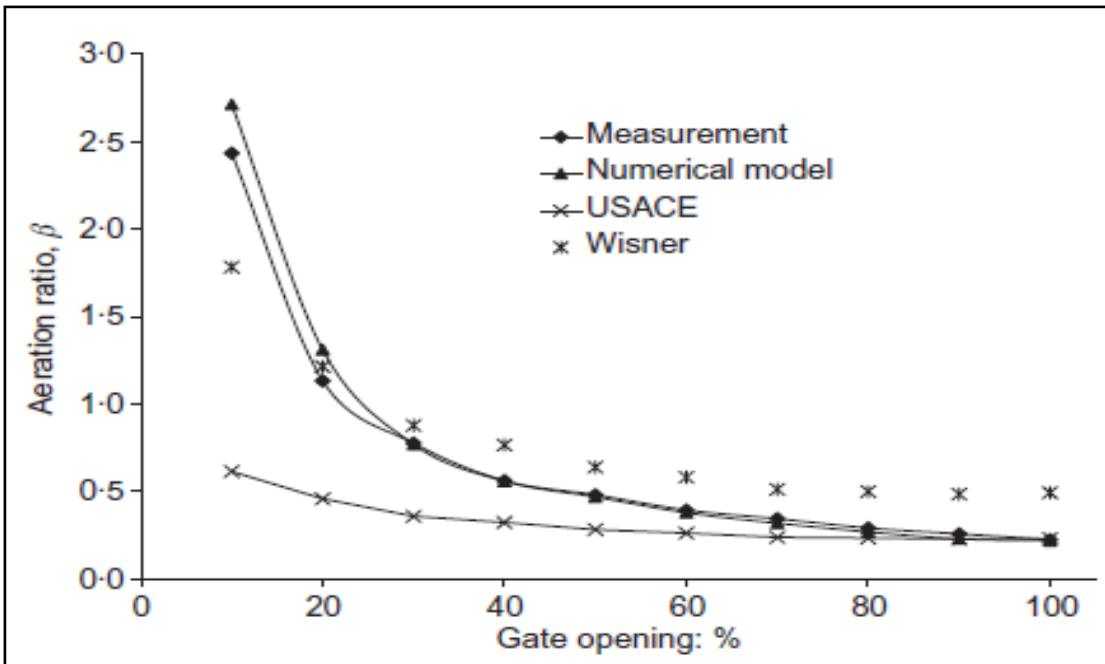
Figure 5.2-5: Aeration demand from research by Najafi et. al. (2007).

The results from the research work follow a similar trend as those for the CFD model described above with differences of course since the models are not geometrically the same. The research study entailed a 1:17 scaled numerical and physical model and only the section of emergency gate was studied. This is another important validation that shows that the CFD modelling of the Berg River Dam provided similar results to those of another research project.

5.2.3   Froude number

The flow velocities through the emergency gate for all gate openings shown in the Tables 5.2.2-1, 5.2.2-2 and 5.2.2-3 above was used to establish and the Froude number, thus confirming the nature of the flow.

The Froude number was calculated using the formula common for rectangular sections seen below.

$$Fr = V/(gy)^{1/2}$$

Where,

V is the flow velocity at the vena contracta

y is the water depth at the vena contracta

Figure 5.2.3-1 below shows the Froude numbers determined for the CFD model, the physical model and those calculated empirically.
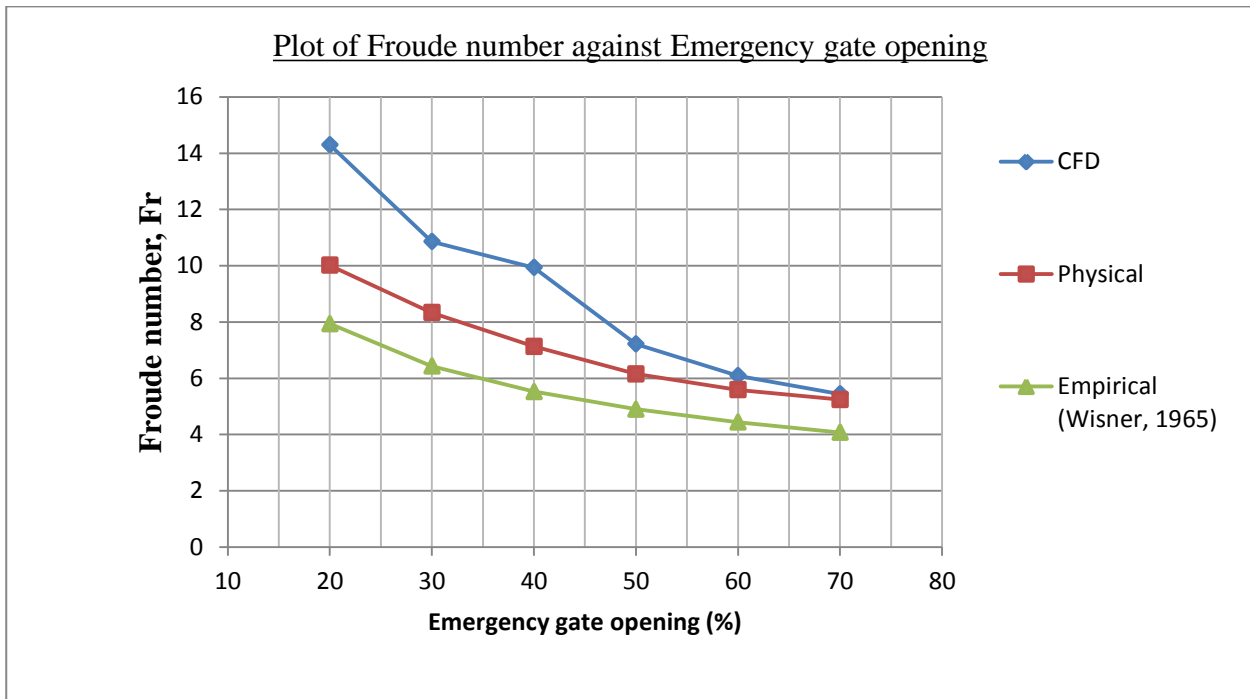
Figure 5.2.3-1: Plot of Froude number at the emergency gate

Froude number plotted in Figure 5.2.3-1 closely follow the same trend and also confirm supercritical flow since all values are greater than 1.

It was noticed that as the flow downstream progressed in the conduit structure, highly aerated damming of fluid in the conduit was observed at 50% and 60% gate openings. These masses resembled hydraulic jumps, so in order to determine whether any hydraulic jump was actually formed in the conduit, the Froude Numbers at various points along the conduit were established to determine whether the flow transitioned from supercritical to subcritical.

The points monitored included the first bend, midway between the first and second bends, and at the second bend. Table 5.2-5 shows the results obtained from calculated Froude numbers.

Table 5.2-5: Froude number at different parts of the floor of the conduit section

Emergency gate opening (%)	Velocity at Bend 1 (m/s)	Velocity at Mid-section (m/s)	Velocity at Bend 2 (m/s)	Froude number at Bend 1	Froude number at Mid-section	Froude number at Bend 2
20	7.5	6.25	6.25	8.86	4.67	6.03
30	6.93	5.04	3.78	6.69	3.44	2.58
40	7.99	6.85	6.85	7.71	4.33	5.12
50	7.42	5.56	3.71	6.20	3.51	2.34
60	8	5	4	5.98	2.79	2.11
70	7.53	4.6	3.47	5.63	2.43	1.83

With the Froude number for all emergency gate openings being more than 1, it was concluded that there was no formation of hydraulic jumps in the conduit since for a hydraulic jump to occur, the flow has to transition from super-critical to sub-critical flow.

Note: A CD-ROM that shows animations created during the CFD simulations for density of fluid in the domain for the various emergency gate openings can be accessed through the supervisor of this research, Prof. G. R. Basson.

CONCLUSIONS AND RECOMMENDATIONS

The purpose of the 3-dimensional CFD study was to investigate the occurrence of the sudden air up-surge in the air vent of the Berg River Dam outlet structure as experienced at the 2008 commissioning tests. The initial assumption was that there was a gate opening during which the aeration demand was not adequately satisfied. The 3-dimensional study was used to investigate the case study and steady state simulations were conducted for static gate openings to investigate the adequacy of the air vent for a range of fixed gate openings.

Simulation results were compared with those from the physical hydraulic model tests. The physical model with a scale of 1:14.066 was tested at the University of Stellenbosch hydraulics laboratory.

The CFD study of steady state fixed gate openings simulated positive air flow down the air vent which agreed with the physical model tests. In the physical model tests, negative air flow could only be obtained while the gate was closing.

The results obtained from the steady state simulations were similar to those of the physical model. However, the numerical model produced higher air flow than the physical model, although the trend in results was the same. Because the simulations were steady state, it was not possible to monitor the variation of parameters with time. Even with the similarity in results from the physical model and numerical model, it was not possible to simulate the sudden air up surge that was experienced in the prototype.

Even though the steady state simulations did not produce the required result, they were not in vain. They enabled not only the establishment and determination of the variables required for further research work but also provided direction for future work.

The steady state simulations helped establish that at static gate opening, the aeration demand could be adequately satisfied since the discharge was constant for specific gate openings.

Since the steady state simulations were not able to produce time dependent results of the varying pressures and velocities that occur during the testing of the Berg River Dam prototype, it is recommended that transient simulations be conducted for a moving gate setting. The results of the transient simulations would create a basis for the comparison of time varying parameters. As a first step the simulations may be performed with fixed gate openings as in the steady state set up and in a further step the creation of a moving gate into the existing geometry should be incorporated.

112

Further research done with a dynamic gate for transient simulations would cause the discharge to vary rapidly with time. As the gate closes, the discharge decreases and the demand for air increases. Inadequacy of the air vent to provide the required aeration demand might force the system to solicit air from the ski jump, a situation that could lead to sudden upstream flow of air.

Increased flow simulation times must be used to ensure that the model is stable and that conservation of mass has been established before results can be extracted for analysis. There may be changes to the flow patterns even after the flow has reached the ski jump. To guarantee the accuracy of the solutions from the simulation, finer meshes should be used although this would require more calculation time, and the quality of the mesh must be kept within acceptable limits.

Smaller time steps are recommended to ensure that divergence of the solution is avoided.

It should be noted, however, that transient simulations will require more processing time since the solutions have to be calculated for time varying parameters.

REFERENCE LIST

Abban, B., Shand, M., Kamish, W., Makhabane, M., Van Zyl, B., & Tente, T. (unknown). *Decision Support System for the Berg River Dam and Supplement Scheme.* University of Stellenbosch, South Africa.

ASHRAE (1981) - American Society of Heating, Refrigerating and Air Conditioning Engineers, Inc. *ASHRAE Handbook Fuundamentals Volume*.

Aydin, I. (2002). Air demand behind high head gates during emergency closure. *Journal Hydraulics Division, vol. 40, 2002, NO. 1*

Borodina, L. K. (1969). Aeration behind low level gates. *Gidrotekhnicheskoe Stroitel'stvo, No. 9, pp. 32-37.*

Calitz. J. A. (2009). *Physical and Mathematical Modelling of air Flow with the Emergency Gate Closure of the Berg River dam.* Stellenbosch University, South Africa.

Campbell, F. B. and Guyton, B. (1953). Air Demand in Gated Conduits. *IAHR Symposium, Minneapolis.*

Chadwick, A., Morfett, J., Borthwick, M. 2004. *Hydraulics in Civil and Environmental Engineering*. New York: Spon Press.

Erbisti, P. C. F. (2004). Design of Hydraulic Gates. *Swets and Zeitlinger B. V., Lisse, Balkema Publishers,* Netherlands.

Falvey, H.T. (1980). Air-water flow in hydraulic structures. *US Department of interior, Water and Power Resources Service*, Engineering monograph No.41

Giesecke, J. (1982). Verschlusse in Grundablassen – Funktion und Ausfuhrung. *Wasserwirtscraft* 72(3): 97-104 (in German).

Hydraulics Research Wallingford. (1990). Charts for the Hydraulic Design of Channels and Pipes. 6th Edition. *Thomas Telford Limited. London.*

Kalinske, A. A. and Robertson, J. W. (1943). Closed conduit flow. ASCE *Transactions 108: 1435-1447*.

Knapp, R. T., Daily J. W., and Hammit, F. G. (1970). Cavitation. McGraw-Hill Book Company, *New York, London.*

Levin, L. (1965). Calcul Hydraulique des Conduits d'Aeration des Vidanges de Fond et Dispositifs Deversants. *L. Houille Blanche,No. 2* (in French).

Lewin, J. (1995). Hydraulic Gates and Valves in free surface flow and submerged outlets. *T. Telford, London*.

Najafi, M. R. and Zarrati, A. R. (2007). Numerical simulation of air-water flow in gated tunnels. *Proceedings of the Institution of Civil Engineers. Water management 163 Issue WM6, pp 289-295.*

Naudascher, E. (1991). Hydrodynamic forces. *IAHR Hydraulic Structures Design Manual* 3. Balkema, Rotterdam, the Netherlands.

Novak, P. Moffat, A.I.B. Naluri, C. and Narayanan, R. (2007). Hydraulic Structures. Fourth Edition. Taylor and Francis Group, Oxon.

Sharma, H. R. (1976). Air entrainment in high head gated conduits. *Proceedings of ASCE, Journal of the Hydraulics Division. vol.102, No.11, pp.1629-1646.*

U. S. Army Corps of Engineers. (1964). *Hydraulic Design Criteria*. Air demand, Regulated outlet works, Sheet 050-1.

Van Vuuren, S. (2003). *Berg River Project Hydraulic Model Testing of the Outlet works Model Scale 1:20.* Sinotech CC, South Africa.

Vischer, D. L. and Hager, W. H. (1998). Dam Hydraulics. *Wiley Series in Water Resources Engineering*, England

Versteeg, H. K. and Malalasekera, W. (2007). The Finite Volume Method. *An Introduction to Computational Fluid Dynamics*. Second Edition. *Pearson edition published*, England.

Wisner, P. (1965). On the role of the Froude criterion for the study of air entrainment in high velocity flows. *Proceedings of the 11th IAHR Congree, USSR, Leningrad.*

APPENDIX A: BRD BOTTOM OUTLET STRUCTURE TRIAL COMMISSIONING TEST REPORT, JUNE 2008

BERG RIVER DAM EMERGENCY GATE COMMISSIONING

RELEASE OF AIR

1. Introduction

Andy Griffiths of Goba and I discussed the possible reasons for the release of very large volumes of air from the air intake shaft during the trial closure of the emergency gate on 12 June 2008.   We concluded that the only way that the volume of air released could arise is through the formation of and entrainment of air by a vortex in the intake shaft. Our reasons are set out below.

2. Design of Air vent

The air vent was designed to allow air to be introduced immediately downstream of the emergency gate on account of the negative pressures that were expected to occur during its partial closure. The final design was based on the 1 in 20 scale hydraulic model tests, which had shown no evidence of vortex formation and had indicated that air **would** be drawn down the air vent.

Immediately after the trial release Prof Gerrit Basson utilized the 1 in 50 scale hydraulic model, that was also used for the original design and is still operational at the University of Stellenbosch, to resimulate partial closure of the emergency gate. This model also showed no evidence of vortex formation and indicated that large volumes of air would be drawn down the air vent.

3. Mechanism for Release of Air from Air vent

Contrary to the design, James Metcalf's air vent velocity measurements shown in Table 1 indicate that, while the emergency gate was closing, very large volumes of air were continuously released from the 1,8 m^2 air vent commencing when the gate was about 30% closed (ie 70% open). The time of commencement of the release of air seems to have coincided with the observations of the following:
o   The time that the cavitation noise in the access shaft to the emergency gate ceased, which indicates the presence of air, and
o   The time that the release of air from the flow commenced in the radial gate house.

James Metcalf's observations indicate that the velocities of air released through the 1,8 m^2 air vent increased from 8,75 m/s (32 km/h) at 13h06 to about 45 m/s (160 km/h) at 13h14, corresponding to air releases increasing from 16 m^3/s to 80 m^3/s as indicated in Table 2. There are only two potential sources of air:
o   The entrainment of air from the downstream end of the conduit at the radial gate: however this would not be possible because of the high velocity of the water flow in the conduit which causes air to be dragged downstream rather than upstream, and because the observations during the trial indicate that for much of the time the conduit was flowing full with considerable volumes of air entrained in the flow. Reports by observers in the housing of the radial gate also indicate that considerable volumes of air were released from the flow as it exited at the radial gate. However the removal of air was also reported and this may have been caused by the suction

116

effect of intermittent fully aerated flow occupying the total area of the opening downstream of the radial gate.

o The only other potential source of air is via a vortex forming in the vertical shaft upstream of the emergency gate, and is the only explanation that is consistent with the velocity observations of the air releases from the air vent and from observations that the flow at the radial gate was highly aerated.

4.   Recommendations for Hydraulic Model Tests

The following recommendations are made to try to gain an improved understanding of the mechanism for the formation of a vortex in the shaft:

o Although the 1 in 40 scale hydraulic model is not sufficiently large to accurately model the formation of vortices, it is nevertheless recommended that this model is utilized to observe the flow patterns as follows:

- For the dam water level and intake level at the time of the trial and with the radial gate fully open check the flow patterns and air entrainment for small incremental closures of the emergency gate similar to those undertaken for the trial. If possible measure the air releases and the flow of water for the various emergency gate openings.
- If no vortex forms repeat the above but introduce mild circular perturbations to the water in the intake shaft either by stirring action or by temporarily blocking the flow through one of the intakes into the tower (try clockwise and counter clockwise rotation).
- Repeat with stronger perturbations until a vortex forms with the gate at about 66% open and then observe the air entrainment and release from the air vent for incrementally reducing openings. If possible measure the flow of water and of air for the various emergency gate openings.
- Repeat for other intake gate selections and water levels in the dam.

o Compare the modeled air releases with those measured by James Metcalf on 12 June.

o Obtain from DWAF the actual flow measurements at the Crump weir downstream, and compare these with the hydraulic model results, if necessary adjusted by computer model routing to account for the times of incremental gate lowering and the plunge pool and channel storage effects upstream of the Crump weir.

o Obtain the records for the pressure cells outside the conduit to check whether these also indicate the reducing pressures in the conduit due to the entrainment of air.

o Prepare a report on the above.

5. Safety Recommendations

The following recommendations are made:

o <u>Air vent:</u> The rectagrids at the top of the air vent were blown 3 m to 4 m into the air as indicated in Table 1 and fortunately only caused a minor injury to James Metcalf but could easily have killed him and the observer from the Cape Argus. Therefore as human lives would be endangered in the event that the emergency gate is purposefully or inadvertently operated in the future, it is strongly recommended that the rectagrid is removed and that the air vent is extended upwards by at least 1,8 m by constructing a reinforced concrete chimney around the air vent.

o <u>Radial Gate House:</u> The accounts of observers that the intermittent release and removal of large volumes of air could perhaps have damaged the radial gate house have already been taken into account and the contractor has been instructed to replace all windows with grids.

It is also understood that there was a considerable amount of water spray in the gate house during the emergency gate closure and earlier during the commissioning tests there was also spray from the leaking gate seals.

As the electrical equipment for operating the radial gate will be exposed to the weather to a greater extent by the removal of the windows and possibly to spray, it is suggested that consideration be given to constructing a small weatherproof enclosure around the electrical equipment in the gate house.

Table 1.   Air vent Velocity Observations By James Metcalf on 12 June 2008

Time	Hand-held Schiltnecht Anemometer **Air vent (±1.5m x 1m) Air Velocity Reading: (32 second average** logged by electronic unit)	Gate Degree Closed	Remarks (NB: Anemometer held down on top of Mentis Grid Cover)
12 June 08	**m/s**		
13h00	Observer not present	0%	Air velocity & direction unknown (suspect <u>ingestion</u> of air – i.e.: "down shaft"
13h01	Ditto	5.5%	
13h02	Ditto	11.1%	
13h03	Ditto	16.7%	
13h04	Observer setting up instrument	22.2%	
13h05	3.5m/s	27.8%	Air Vel Direction unknown
13h06	8.75m/s	33.3%	Notebook in which air velocity readings were being recorded handed to second observer (Cape Argus Reporter) since up-velocity (out of shaft) causing notebook to be "blown away"
13h07	12.44m/s	38.9%	Up-shaft air flow
13h08	14.2m/s	44.4%	Ditto
13h09	19.8m/s	50%	Ditto
13h10	21.7m/s	55.5%	Increasing difficulty in holding anemometer down on shaft top grid cover due to high-velocity outflow (anemometer wooden case became air-borne at about this stage)
13h11	22.3m/s	61.1%	Air flows "surging" constantly at (say) 10 cycles per minute and getting stronger all the time
13h12	26.0m/s	66.7%	Observer finds it increasing difficult to hold down anemometer and to hold his arm horizontal whilst lying down on the shaft top cover, due to progressively rising air up-flow velocity
13h13	35 m/s	72.2%	Last reading before……..
13h14	Probably of the order of 45m/s (160km/hr)	77.8%	Mentis grid cover blown off top of shaft, lifted to a height of about 3 or 4 metres, tipping observer off the shaft top and against the

118

Time	Hand-held Schiltnecht Anemometer **Air vent (±1.5m x 1m) Air Velocity Reading: (32 second average** logged by electronic unit)	**Gate Degree Closed**	**Remarks** (NB: Anemometer held down on top of Mentis Grid Cover)
			upstream concrete wall, and then falling back to the ground, striking/injuring[1] the observers right foot (which was aligned along the toe of the wall
13h15	?	83.3%	Anemometer retrieved from the top of the shaft (loss prevented by being attached to the output cable to the electronic unit)
13h16	?	88.9%	No further readings
13h17	?	94.4%	
13h18	?	100%	

Table 2: Air Velocities and Flows Released from 1.8 m^2 Air vent

Time	Air Velocity		Air Flow
	m/s	km/hr	cu m/s
13h06	8.75	32	16
13h07	12.44	45	22
13h08	14.2	51	26
13h09	19.8	71	36
13h10	21.7	78	39
13h11	22.3	80	40
13h12	26	94	47
13h13	35	126	63
13h14	45	162	81

Mike Shand
30 June 2008

---

[1] "Ring toe" found to be crushed; writer is taken to a Franschhoek surgery wef ±2pm. Wound inspected by Dr. Alex. Heywood at about 3 pm, stitched up & dressed & appropriate medication given

119